3.4 Cooperative Phenomena in Complex Macroscopic Systems

Nonequilibrium superconductivity emerging from synergistic effects of light and phonons in strongly correlated systems

Kota IDO, Takahiro OHGOE and Masatoshi IMADA
Department of Applied Physics, The University of Tokyo,
Hongo 7-3-1, Bunkyo-ku, Tokyo 113-8656

Recently, laser-controlled superconductivity (SC) has been studied extensively to go beyond the limit of superconducting critical temperature T_c in equilibrium. One of the approaches is selective excitations of phonon modes of correlated electron materials by strong laser irradiation. Surprisingly, in the case of a bi-layered cuprate, indication of superconductivity above T_c has been reported [1,2]. This fascinating experiment has motivated theoretical studies for understanding its mechanism.

On the other hand, proposals for an alternative strategy ascribed to a more generic mechanism are also desirable. This is because the strategy based on coherent phonon excitations does not seem to be general in correlated electron materials at present due to strong restriction on the details of phonon modes in materials. Recently, we have proposed an alternative way to enhance SC in a correlated electron system without lattice degrees of freedoms [3]. In this study, we have shown that strong and non-resonant laser irradiation to a charge uniform state dynamically enhances SC without deteriorating into inhomogeneities that suppress SC in equilibrium. However, this approach can be applied only to uniform states in cuprates. Since inhomogeneous states were observed in a number of cuprates below optimal doping [4], it is important to verify whether strong and non-resonant laser irradiation dynamically melts static inhomogeneity and enhances SC.

Our purpose in this project is to clarify microscopic origin of the light-enhanced SC observed in the experiments. In addition, we also aim to clarify what happens when strong lasers are irradiated to equilibrium systems with inhomogeneity. Here, we summarize our main achievements for each topic.

(i) *Development of time-dependent variational Monte Carlo method for electron-phonon coupled systems:* In order to analyze an effective model for cuprates with light-driven phonon excitations, we need to treat not only strong electron correlations but also many phonons excited by laser irradiation. For this purpose, we extended a many-variable variational Monte Carlo (mVMC) method to nonequilibrium electron-phonon coupled systems. As a trial state, we adopt a tensor product state of an electron wave function and a phonon wave function with an electron-phonon correlation factor [5]. By introducing a

large number of variational parameters to the phonon part, we can treat multi-phonon excitations by light.

As benchmarks of the mVMC method, we calculated relaxation dynamics after an electron-phonon interaction quench protocol of the one-dimensional Holstein model. We found that our trial wave function well reproduces the exact results for the time evolution of double occupancy and charge correlations. This result shows that the mVMC method offers an efficient and accurate way to study challenging problems of nonequilibrium electron-phonon coupled systems. The analysis of an effective model for the cuprates with phonons under laser irradiation will be reported elsewhere.

(ii) *Laser-enhanced superconductivity caused by dynamically melting charge inhomogeneity:* By using the mVMC method [6,7], we numerically study dynamics of *d*-wave SC and charge inhomogeneity when laser pulses are irradiated to an inhomogeneous ground state in a two-dimensional correlated electron system. We found that strong and non-resonant laser irradiation can melt charge inhomogeneity, and enhance *d*-wave SC. We observed that the lifetime of such enhanced SC is prolonged by keeping the laser intensity constant in the middle of the laser irradiation. Our findings will shed light on a new way to realize SC that is not attainable in equilibrium in strongly correlated electron systems.

References

[1] W. Hu *et al.*: Nat. Mater. **13** (2014) 705.

[2] S. Kaiser *et al.*: Phys. Rev. B **89** (2014) 184516.

[3] K. Ido, T. Ohgoe, and M. Imada: Sci. Adv. **3** (2017) e1700718.

[4] R. Comin and A. Damascelli: Annu. Rev. Condens. Matter Phys. **7**, 369 (2016).

[5] T. Ohgoe, and M. Imada, Phys. Rev. B. **89** 195139 (2014).

[6] D. Tahara and M. Imada: J. Phys. Soc. Jpn. **77** (2008) 114701.

[7] K. Ido, T. Ohgoe, and M. Imada: Phys. Rev. B **92** (2015) 245106.

Determination of Scattering Length of Bose-Hubbard Model by Quantum Monte Carlo Simulations[1]

Naoki KAWASHIMA
Institute for Solid State Physics, University of Tokyo
Kashiwa-no-ha, Kashiwa, Chiba 277-8581

The Bose-Hubbard model is the simplest non-trivial model for interacting boson system. It is widely believed that, in the dilute limit, the model is equivalent to the continuous model characterized by a single parameter, i.e., the s-wave scattering length. However, there has been no quantitative estimation of the scattering length in the unit of lattice constant. In the ISSP supercomputer project of SY2017, we aim at establishing the quantitative correspondence between the lattice model and the continuous-space model.

Here, the Bose-Hubbard model defined as

$$H = -t \sum_{(ij)} (b_i^\dagger b_j + \text{h.c.}) - \mu \sum_i b_i^\dagger b_i,$$

which is compared in our project to

$$H = \int d\mathbf{x} \phi^\dagger(\mathbf{x}) \left(-\frac{\hbar^2}{2m} \nabla^2 \right) \phi(\mathbf{x}) + \int d\mathbf{x} d\mathbf{x}' \phi^\dagger(\mathbf{x}') \phi^\dagger(\mathbf{x}) V(\mathbf{x}' - \mathbf{x}) \phi(\mathbf{x}) \phi(\mathbf{x}')$$

with

$$V(\mathbf{x}) \equiv \begin{cases} \infty & (|\mathbf{x}| \le a_s) \\ 0 & (|\mathbf{x}| > a_s) \end{cases}$$

We carried out Monte Carlo simulation on the Bose-Hubbard model in dilute region, $10^{-3} < na^3 < 10^{-1}$. We used our original package DSQSS[2], which can be downloaded from the GITHUB and can be used under GPL license. We varied the system size L and the inverse temperature β to confirm that the result does not depend on these parameter beyond the statistical error, i.e., our result can be identified with those at zero temperature in the thermodynamic limit.

Figure 1 is our result compared with the analytical predictions made by Lee, Huang and Yang [3]. From this comparison we estimated the s-wave scattering length in the unit of the lattice constant as $a_s/a = 0.315$.

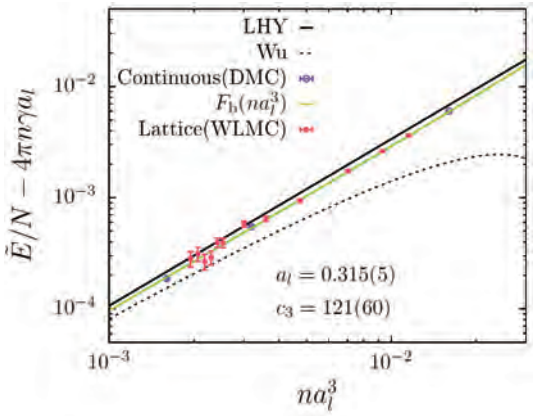

Figure 1: The correction in the normalized energy. The three curves labeled as "LHY", "Wu", and "F_b" represent the analytical prediction up to the first correction, up to the second correction and the third (logarithmic) correction, respectively. The open symbols labeled as "Continuous" are the results of the diffusion Monte Carlo for the continuous-space model whereas the closed symbols are for the present calculation of the lattice system.

[1] This report is based on A. Masaki-Kato, Y. Motoyama and N. Kawashima (unpublished).
[2] https://github.com/qmc/dsqss/wiki
[3] T. D. Lee, K. Huang and C. N. Y. Yang Phys. Rev. 106, 1135 (1957).

Study on Complex Systems by Generalized-Ensemble Algorithms

Takuya HAYASHI, Yuhei TACHI, and Yuko OKAMOTO

Department of Physics, Graduate School of Science, Nagoya University

Furo-Cho, Chikusa-ku, Nagoya, Aichi 464-8602

Despite the experimental discovery of the residual entropy of ice Ih in the 1930's [1], highly accurate measurements have yet to be made in experiments. The calculation started from Pauling in the 1930's [2]. As a recent calculation, there are results [3,4] by multicanonical simulations [5]. In this work, we aim to drastically improve the accuracy in large scale and complex systems.

The entropy is proportional to a logarithm of the density of states. In Refs. [3,4] multicanonical weight factor was obtained by the Wang-Landau method [6], and a multicanonical production run was performed to obtain an accurate estimate of the density of states.

In order to obtain the multicanonical weight factor for a larger system, we propose to combine the multicanonical replica-exchange method [7] and replica-exchange Wang-Landau method [8]. In order to confirm the effectiveness of this new method, test simulations were performed with the 2-dimensional Ising model (with the number of spins up to 128×128), and we found that this combination gives the most effective method for the determination of the density of states (a manuscript is in preparation). We are now ready to perform simulations to improve the value of the residual entropy of ice.

We have also studied an artificial glycan cluster in which 24 GM1 glycans were transplanted to a metal-ligand complex using cluster B. The complex with GM1 glycans was developed to investigate the interaction between amyloidgenic proteins and GM1 glycan clusters [9]. GM1 glycan is glycan moiety in glycolipid called GM1 ganglioside. The structural information of the GM1 glycan clusters is important for understanding the mechanism of glycan cluster recognition of amyloidgenic proteins. Therefore, we focused on the structural properties of GM1 glycans on the metal-ligand complex.

In this study, molecular dynamics (MD) simulations of the artificial glycan cluster and a monomeric GM1 glycan were performed to compare the structural distribution of the GM1 glycan on the complex and that of the monomeric GM1 glycan.

In this simulation, we found that about 65% GM1 glycans on the complex forms clusters by hydrogen bonding. It was also found that GM1 glycans interacts with the

ligands on the complex by tilting. Furthermore, we revealed that some local minimum structures of GM1 glycans on the complex are stabilized as the monomeric GM1 glycan (a manuscript is in preparation).

The above results give important information for investigating the mechanism of the glycan cluster recognition of amyloidgenic proteins. In the future work, we plan to perform the binding MD simulations of amyloidgenic proteins to the artificial glycan cluster.

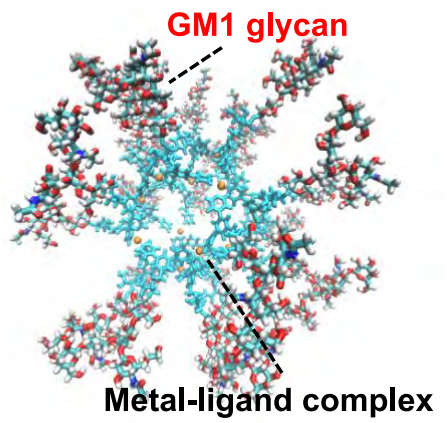

Fig. 1: Metal-ligand complex with GM1 glycans.

References

[1] J. D. Bernal and R. H. Fowler: J. Chem. Phys. **1** (1933) 515.

[2] L. Pauling, J. Am. Chem. Soc. **57** (1935) 2680.

[3] B. A. Berg, C. Muguruma, and Y. Okamoto, Phys. Rev. B **75** (2007) 092202.

[4] B. A. Berg, C. Muguruma, and Y. Okamoto, Mol. Sim. **38** (2012) 856.

[5] B. A. Berg and T. Neuhaus, Phys. Rev. Lett. **68** (1992) 9.

[6] F. Wang and D. P. Landau, Phys. Rev. Lett. **86** (2001) 2050.

[7] Y. Sugita and Y. Okamoto, Chem. Phys. Lett. **329** (2000) 261.

[8] T. Vogel, Y. W. Li, T. Wüst and D. P. Landau, Phys. Rev. Lett. **110** (2013) 210603.

[9] S. Sato, Y. Yoshimasa, D. Fujita, M. Yagi-Utsumi, T. Yamaguchi, K. Kato, and M. Fujita, Angew. Chem. Int. Ed. **54** (2015) 8435.

Coarse grained MD simulation for fracture and reinforcement of polymer materials

Katsumi HAGITA

Department of Applied Physics, National Defense Academy, Yokosuka, Kanagawa 239-8655

We investigated fracture behaviors of polymers such as morphology changes and chain breaking by uniaxial elongations. Understanding of fracture mechanisms with molecular level is considered to be important on reinforcement of polymer materials. We performed coarse grained (CG) molecular dynamics (MD) simulations of polymer materials. Here, we considered Kremer-Grest (KG) model, united atom (UA) model and reactive force field (ReaxFF) MD. KG is bead spring model. UA and ReaxFF can be regarded as CG of all atomistic MD simulations and DFT simulations, respectively. These simulation methods can be performed by LAMMPS (Large-scale Atomic/Molecular Massively Parallel Simulator), which was used in the present studies. We also studied Dissipative particle dynamics (DPD) which is a stochastic simulation method that can handle larger time scales than the KG model. This year, we focused on ABA tri-block copolymers (BPCs) and crystallized polyethylene (PE).

For ABA tri-BCPs, we studied morphology changes via two-dimensional scattering patterns (2DSPs) for correspondences between simulations and experiments. Recently, we proposed Thinning Approximation (TA) to calculate 2DSPs under shear flows for KG model [1]. We performed CGMD simulations of KG model of ABA tri-BCPs for various fractions. Systematic changes of 2DSPs under uniaxial elongations were observed by using TA [2]. Also, we performed CGMD simulations of KG model to examine filler-filled systems such NC-clay nanocomposites [3], and nano-particle (NP) filled rubbers [4]. On the study of NC-clay nanocomposites, we could reproduce the stress-strain curve and the change of 2DSPs during elongation at the same time. For the NP-filled rubbers, we found that effect of polymer-NP interactions and nanostructures on glass transition temperature.

In order to investigate the fracture behaviors from the equilibrium structure of phase separated ABA tri-BPCs by elongations, we considered an improvement of segmental repulsive potential (SRP) of DPD simulations. To reduce bond crossing probabilities and keep the equilibrium structure before and after introducing of SRP, we proposed multipoint SRP [5].

As studies behaviors of 2DSPs of NP-filled rubbers, we proposed filler network model of

filled rubber materials in order to study system size dependence of 2DSPs and obtain a rough model to reproduce structure-property relationship for machine learning studies [6].

To study fracture of realistic materials, we considered crystallization of PE chains. As produces in our usual life, branched PE chains such as high- and low-density PE (HDPE and LDPE) are used. We found that branched junctions are mainly localized in amorphous layer. To study formations of amorphous layers, we compared ring and linear PE polymers. Here, amorphous layers have important role on fractures of PE materials. We found that crystallization of ring PE polymers is faster than that of linear PE polymers [7]. In addition, we also investigated the topological effect of a knot of a ring on crystallization of ring PE polymers [8]. To reproduce chain breaking, we used ReaxFF MD simulations. In our study, UAMD was used to prepare crystallized PE and ReaxFF MD was used to study chain breaking under stretching.

To enhance material researches including developments of real materials, we examined AI based information analysis methods. As the first example, we studied image classification of images of NPs in rubbers [9]. As the second example, we considered super resolution for asymmetric resolution of FIB-SEM (focused ion beam scanning electron microscopy) 3D imaging of NPs in rubbers [10].

References

[1] K. Hagita, T. Murashima, H. Takano, and T. Kawakatsu: J. Phys. Soc. Jpn. **86** (2017) 124803.

[2] K. Hagita, K. Akutagawa, T. Tominaga, and H. Jinnai: in preparation.

[3] K. Hagita, Y. Shudo, and M. Shibayama: Submitted to Polymer.

[4] K. Hagita and H. Morita: Submitted to Macromolecules.

[5] N. Iwoaka, K. Hagita, and H. Takano: in preparation.

[6] K. Hagita, T. Tominaga, T. Hatazoe, T. Sone, and H. Takano: J. Phys. Soc. Jpn. **87** (2018) 014802.

[7] K. Hagita, S. Fujiwara, and N. Iwaoka: in preparation.

[8] K. Hagita, E. Uehara and T. Deguchi: in preparation.

[9] K. Hagita, T. Tominaga, T. Sone, I. Takahashi, C. Lee, and M. Ogino: Nippon Gomu Kyokaishi **91** (2018) 3-8 in Japanese.

[10] K. Hagita, T. Higuchi and H. Jinnai: Scientific reports **8** (2018) 5877.

Numerical Studies on Finite Temperature Excitation Spectra of Quantum Spin Liquids

Youhei Yamaji
Deparment of Applied Physics, The University of Tokyo
Hongo 7-3-1, Bunkyo-ku, Tokyo 113-8656

A growing demand for finite-temperature simulation of excitation spectra has originated from experimental researches on many-body quantum systems. Raman scattering and inelastic neutron scattering measurements on a class of quantum magnets, *Kitaev materials* [1], have brought attention to the temperature dependence of the excitation spectra. Shortly after the finding of the quantum spin liquid in the Kitaev model [2], it has been proposed that the Kitaev model captures low-energy spin degrees of freedom in honeycomb networks of heavy transition metal ions, which are typified by an iridium oxide α-Na_2IrO_3 [3]. So far, the Kitaev materials including α-A_2IrO_3 (A=Na, Li), α-$RuCl_3$, β-Li_2IrO_3, and γ-Li_2IrO_3 exhibit spontaneous time-reversal symmetry breakings. However, these materials expected in proximity to the Kitaev's spin liquid stimulate the experimental research on the excitation spectra at finite temperatures, which requires theoretical counterparts. In addition to the theoretical studies on Raman spectra and dynamical spin structure factors of the simple Kitaev model at zero temperature [4] and finite temperatures [5], theoretical and numerical studies on the Kitaev-like Hamiltonian on variety of tricoordinate networks are highly desirable.

This year, we have developed an $\mathcal{O}(N_{\rm F})$ algorithm for simulating exact finite-temperature excitation spectra in frequency domain [6], where $N_{\rm F}$ is the dimension of the Fock space of the target system, by combining the typical pure state approach [7] and the shifted Krylov subspace method [8]. We applied the present algorithm to the simplest effective Hamiltonian of the two-dimensional Kitaev-like systems on honeycomb lattices, namely, the Kitaev-Heisenberg model on a honeycomb lattice [9] that consists of S=1/2 spins. The nearest-neighbor bonds on the honeycomb lattice have three different directions. When the three bonds are labeled as x, y, and z, the Kitaev-Heisenberg Hamiltonian,

$$\hat{H} = \sum_{\gamma=x,y,z} \sum_{\langle i,j\rangle\in\gamma} \hat{H}_{ij}^{(\gamma)}, \tag{1}$$

is defined by the exchange coupling for the γ ($= x, y, z$) bond,

$$\hat{H}_{ij}^{(\gamma)} = J\vec{\hat{S}}_i \cdot \vec{\hat{S}}_j + K\hat{S}_i^{\gamma}\hat{S}_j^{\gamma}, \tag{2}$$

where $K = J_0 \sin\varphi$ is the Kitaev coupling constant and $J = (J_0/2)\cos\varphi$ is the Heisenberg exchange coupling constant. Below, we set the energy unit as $J_0 = 1$.

We have focused on the proximity of the phase boundary between the spin liquid phase and a zigzag ordered phase around $\varphi \simeq 92.2°$, and examined temperature dependence of dynamical spin structure factors $S(\vec{Q},\omega)$. We found that the crossover from a spin-excitation continuum, which is a characteristics of the quantum spin liquid, to a damped high-energy magnon mode occurs at temperatures higher than the energy scale of the Heisenberg exchange couplings or the spin gap that is a signature of the quantum spin liquid at zero

temperature. The crossover and the closeness to the quantum spin liquid are quantitatively measured by a dimensionless ratio of the width of the excitation continuum or the damped magnon spectrum and the energy at which the spectral weight becomes maximum. As shown in Fig. 1, we calculated $S(\vec{Q},\omega)$ at $\vec{Q} = \Gamma$ $(= \vec{0})$. To extract the peak width, we fit the high energy peak by an asymmetric Lorentzian function,

$$s(\omega) = \frac{\gamma_{\rm f}}{\gamma_{\rm f}^2 + (\hbar\omega - \epsilon_{\rm f})^2} \left\{ a + \frac{b}{1 + e^{c(\hbar\omega - \epsilon_{\rm f})}} \right\}, \quad (3)$$

where a, b, c, $\gamma_{\rm f}$, and $\epsilon_{\rm f}$ are fitting parameters. The dimensionless ratio of $\epsilon_{\rm f}$ and $\gamma_{\rm f}$ is an estimate of the peak width and characterizes the finite-temperature crossover from the continuum excitations to damped magnon as summarized in Fig. 2. The present results shed new light on analysis of neutron scattering and other spectroscopy measurements on the spin-liquid candidates.

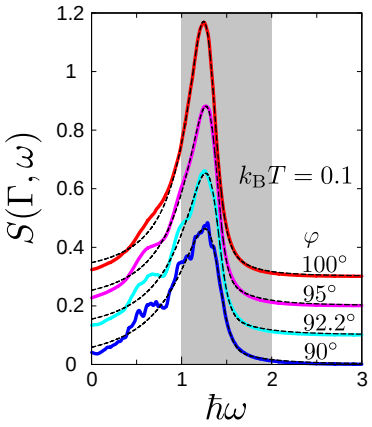

Figure 1: $S(\Gamma,\omega)$ of a 24 site cluster at $k_{\rm B}T = 0.1$ for $\varphi = 90°$, 92.2°, 95°, and 100°. The broken curves represent the asymmetric Lorentzian function $s(\omega)$ defined in Eq.(3) fitted to $S(\Gamma,\omega)$ in $1 \le \hbar\omega \le 2$. These curves are horizontally shifted for visibility.

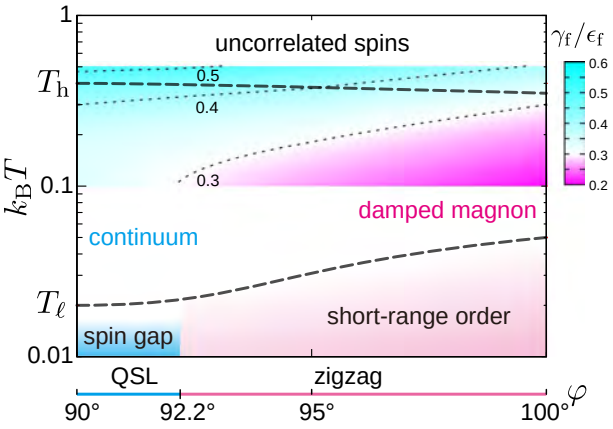

Figure 2: Summary of temperature dependence of $\gamma_{\rm f}/\epsilon_{\rm f}$ and temperature scales of the Kitaev-Heisenberg model for $90° \le \varphi \le 100°$. The two temperature scales $T_{\rm h}$ and T_ℓ for the 24 site cluster at which temperature dependence of heat capacity shows peaks.

References

[1] As reviews, S. Trebst: arXiv:1701.07056.

[2] A. Kitaev: Ann. Phys. **321** (2006) 2.

[3] G. Jackeli and G. Khaliullin: Phys. Rev. Lett. **102** (2009) 017205.

[4] J. Knolle, D. L. Kovrizhin, J. T. Chalker, and R. Moessner: Phys. Rev. Lett. **112** (2014) 207203; J. Knolle, G.-W. Chern, D. L. Kovrizhin, R. Moessner, and N. B. Perkins: Phys. Rev. Lett. **113** (2014) 187201.

[5] J. Nasu, J. Knolle, D. L. Kovrizhin, Y. Motome, and R. Moessner: Nat. Phys. **12** (2016) 912; J. Yoshitake, J. Nasu, and Y. Motome: Phys. Rev. Lett. **117** (2016) 157203.

[6] Y. Yamaji, T. Suzuki, and M. Kawamura: arXiv:1802.02854.

[7] S. Lloyd Ph.D. Thesis, Rockefeller University, 1988; A. Hams and H. De Raedt: Phys. Rev. E **62** (2000) 4365.

[8] A. Frommer: Computing **70** (2003) 87.

[9] J. Chaloupka, G. Jackeli and G. Khaliullin: Phys. Rev. Lett. **105** (2010) 027204.

Randomness-induced quantum spin liquid behavior in the *s*=1/2 random *J1-J2* Heisenberg antiferromagnets on the honeycomb and square lattices

Kazuki Uematsu and Hikaru Kawamura

Graduate School of Science, Osaka University, Toyonaka 560-0043

The quantum spin liquid (QSL) state without any spontaneously broken Hamiltonian symmetry, which accompanies no magnetic long-range order down to low temperatures, has long received much attention. For the realization of such QSL state, geometrical frustration is considered to be essential, and frustrated magnets have been the main target of the quest for QSL materials. In particular, the *s*=1/2 organic triangular-lattice salts and *s*=1/2 inorganic kagome-lattice compound herbertsmithite are well-studied examples, which were reported in common to exhibit the QSL-like behaviors down to very low temperatures with gapless (or nearly gapless) behaviors.

Despite such recent experimental progress, the true origin of the experimentally observed QSL-like behaviors still remains not fully understood and is under hot debate. In many theoretical studies, it has been assumed that the system is sufficiently clean so that the possible effect of randomness or inhomogeneity is negligible and unimportant. Meanwhile, one of the present authors (H.K.) and collaborators have claimed that the QSL-like behaviors recently observed in triangular-lattice organic salts and kagome-lattice herbertsmithite might be the randomness-induced one, the random-singlet state [1-3]. The advocated random-singlet state is a gapless QSL-like state where spin singlets of varying strengths are formed in a hierarchical manner on the background of randomly distributed exchange interactions Jij. The state may also be regarded as a sort of ``Anderson-localized resonating valence bond (RVB) state". Indeed, it was demonstrated that the random-singlet state exhibited the *T*-linear specific heat and the gapless susceptibility with an intrinsic Curie tail, accompanied by the gapless and broad features of the dynamical spin structure factor.

In this year's project, in order to examine the genericity of the proposed randomness-induced QSL state (random-singlet state) , we have extended our previous calculations in search the random-singlet state in the geometrically frustrated lattices like triangular and kagome lattices to unfrustrated, *i.e.*, bipartite lattices like honeycomb and square lattices. Frustration is introduced not by the underlying lattice geometry, but by the

competition between the nearest-neighbor and the next- nearest-neighbor intereactions J_1 and J_2. We compute both the ground-state and finite-temperature properties of both the honeycomb and square models by means of the the exact diagonalization and the Hams-de Raedt methods. The ground-state phase diagram of the models is then constructed in the randomness versus the frustration (J_2/J_1) plane, with the aim of clarifying the effects of randomness and frustration in stabilizing a variety of distinct phases. The results on the honeycomb-lattice model was published in [4].

We have found that the random-singlet state similar in its nature to the one previously found in the geometrically frustrated triangular and kagome lattices are stabilized in a rather wide range of the parameter space even for the J_1-J_2 model on the honeycomb- and square-lattice models so long as the extent of frustration exceeds a critical value. We then conclude that the randomness-induced QSL state, the random-singlet state, is a generic state expected to be realized in quantum magnets in the presence of strong frustration and randomness.

References

[1] K. Watanabe, H. Kawamura, H. Nakano, and T. Sakai, J. Phys. Soc. Jpn. **83**, 034714 (2014).

[2] H. Kawamura, K. Watanabe, and T. Shimokawa, J. Phys. Soc. Jpn. **83**, 103704 (2014).

[3] T. Shimokawa, K. Watanabe, and H. Kawamura, Phys. Rev. B **92**, 134407 (2015).

[4] K. Uematsu and H. Kawamura, J. Phys. Soc. Jpn. **86**, 0447704 (2017).

Slow-Slip Phenomena Represented by the One- and Two-Dimensional Burridge-Knopoff Models of Earthquakes

Hikaru Kawamura and Jun Akutagawa

Graduate School of Science, Osaka University, Toyonaka, Osaka 560-0043

An earthquake is a stick-slip dynamic instability of a pre-existing fault driven by the motion of a tectonic plate. Numerical simulations of earthquakes based on a simplified statistical model, the so-called Burridge--Knopoff (BK) model, are popular in statistical physics, and they provide considerable information about the statistical properties of earthquakes[1]. Although the BK model has been successful in describing earthquakes, almost all studies so far have been limited to the high-speed rupture of earthquakes or to main shocks.

Meanwhile, recent development in modern GPS technology and in high-density GPS and seismograph networks has revealed a rich variety of slow-slip phenomena, including afterslips, silent earthquakes, deep tremors, *etc.*, where the fault sliding velocity is several orders of magnitudes slower than that of the standard high-speed rupture. Thus, the concept of seismicity has been broadened dramatically. Then, to gain a complete understanding of earthquake phenomena, one needs to incorporate these slow-slip phenomena.

It is a challenge to understand such a wide variety of seismicity from a general physical viewpoint, including slow slips. Therefore, questions such as what are the characteristics of slow-slip phenomena, how it differs from the standard high-speed rupture of a main shock, what conditions cause them to occur, *etc*, need to be answered.

In this year's project, we have addressed this issue from the statistical-physics viewpoint by employing the 1D and 2D BK models obeying the rate-and-state dependent friction (RSF) law. We successfully reproduce a variety of seismic phenomena, including high-speed rupture of main shocks, its precursory nucleation processes, afterslips, and silent earthquakes, by varying only a few fundamental parameters of the model. The results on the 1D model was published in [2]. Regarding the occurrence of slow-slip phenomena, the relative magnitude of the frictional parameters a and b characterizing the RSF law turns out to be crucial.

References

[1] For review, see, H. Kawamura, T. Hatano, N. Kato, S. Biswas and B.K. Chakrabarti, Rev. Mod. Phys. 84, 839-884 (2012).

[2] H. Kawamura, M. Yamamoto and Y. Ueda, J. Phys. Soc. Jpn. 87, 053001-(1-4) (2018).

Molecular Dynamics Simulation of Complex Fluids

Yuta ASANO, Hiroshi WATANABE, and Hiroshi NOGUCHI
Institute for Solid State Physics, University of Tokyo
Kashiwa-no-ha, Kashiwa, Chiba 277-8581

The addition of an extremely small amount of long-chain polymer into a Newtonian fluid causes a dramatic change in the fluid behavior. Turbulent drag reduction [1] and the change in vortex structure in Kármán vortex street [2] are the major examples of these phenomena. Because almost all industrial flows are accompanied by the turbulence and vortices, polymer effects on fluids have been intensively studied for energy saving, environmental protection, and so forth. Despite the dramatic change of the flow behavior by adding polymers is an important issue in engineering fields, the detailed mechanism remains unclear due to the difficulty of the polymer rheology in flow. So far, it is considered that the relation between the polymer and the vortical motion plays a key role in the change in fluid behavior. Therefore, in order to elucidate the mechanism of the phenomena, it is necessary to investigate polymer behavior in the vortex as directly as possible.

In the present study, we investigated the polymer effects on the Kármán vortex behind a circular cylinder by a molecular dynamics (MD) simulation using ISSP supercomputer [3]. Here, two-dimensional MD simulations were carried out to elucidate the polymer effects on the Kármán vortex street. A solvent particle and polymer molecule are modeled by Weeks–Chandler–Andersen (WCA) particle [4] and Kremer–Grest model [5], respectively. The circular cylinder is modeled by a set of WCA particles whose positions are fixed. The simulations were performed for the reference liquid (no polymer) and the polymer solutions. As for the polymer solutions, short- and long-polymer chains are considered. The number of the segment of the short- and long-polymer are $N_{\mathrm{s}} = 10$ and 100, respectively. The polymer concentrations are $\phi = 0.024$, 0.043, 0.085, and 0.107 in each type of polymer. These concentrations are less than the overlap concentration.

The characteristics of the vortex shedding are distinctly different for short and long polymer solutions (see Fig. 1). The characteristics of the short-polymer solution and the reference liquid are almost identical. On the other hand, the long-polymer solution exhibits two different behaviors from the reference liquid. One is a reduction in the vortex shedding frequency, and the other is a broadening of the lift coefficient spectrum. These facts are consistent with the experiments [6]. Because the gyration radius and the orientational order of the long-polymer are highly inhomogeneous in wake region, we conclude that the extensional property of the polymer plays an important role in suppression of the vortex shedding.

References

[1] G. E. Gadd: Nature **206** (1965) 463.

[2] G. E. Gadd: Nature **211** (1966) 169.

[3] Y. Asano, H. Watanabe, and H. Noguchi: J. Chem. Phys. **148** (2018) 144901.

[4] J. D. Weeks, D. Chandler, and H. C. Andersen: J. Chem. Phys. **54** (1971) 5237.

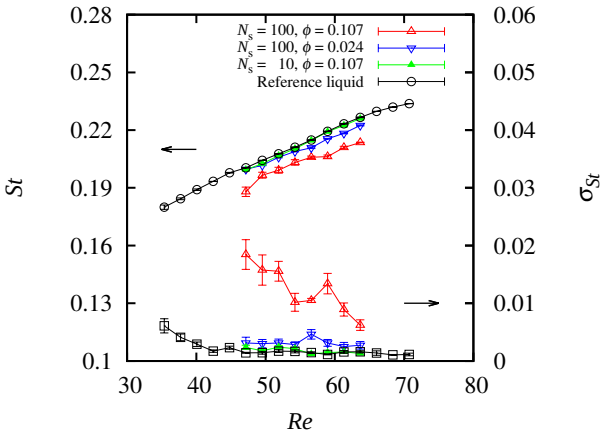

Figure 1: The Strouhal number St and the spectral width σ_{St} as a function of the Reynolds number Re.

[5] K. Kremer and G. S. Grest: J. Chem. Phys. **92** (1990) 5057.

[6] J. R. Cressman, Q. Bailey, and W. I. Goldburg: Phys. Fluids **13** (2001) 867.

Bilayer sheet protrusions and vesicle budding induced by chemical reactions

Koh M. NAKAGAWA and Hiroshi NOGUCHI
Institute for Solid State Physics, University of Tokyo, Kashiwa, Chiba 277-8581

In living cells, membrane composition continually changes by lipid metabolism. However, the effects of non-constant membrane composition on shape transformations of cells are not understood so well. We have studied membrane shape transformations under hydrolysis and condensation reactions using dissipative particle dynamics simulation [1]. The hydrolysis and condensation reactions result in the formation and dissociation of amphiphilic molecules, respectively as shown in Fig. 1. Because the dissociated hydrophilic and hydrophobic molecules are typically dissolved in surrounding fluids and embedded in the bilayer, we refer to them as the hydrophilic solute (HS) and embedded oil (EO), respectively.

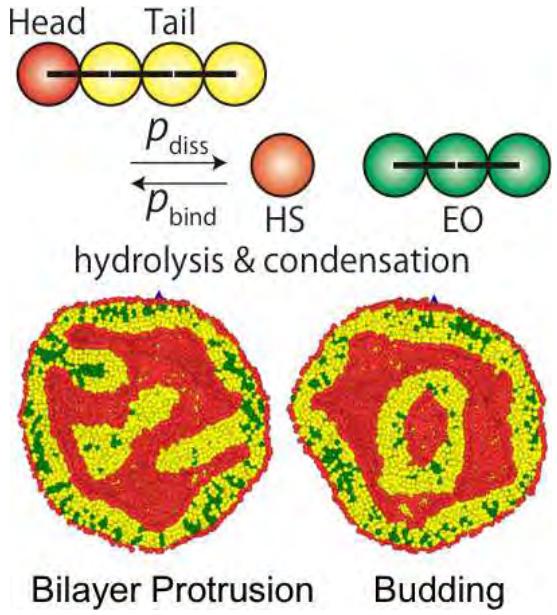

Figure 1: Top: Schematic picture of hydrolysis and condensation reactions. Bottom: Snapshots of bilayer sheet protrusions (BP) and budding of vesicles at a low reduced volume.

Asymmetric reactions between the inner and outer leaflets of a vesicle can transport amphiphilic molecules between the leaflets via EO diffusion. We consider high HS density in the inner fluid of the vesicle and investigate how the transport into the inner leaflet changes the membrane shapes. We found that the resulting area difference between the two leaflets induces bilayer sheet protrusion (BP) and budding at low reduced volumes of the vesicles (see the snapshots in Fig. 1), whereas BP only occurs at high reduced volumes.

The probabilities of these two types of transformations depend on the shear viscosity of the surrounding fluids compared to the membrane as well as the reaction rates. For a high surrounding fluid viscosity, BP formation occurs at high reaction rates. but for a low viscosity, budding always occurs before BP formation. A higher surrounding fluid viscosity leads to more BP formation. Thus, the viscosity of the surrounding fluids affects budding more than it does BP formation, while the viscosity in the membrane affects BP formation more. The inhomogeneous spatial distribution of the hydrophobic reaction products forms the nuclei of BP formation, and faster diffusion of the products enhances BP formation. Our results revealed that adjustment of the viscosity is important to control membrane shape transformations.

References

[1] K. M. Nakagawa and H. Noguchi: Soft Matter **14**, 1397 (2018).

Dynamical properties of effective models for α-$RuCl_3$

Takafumi SUZUKI
Graduate school of Engineering, University of Hyogo
Shosha, Himeji, Hyogo, 671-2280

In this project, we have studied dynamical properties of effective models for α-$RuCl_3$ [1, 2]. A honeycomb lattice magnet α-$RuCl_3$ is considered to be a candidate material for the Kitaev spin liquid because the strong Kitaev-type anisotropic interaction works between Ru^{3+} ions thanks to the edge-shared $RuCl_6$ octahedra. Many effective models for this compound have been proposed so far. However, the discussions for the proper model for this compound have not been converged yet.

In this study, we have focused on four effective models [3, 4, 5, 6]. Three of them have been proposed by the ab-initio calculations[3, 4, 5] and the other has been obtained by the ab-initio-guided method [6]. For these four models, we have calculated dynamical spin structure factors and thermal properties by using the numerical exact diagonalization method. From the results obtained from these four effective models, we have found that the four models fail to explain heat-capacity measurements whereas two of the four models succeed in explaining inelastic-neutron-scattering experiments. In the four models, the heat capacity shows a prominent peak at a high temperature when the temperature decreases. However, the peak temperature in the heat capacity is too low in comparison with that observed in the experiments.

In order to explain both the inelastic-neutron-scattering and heat-capacity experiments, we have proposed an effective model that includes the strong ferromagnetic Kitaev coupling. From the numerical calculations, we have confirmed that our model quantitatively reproduces both inelastic-neutron-scattering experiments and heat-capacity experiments. To further examine the adequacy of our model, we have calculated the field dependence of the polarized terahertz spectra. The obtained results have succeeded in explaining the experimental results: the spin-gapped excitation survives up to the critical field where the zigzag magnetic order disappears and the spin gap increases almost linearly above the critical field.

Based on these numerical results, we argue that, rather than the strong Kitaev interactions, the interactions such as off-diagonal interactions and weak Heisenberg interactions between nearest-neighbor pairs are important to explain the low-energy magnetic excitation in α-$RuCl_3$.

References

[1] T. Suzuki and S. Suga, Phys. Rev. B in press.

[2] T. Suzuki and S. Suga, J. Phys.: Conf. Sers, **969**, 012123 (2017).

[3] H.-S. Kim and H.-Y. Kee, Phys. Rev. B **93**, 155143 (2016).

[4] S. M. Winter, Y. Li, H. O. Jeschke, and R. Valenti, Phys. Rev. B **93**, 214431 (2016).

[5] R. Yadav, N. A. Bogdanov, V. M. Katukuri, S. Nishimoto, J. van den Brink, and L. Hozoi, Sci. Rep. **6**, 37925 (2016).

[6] S. M. Winter, K. Riedl, A. Honecker, and R. Valenti, Nature Comm. **8**, 1152 (2017).

Novel phases in classical and quantum frustrated spin systems

Tsuyoshi OKUBO
Department of Physics, The University of Tokyo
7-3-1 Hongo, Bunkyo-ku, Tokyo 133-0033

Anisotropic interactions due to the strong spin-orbit interaction have attracted recent interest. In Na_2IrO_3 and α-$RuCl_3$, effective spins $J_{\rm eff} = 1/2$ form the two-dimensional honeycomb lattice and they interact through the Kitaev interaction. The Kitaev interaction is an anisotropic interaction $S_i^\gamma S_j^\gamma$ with easy axis γ depending on the direction of the interacting bonds. In the case of $S = 1/2$ quantum spins with the Kitaev interaction only (Kitaev model), its ground state is proved to be a quantum spin liquid state [1]. In real compounds other interactions such as the isotropic Heisenberg interaction, the further neighbor interactions, and the off-diagonal interactions exist in addition to the Kitaev interaction [2–4]. These interaction might stabilize magnetically ordered states.

In order to clarify the effect of additional interactions, we have investigated two kinds of systems, *ab initio* Hamiltonian of Na_2IrO_3 [4,5] and Kitaev-Gamma model [6,7], by means of an infinite Tensor Product State (iTPS) method. In this iTPS method, we represent the ground state wave-function of the infinite system as a two-dimensional network of tensors. By optimizing each tensor so as to minimize the energy, we obtain wave-functions close to the ground state.

Based on iTPS calculations, we showed that the ground state of Na_2IrO_3 calculated from the *ab initio* Hamiltonian was the zigzag state [5]. The zigzag state is consistent with experimental observations, which could not be explained from the simple Kitaev-Heisenberg model. We also showed that in the parameter space away from the *ab initio* value of Na_2IrO_3, variety of magnetically ordered state were stabilized. It suggests that rich magnetic structures may appear in A_2IrO_3.

As an effective model for α-$RuCl_3$, we also investigated the ground state phase diagram of Kitaev-Gamma model where an off-diagonal interaction, the gamma term, exists in addition to the Kitaev interaction [6, 7]. The Hamiltonian of the model is given by

$$\mathcal{H} = \sum_{\gamma \in x,y,z} \mathcal{H}_\gamma, \tag{1}$$

and on z-bond,

$$\mathcal{H}_z = \sum_{\langle i,j \rangle_z} [K S_i^z S_j^z + \Gamma (S_i^x S_j^y + S_i^y S_j^x)]. \tag{2}$$

Similar to the Kitaev model, the classical ground state of the pure gamma model, where only the gamma term exists, is macroscopically degenerated and thus, one can expect possible quantum spin liquid state induced by quantum fluctuations. Actually, based on the exact diagonalization (ED) and the infinite density matrix renormalization group (iDMRG), previous studies indicated that the Kitaev spin liquid survives wide regions when the gamma term was included and it was adiabatically connected to the ground state of the pure gamma model [6, 7]. In the iTPS calculations, however, we found that magnetically ordered states had lowest energies than the Kitaev spin liquid state in wide regions, and the Kitaev

spin liquid was stabilized at only the vicinity of the pure Kitaev model. The discrepancy from the previous studies might be explained by the effect of anisotropy, which was included in the previous calculations explicitly (ED) or implicitly due to the cylindrical geometry (iDMRG).

References

[1] A. Kitaev: Ann. Phys. **321** (2006) 2.

[2] G. Jackeli, and G. Khaliullin: Phys. Rev. Lett. **102** (2009) 017205.

[3] J. Chaloupka, G. Jackeli, and G. Khaliullin: Phys. Rev. Lett. **105** (2010) 027204.

[4] Y. Yamaji, Y. Nomura, M. Kurita, R. Arita, and M. Imada: Phys. Rev. Lett. **113** (2014) 107201.

[5] T. Okubo, K. Shinjo, Y. Yamaji, N. Kawashima, S. Sota, T. Tohyama, and M. Imada: Phys. Rev. B **96** (2017) 054434.

[6] A. Catuneanu, Y. Yamaji, G. Wachtel, H.-Y. Kee, and Y. B. Kim: arXiv:1701.07837.

[7] M. Gohlke, G. Wachtel, Y. Yamaji, F. Pollmann, and Y. B. Kim: Phys. Rev. B **97** (2018) 075126.

Randomness Effects on Quantum Spin Systems Coupled to Lattice Degrees of Freedom

Chitoshi YASUDA and Shouta MIYARA
Department of Physics and Earth Sciences, Faculty of Science, University of the Ryukyus, Nishihara, Okinawa 903-0213, Japan

Since the inorganic compound $CuGeO_3$ was synthesized, randomness effects of the spin-Peierls (SP) system have attracted considerable attention. When nonmagnetic impurities are doped in the SP compound, an antiferromagnetic long-range order (AFLRO) is induced. The mechanism is understood by a cluster of magnetic moments induced near an impurity, which is called an 'effective spin'. By substituting nonmagnetic atoms for magnetic atoms, effective spins are induced near the nonmagnetic atoms. Since the effective spins interact through a sea of spin-singlet pairs, the AFLRO is induced [1]. However, Cu nuclear quadrupole resonance (NQR) data contradictory to this interpretation was reported for $CuGe_{1-x}Si_xO_3$: the effective spins are not induced near diluted sites [2]. We need to take the lattice degrees of freedom into account in order to investigate positions of the effective spins.

In this project, we investigated the appearance of the AFLRO induced by site dilution in an $S = 1/2$ two-dimensional antiferromagnetic Heisenberg model composed by the intrachain interaction J coupled to the lattice distortion and the interchain interaction J'. The method is the quantum Monte Carlo (QMC) simulation with the continuous-imaginary-time loop algorithm [3]. Since this QMC simulation is suitable to parallel computing, we mainly performed parallel computing with the Message Passing Interface.

The staggered magnetizations M_s at zero temperature were evaluated by assuming that the effective spins arise away from diluted sites for $J'/J = 0.3$ and 0.2. This assumption is necessary to recreate the NQR result for $CuGe_{1-x}Si_xO_3$. The value of M_s for system size $N = 64 \times 64$ converges a constant value at the temperature $T/J = 0.0001$. Since the dilution-induced AFLRO for J' calculated is a physical phenomenon that occurs at a very small energy scale, we have needed the large scale numerical simulations.

We found that the AFLRO is induced by site dilution even when effective spins arise away from diluted sites. The values of M_s, however, become smaller than those in bond-alternated systems with the same parameters, where effective spins are induced near diluted sites. The decrease in M_s indicates that the AFLRO is difficult to induce in the system with the lattice degrees of freedom. By calculating the distribution of the correlation function, the dimerization order parameter, and the local-field susceptibility, we concluded that the disturbance of the singlet-pair sea and the weakening of the effective spin are the origins of the decrease in M_s. On the other hand, the width of the effective spin in the system with the lattice degrees of freedom is the similar to that in the bond-alternated system. It is expected that the locality of the effective spin is important for the appearance of the AFLRO by dilution.

References

[1] C. Yasuda, *et al.*: Phys. Rev. B **64**, 092405 (2001); J. Phys. Soc. Jpn. **75**, 124704 (2006).

[2] J. Kikuchi, *et al.*: Phys. Rev. Lett. **88**, 037603 (2002).

[3] S. Todo and K. Kato, Phys. Rev. Lett. **87**, 047203 (2001).

Excitation dynamics of two-dimensional quantum spin systems

Akiko MASAKI-KATO

RIKEN Center for Computational Science,

Wako, Saitama 351-0198

The ground state property of two-dimensional quantum lattice models such as two-dimensional quantum Heisenberg spin systems has been theoretically understood rapidly in recent years. On the other hand, excitation dynamics are not well understood even in simple models such as S=1/2 square lattice antiferromagnetic Heisenberg models (SLAHM). For example, although the staggered order in which the adjacent spins are antiparallel each other is realized, the staggered magnetic moment is 40% smaller than that expected in the classical Néel order due to the quantum fluctuation. How this giant quantum effect is reflected in the ground state and how it appears in the excitation dynamics have been discussed as an essential problem of quantum spin systems since it was discovered in high-T_c cuprates [1]. As consensus of the experiment results until recent years, it can be mentioned that the magnon excitation spectrum of the wave number $\mathbf{k} = (\pi, 0)$ becomes much broader than that of $\mathbf{k} = (\pi/2, \pi/2)$, and the peak position also shifts to the lower energy side [2,3]. These features are observed not only with high-T_c cuprates but also with other materials. That is, experimental results suggest that this is the universal nature of S=1/2 SLAHM without being attributed to specific properties of each material. According to the linear spin-wave theory, the magnon excitation energy at these two wavenumbers is the same and it is expected to behave similarly. Furthermore, the incoherent excitation observed at these wave numbers can not be explained by the linear spin wave theory. Recent neutron scattering experiments with metal-organic compound Cu(DCOO)2・4D2O (CFTD) have argued that the source of incoherent excitation at wave number $\mathbf{k} = (\pi, 0)$ is spinon excitation. However, no effective theoretical interpretation has been obtained so far.

One of the reasons why the excitation dynamics of low-dimensional quantum lattice system is poorly understood is that it is not easy to calculate the dynamic physical quantity even when the numerical calculation method has dramatically advanced recently.

The worldline QMC method[4] based on Feynman's path integral representation is one of the most powerful tool that can be obtained an exact solution within the range of the statistical error with respect to the equilibrium state of the quantum lattice system free from the negative

sign problem at the finite temperature. With this method it is possible to treat huge lattice systems of thousands to millions sites. However conventional spectrum estimation methods such as the maximum entropy method are not sufficiently accurate and it is difficult to quantitatively discuss line shapes of unexplained excitation spectra because bias such as prior knowledge and artificial tuning parameters work strongly. Recently, a new numerical analytic continuation method which is the hybrid of the stochastic optimization method and consistent constraints (SOCC) method proposed by Mishchenko *et al*, who is a co-worker of us, have been succeeded [5]. SOCC method is unbiased method for estimating the spectrum function with statistical error-bars. With this method, it was possible to evaluate delta function like peaks and widths of peaks for which MEM is not good.

We calculated on the excitation spectra of S=1/2 SLAHM which is an effective model of CFTD at two distinctive wavenumbers **k** using QMC+SOCC method. To obtain imaginary time correlations with ultra-high precision by QMC calculation, we executed huge-scale parallel computations using supercomputer in *ISSP*. I have obtained results that quantitatively and precisely coincide with the neutron scattering experiment result for CFTD. A remarkable feature is that the sharp peak at $\mathbf{k} = (\pi/2, \pi/2)$ suggests the existence of symmetric well-defined magnon excitation, while the peak at $\mathbf{k} = (\pi, 0)$ is broad and asymmetric. As a result of investigating the temperature dependence, the delta function like peak grow at $\mathbf{k} = (\pi/2, \pi/2)$, whereas at $\mathbf{k} = (\pi, 0)$, no change was observed when the temperature was sufficiently low. It indicates that the excitation of this model has the incoherent property [6].

References

[1] N. B. Christensen, et al., Proc. Nati. Acad. Sci. USA (2007) and so on.

[2] B. Dalla Piazza *et al*., Nat. Phys. **11**, 62 (2015)

[3] N. S. Headings *et al*., Phys. Rev. Lett. 105, 247001 (2010) and so on.

[4] A. Masaki-Kato *et al*., Phys. Rev. Lett. 112, 140603 (2014); dsqss [https://github.com/qmc/dsqss]; and so on.

[5] O. Goulko *et al*., Phys. Rev. B 95, 014102 (2017).

[6] Akiko Masaki-Kato *et al*., submitted (2018).

Finite-Sized effects and hysteresis in chiral helimagnets

Yusuke Kato
Department of Basic Science, The University of Tokyo
Komaba 3-8-1, Meguro-ku, Tokyo 153-8902

We have studied two subjects of mono-axial chiral helimagnets using class C.
(i)We examined the properties of isolated chiral soliton as constituent of chiral soliton lattice in mono-axial chiral helimagnets at finite temperatures with use of three-dimensional lattice model[1]. In the plane of magnetic field and temperature, we numerically found the instability line of isolated chiral soliton, the region where the interaction between two solitons is repulsive/attractive and the region where the isolated chiral soliton can not exist. We found that the three regions correspond to the continuous phase transition of nucleation-type (repulsive soliton region), the discontinuous phase transition (attractive soliton region) and the continous phase transition of instability-type (no soliton region). This coincidence between the properties of soliton and the type of phase transition implies crucial role of chiral soliton in the mechanism for the phase transition. In this study, we used the supercomputers to examine the properties of isolated soliton and the types of phase transition in the mean-field theory.
(ii) We argue that the surface barrier is an underlying mechanism for large hysteresis observed in magneto-resistance (MR) measurement for micrometer-sized samples of mono-axial chiral magnet CrNbS[2]. The hysteresis of MR in those specimens consists of conspicuous jump at the field $H_{\rm b}$ in decreasing field process and relatively gradual change in field increasing process. We attribute the large jump in the decreasing field process to the disappearance of the surface barrier. This interpretation is justified through agreement between the experimental results at 10K (which is much lower than the transition temperature $T_{\rm c} \sim 130$K in zero field) and theoretical result of a universal ratio $H_{\rm b}/H_{\rm c} = 4/\pi^2 \sim 0.4$ (with thermodynamic critical field $H_{\rm c}$) at zero temperature in the configuration of the least demagnetization effect. We discuss that surface barrier is regarded as a common property shared among various systems (superconductors, chiral magnets and chiral liquid crystals) with nucleation type of continuous phase transition. In early state of this study, we used the supercomputers to examine the metastable properties of chiral magnet in the mean-field type relaxation method. We also used it to discuss the experimental results on hysteretic properties in magnetization-curve in this material in [3]
A doctor degree has been given on the basis of the two studies[4].

References

[1] M. Shinozaki, S. Hoshino, Y. Masaki, A. O. Leonov, J. Kishine and Y. Kato: submitted to JPSJ.

[2] M. Shinozaki, Y. Masaki, R. Aoki, Y. Togawa and Y. Kato: submitted to PRB.

[3] M. Mito, et al, PRB **97**, 024408 (2018).

[4] M. Shinozaki, Doctor Thesis (2017) The University of Tokyo.

Nonequilibrium relaxation analysis for critical properties of the antiferromagnetic triangular Heisenberg model

Y. Ozeki and R. Tobise

Graduate School of Informatics and Engineering, The University of Electro-Communications

We investigate the phase transition and critical properties for the antiferromagnetic (AF) triangular Heisenberg model by means of the nonequilibrium relaxation (NER) method [1]. While it has been well-known that there is no long-range order with continuous symmetry-breaking in 2D continuous spin systems, a topological phase transition has been explored in this model and discussed for a long time [2]. Previously, we analyzed the relaxation of the z-component for the chiral order parameter, $\kappa(t)$, from a 120° structure in the XY-plane, and estimated the precise transition temperature as $T_{\rm KT} = 0.2767$ using the NER method with recently improved dynamical scaling analysis [3], where we assumed the transition type as the Kosterlitz-Thouless (KT) one.

In the present study, we estimate the static and dynamical critical exponents z and η, where just these two critical exponents exist independently in the KT transition. Together with the relaxation of order parameter, the NER of fluctuation $f_{\kappa\kappa}(t) \equiv N\left[\langle\kappa(t)^2\rangle/\langle\kappa(t)\rangle^2 - 1\right]$. is used for the analysis. The asymptotic forms for these dynamical functions are expected as $\kappa \sim t^{-\eta/2z}$ and $f_{\kappa\kappa} \sim t^{2/z}$, which provide the estimations for z and η. Calculations are carried out for 1001×1002 triangular lattice with a skew boundary condition at the transition temperature obtained above up to an observation time of 2000 Monte Carlo steps (MCSs). About 3×10^6 samples are taken for statistical averaging. Making numerical derivatives for $f_{\kappa\kappa}(t)$ and $\kappa(t)$, we evaluate the functions $z(t)$ and $\eta(t)$, which converge to $z = 1.90$ and $\eta = 0.370$ asymptotically, as shown in Figs. 1-2. The present estimations suggest that the static exponent η is much deviated from those for the FM-XY model $\eta = 0.25$ and for the triangular AF-XY model $\eta \sim 0.31$, while the dynamical one z are almost the same with those model $z \sim 2$. This indicates that the universality class of the triangular AF Heisenberg model would be distinct with that of the triangular AF XY model. Farther investigations are necessary to settle these problems.

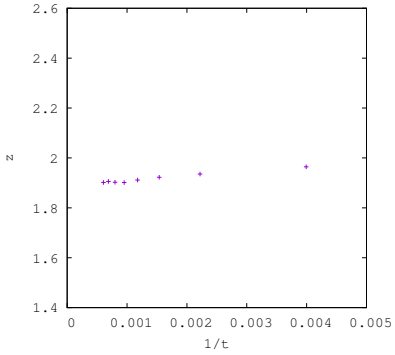

Figure 1: Local exponent $z(t)$.

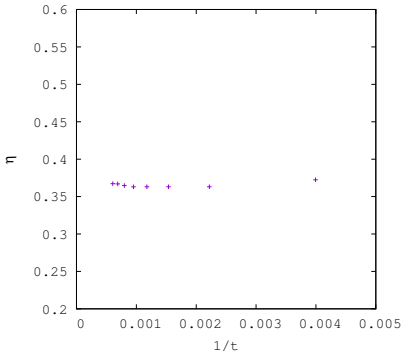

Figure 2: Local exponent $\eta(t)$

References

[1] Y. Ozeki and N. Ito, Phys. Rev. B**68** 054414 (2003); Y. Ozeki and N. Ito, J. Phys.: Math. Theor. **40** R149 (2007).

[2] H. Kawamura and S. Miyashita, J. Phys. Soc. Jpn. **53** 4138 (1984); H. Kawamura, et. al., J. Phys. Soc. Jpn. **79** 023701 (2010).

[3] Y. Echinaka and Y. Ozeki, Phys. Rev. E**94** 043312 (2016).

Molecular dynamics simulations to reveal aggregation mechanism of amyloid-β peptides

Satoru G. Itoh and Hisashi Okumura

Research Center for Computational Science,

Institute for Molecular Science, Okazaki, Aichi 444-8585

Protein aggregates such as oligomers and amyloid fibril, which is a fibrous aggregate of proteins, are known to be associated with more than 40 human neurodegenerative diseases (Fig. 1). For example, Alzheimer's disease is related to amyloid-β (Aβ) peptides, and Parkinson's disease is caused by α-synuclein. To overcome these diseases, it is essential to understand the formation mechanism of protein oligomers and amyloid fibrils. For this purpose, we have been performed several molecular dynamics (MD) simulations of oligomers and amyloid fibrils: We have revealed (a) the aggregation mechanism of Aβ fragments [1,2], (b) structural difference between two ends of the Aβ amyloid fibril [3], and (c) disruption process of Aβ amyloid fibril by supersonic wave [4]. As for the aggregation of Aβ, we have dealt with relatively simple systems such as Aβ fragments (not full length) in pure solvent so far, but we tried more realistic systems including the full length Aβ peptides in this fiscal year.

Aβ has two types, Aβ 40 (40 residues) and Aβ 42 (42 residues), which differ in the number of amino acids in the C-terminal region. It is known that the oligomerization and amyloid formation speed of Aβ42 are faster than those of Aβ40, but it is not clear why such a difference occurs. Initial formation of amyloid fibrils in the brains of Alzheimer's disease patients is thought to be caused by aggregation of Aβ42 rather than Aβ40. Understanding the difference in aggregation mechanism of Aβ40 and Aβ42 is also essential for the development of Alzheimer's disease treatment. We performed a Hamiltonian replica-permutation MD simulation, the method of which was developed by our group, on each of the Aβ 40 dimer and Aβ 42 dimer systems and examined the effect of the C-terminal region on oligomer formation. As a result, we found that Aβ42 forms intermolecular β-sheet more than Aβ40. We also found that this difference is caused by the fact that Aβ42 tends to form a β-hairpin more easily and a stable intermolecular β-sheet is formed between this β-hairpin and another Aβ42.

We plan to increase the statistic by performing the simulations further and investigate the details of the dimerization mechanism of Aβ40 and Aβ42 and its differences.

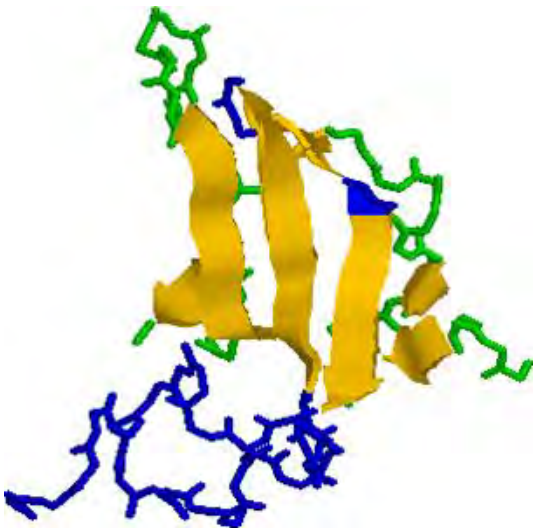

Fig. 1: Aggregated Aβ peptides of Aβ peptides.

References

[1] S. G. Itoh and H. Okumura: J. Phys. Chem. B **118** (2014) 11428.

[2] S. G. Itoh and H. Okumura: J. Comput. Chem. **120** (2016) 6555.

[3] H. Okumura and S. G. Itoh: Sci. Rep. **6** (2016) 28422.

[4] H. Okumura and S. G. Itoh: J. Am. Chem. Soc. **136** (2014) 10549.

Elucidation of softness hidden in glass-forming liquids

Kang KIM[1] and Hayato SHIBA[2]
[1]*Division of Chemical Engineering, Graduate School of Engineering Science, Osaka University, Toyonaka, Osaka 560-8531*
[2]*Institute for Materials Research, Tohoku University 2-1-1, Katahira, Aoba-ku, Sendai 980-8577*

We are investigating the universal feature for emergence of softness in glass-forming liquids. One of our recent findings is long-wavelength fluctuation in two-dimensional (2D) glassy liquids forming originating in the same mechanism as Mermin-Wagner theorem. In this year, we have performed several extended analyses of 2D fluctuations. One is the normal mode analysis of 2D and 3D supercooled liquid for Lennard-Jones binary mixtures with Kob-Andersen parameters, so that we can establish the Debye asymptote, in a more quantitative manner than the estimation using the velocity autocorrelation function performed in our previous publication [1]. We have especially working on solution of sparse Hessian matrix, with more than 10^{13} matrix elements, to elucidate its low-frequency vibration behaviors. In addition, we began to investigate the response of 2D liquids to the external field, owing to the mechanical softness that is inherent to the 2D glassy systems. The details are under preparation for our forthcoming publication [2].

In addition, we have developed to new methodologies to clarify the unified mechanism for emergence of fragility in various types of glassy liquids. We are developing classical molecular models with tunable fragilities, in order to investigate its correlation with the viscous relaxation, diffusion, and energy transport. Up to now, we clarified that the diffusion is associated with breakage of hydrogens and stress relaxation, and emergence of rigidity is decoupled from these, by investigating the breakdown mechanism of Stokes-Einstein relaxation in water systems [3]. Its relation to anomalous properties of glasses, including Boson peak and hidden structural ordering, is now under investigation.

References

[1] H. Shiba, Y. Yamada, T. Kawasaki, and K. Kim: Phys. Rev. Lett. **117**, 245701 (2016).

[2] H. Shiba, T. Kawasaki, and K. Kim: in preparation.

[3] T. Kawasaki and K. Kim: Sci. Adv **3**, e1700399 (2017).

The effect of bond-randomness on the quantum magnetisms in low dimension

TOKURO SHIMOKAWA[1] and HIKARU KAWAMURA[2]
[1]*Okinawa Institute of Science and Technology Graduate University, Onna, Okinawa, 904-0495, Japan*
[2]*Department of Earth and Space Science, Graduate School of Science, Osaka University, Toyonaka, Osaka 560-0043, Japan*

S=1/2 antiferromagnetic Heisenberg model on the kagome lattice with nearest-neighbor interaction is well known as a candidate of the possible realization of a quantum spin liquid (QSL) state. In spite of the tremendous efforts, the true natures still remain unclear.

We investigate the effect of the bond-randomness to the thermal properties of the S=1/2 kagome antiferromagnet by means of Hams-de Raedt (thermal pure quantum state) method [1, 2, 3]. This method enables us to compute exact finite-temperature physical quantities for larger system sizes than those treated by the conventional exact diagonalization method and the negative sign problem does not occur. We treat here up to 36-site kagome cluster which has full symmetry of the infinite kagome lattice under periodic boundary condition.

In the 36-site cluster, we identified before the additional 3rd and 4th peaks in the low-temperature specific heat and found that the 3rd peak is associated with a crossover phenomenon occurring between the QSL states with distinct magnetic short-ranged orders (SROs). We investigate here the effect of the bond-randomness to the crossover phenomenon observed in the regular kagome-lattice antiferromagnet. We find that the low-temperature specific heat shows T-linear behavior in the strong randomness case even in the 36-site cluster as reported in smaller system sizes by means of the exact diagonalization method [4]. Almost no size dependence of the T-linear specific heat is also confirmed from 12 to 36-site clusters in the strong randomness case.

Our results were obtained by using CPU node of system B. Our MC code is executed in parallel by using OpenMP technique.

References

[1] M. Imada and M. Takahashi,J. Phys. Soc. Jpn. **55**, 3354 (1986).

[2] A. Hams and H. De Raedt, Phys. Rev. E **62**, 4365 (2000).

[3] S. Sugiura and A. Shimizu, Phys. Rev. Lett. **111**, 010401 (2013).

[4] H. Kawamura, K. Watanabe, and T. Shimokawa, J. Phys. Soc. Jpn. **83**, 103704 (2014)

Multiple-Q states of the frustrated Heisenberg model on the honeycomb lattice

TOKURO SHIMOKAWA[1] and HIKARU KAWAMURA[2]
[1]*Okinawa Institute of Science and Technology Graduate University, Onna, Okinawa, 904-0495, Japan*
[2]*Department of Earth and Space Science, Graduate School of Science, Osaka University, Toyonaka, Osaka 560-0043, Japan*

Motivated by recent theoretical study by Okubo *et al* [1] of the possible realization of the triple-q skyrmion-lattice state in the J_1-J_2 or J_1-J_3 triangular-lattice Heisenberg model, we here investigate the ordering properties in the J_1-J_2 classical honeycomb-lattice Heisenberg model under magnetic field.

The Hamiltonian of the honeycomb-lattice Heisenberg model is given by,

$$\begin{aligned}\mathcal{H} = &- J_1 \sum_{\langle i,j \rangle} \mathbf{S}_i \cdot \mathbf{S}_j - J_2 \sum_{\langle\langle i,j \rangle\rangle} \mathbf{S}_i \cdot \mathbf{S}_j \\ &- H \sum_i S_i^z, \end{aligned} \tag{1}$$

where $\mathbf{S}_i = (S_i^x, S_i^y, S_i^z)$ is the classical Heisenberg spin with the fixed length of $|\mathbf{S}_i| = 1$ located at the i-th site on the honeycomb lattice, $J_1 < 0$ and $J_2 < 0$ represent the antiferromagnetic NN and NNN interactions, while the $\sum_{\langle i,j \rangle}$ and $\sum_{\langle\langle i,j \rangle\rangle}$ are taken over the NN and NNN pairs J_1 and J_2, respectively.

This model has been known that the ground state of the model in zero field exhibits, for $J_2/J_1 > 1/6$, a single-q helical order with an incommensurate wavevector with an infinite ring-like degeneracy in the q-space, while, for $J_2/J_1 \leq 1/6$, the standard two-sublattice antiferromagnetic order [2]. Finite-temperature ordering properties in zero field have also been investigated by Okumura *et al* [3], and then only a single-q helical ordered state has been found as an quasi-long ranged ordered state. The in-field ordering process of the present honeycomb-lattice model is a remaining big issue since the interplay between macroscopic degeneracy in the ground state and fluctuations might lead to a intriguing behavior.

We focus here to the region $1/6 < J_2/J_1 < 0.2$ in which the incommensurability is very strong. We succeed to find an exotic multiple-q state by means of extensive monte carlo (MC) method. The corresponding real-space spin texture seems to be like a "water ripple", therefore, we call the new multiple-q state as "ripple state". We also find appearance of the vector chiral domain in the new state and the relationship to the spin-liquid compound, $Bi_3Mn_4O_{12}(NO_3)$ is discussed. [4]

Our results were obtained by using CPU node of system B. Our MC code is executed in parallel by using both OpenMP and MPI techniques.

References

[1] T. Okubo, S. Chung, and H. Kawamura, Phys. Rev. Lett. **108**, 017206 (2012).

[2] S. Katsura, T. Ide, and T. Morita: J. Stat. Phys. **42**, 381 (1986).

[3] S. Okumura, H. Kawamura, T. Okubo, and Y. Motome, J. Phys. Soc. Jpn. **79**, 114705 (2010).

[4] T. Shimokawa, and H. Kawamura, to be submitted.

Numerical Diagonalization Study on the Spin Gap of Frustrated Systems

T. SAKAI[1,2,3], H. NAKANO[1,2], Y. Hasegawa[1,2], T. SHIMOKAWA[4], and A. Shimada[5]
[1]*Graduate School of Material Science, University of Hyogo, Kouto, Kamigori, Hyogo 678-1297, Japan*
[2]*Research Center for New Functional Materials, University of Hyogo, Kouto, Kamigori, Hyogo 678-1297, Japan*
[3]*Synchrotron Radiation Research Center, Kansai Photon Science Institute, Quantum Beam Science Research Directorate, National Institute for Quantum and Radiological Science and Technology (QST) SPring-8, Kouto, Sayo, Hyogo 679-5148, Japan*
[4]*Okinawa Institute of Science and Technology Graduate University, Okinawa, Japan*
[5]*Graduate School of Science, Kyoto University, Kyoto 606-8502, Japan*

The S=1/2 kagome-lattice antiferromagnet is one of interesting frustrated quantum spin systems. The systems exhibit the quantum spin fluid behavior, which was proposed as an origin of the high-Tc superconductivity. The spin gap is an important physical quantity to characterize the spin fluid behavior. Whether the S=1/2 kagome-lattice antiferromagnet is gapless or has a finite spin gap, is still unsolved issue. Because any recently developped numerical calculation methods are not enough to determine it in the thermodynamic limit. Our large-scale numerical diazonalization up to 42-spin clusters and a finite-size scaling analysis indicated that the S=1/2 kagome-lattice antiferromagnet is gapless in the thremodynamic limit[1, 2, 3]. It is consistent with the U(1) Dirac spin liquid theory of the kagome-lattice antiferromagnet[4, 5]. On the other hand, the density matrix renormalization group calculations supported the gapped Z2 topological spin liquid theory[yan,hotta]. We propose one of better methods to determine whether the spin excitation is gapless or gapped, based on the finite-size scaling analysis of the spin susceptibility calculated by the numerical diagonalization. The present work indicates that the kagome-lattice antiferromagnet is gapless, as well as the triangular-lattice one[8, 9, 10].

References

[1] H. Nakano and T. Sakai: J. Phys. Soc. Jpn. 80 (2011) 053704.

[2] H. Nakano and T. Sakai, J. Phys. Soc. Jpn. 84 (2015) 063705.

[3] T. Sakai and H. Nakano, Phys. Rev. B 83 (2011) 100405(R).

[4] Y. Ran, M. Hermele, P. A. Lee and X. -G. Wen: Phys. Rev. Lett. 98 (2007) 117205.

[5] Y. Iqbal, F. Becca, S. Sorella and D. Poilblanc: Phys. Rev. B 87 (2013) 060405(R).

[6] S. Yan, D. A. Huse and S. R. White: Science, 332 (2011) 1173.

[7] S. Nishimoto, N. Shibata and C. Hotta: Nature Commun. 4 (2013) 2287.

[8] T. Sakai and H. Nakano: POLYHEDRON 126 (2017) 42.

[9] H. Nakano and T. Sakai: J. Phys.: Conf. Ser. 868 (2017) 012006.

[10] T. Sakai and H. Nakano: to appear in Physica B.

Numerical Study on Spin Flop Phenomena in Low-Dimensional Quantum Spin Systems

T. SAKAI[1,2,3], H. NAKANO[1,2], Y. Hasegawa[1,2], T. SHIMOKAWA[4], and A. Shimada[5]
[1]*Graduate School of Material Science, University of Hyogo, Kouto, Kamigori, Hyogo 678-1297, Japan*
[2]*Research Center for New Functional Materials, University of Hyogo, Kouto, Kamigori, Hyogo 678-1297, Japan*
[3]*Synchrotron Radiation Research Center, Kansai Photon Science Institute, Quantum Beam Science Research Directorate, National Institute for Quantum and Radiological Science and Technology (QST) SPring-8, Kouto, Sayo, Hyogo 679-5148, Japan*
[4]*Okinawa Institute of Science and Technology Graduate University, Okinawa, Japan*
[5]*Graduate School of Science, Kyoto University, Kyoto 606-8502, Japan*

The spin flop is one of interesting magnetic phenomea. It was initially proposed as a first-order phase transition accompanied by the change of the direction of the Néel order. It has been supposed to occur only in antiferromagnets with the easy-axis anisotropy. However, our previous large-scale numerical diagonalization study indicated that a spin-flop-like magnetization jump in someantiferromagnets without any spin anisotropy[1, 2, 3]. The systems which exhibit such a magnetization jump are the S = 1/2 square-kagome- and Cairo-pentagon-lattice antiferromagnets. The magnetization jump is supposed to induced by the strong spin frustration. However, the detailed mechanism is still an open problem. Thus we study on the spin flop phenomena of these frustrated systems using the exact small cluster analysis. As a result, it is found that the magnetization jump is induced by an entangled state[4].

References

[1] H. Nakano and T. Sakai: J. Phys. Soc. Jpn. 82 (2013) 083709.

[2] H. Nakano, M. Isoda and T. Sakai: J. Phys. Soc. Jpn. 83 (2014) 053702.

[3] H. Nakano, T. Sakai and Y. Hasegawa: J. Phys. Soc. Jpn. 83 (2014) 084709.

[4] Y. Hasegawa, H. Nakano and T. Sakai: submitted to Phys. Rev. B.

Efficient Sampling Simulation of the Soft Modes Significantly Contribute to Protein Properties

Kazuhiro TAKEMURA, Duy TRAN, Hisham DOKAINISH, Jacob SWADLING, Hiroaki HATA, Kenichiro TAKABA, Ai SHINOBU, and Akio KITAO

School of Life Science and Technology, Tokyo Institute of Technology

Ookayama, Meguro, Tokyo 152-8550

Proteins carry their function by interacting with other proteins or ligands. Thus, accurate prediction of protein-protein/ligand complex structures is a key to understanding their function. We proposed the Concentrated ligand Docking (ColDock) method, an efficient but accurate method to generate protein-ligand complex structures using molecular dynamics (MD) simulations at relatively high ligand concentrations. The procedure of ColDock for a given protein-ligand pair is as follows. (i) Multiple ligands are distributed randomly around the protein at relatively high concentration (~100 mM). (ii) Multiple short (100 ns) independent MD simulations are conducted. To prevent ligand aggregations which might be caused by high concentration, extra repulsive forces are applied between ligands (Fig.1). (iii) Ligands in contact with the protein are selected. (iv) The selected ligands are clustered according to root-mean-square-deviation (RMSD). Ligand poses are predicted as the representatives poses of each of the dominant clusters.

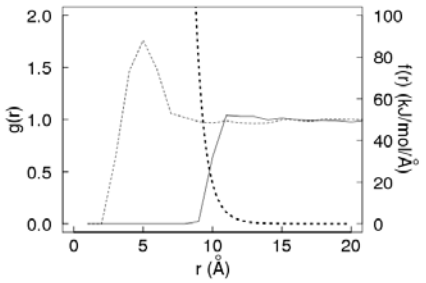

Fig.1 Pair distribution functions, g(r)s, of ligand with (solid line) and without (broken line) repulsive force, f(r) (dotted line)

We applied ColDock to four systems; FK506 binding protein in complex with 1) dimethylsulfoxide (DMS) and 2) methyl sulfinyl-methyl sulfoxide (DSS), 3) a complex of human plasminogen kringle 4 with ε-aminocaproic acid (ACA), and 4) the X-linked inhibitor of apoptosis protein in complex with 4-(4-bromo-1H-pyrazol-1-yl) piperidinium (BPP). We used the protein structure in holo form (taken from the crystal complex structure for DMS, ACA, and BPP as an initial test. To examine the performance of ColDock we later used the protein structures in apo form for all four systems.

Since ligands bound to the correct

position are stably held at that position, the population of ligands at the correct binding site is expected to be high. The assumption was verified by analyzing probabilities of ligand contact per residue (Fig.2). As expected, residues with high contact probability (dark region in Fig.2) are located around the correct binding site. Ligands in contact with the protein from all MD snapshot were gathered, then RMSD-based clustering was conducted. To reduce the computational cost for clustering, only ligands in contact with 6 or more residues were selected.

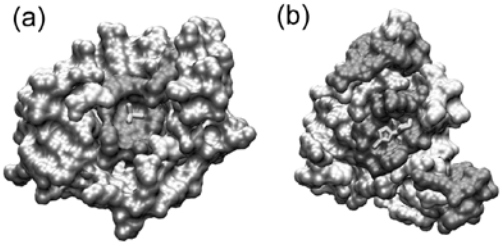

Fig.2 Probabilities of ligand contact per residue in DMS (a) and BPP (b). Darker regions represent residues with high contact probability. Ligands in the crystal structure of the complex are shown for reference.

Despite the simplicity of the procedure, ColDock successfully predicted the structure of the three complexes starting from the holo structure. Ligand RMSDs (RMSD of ligand from the crystal structure after superposing protein structures) for DMS, ACA, and BPP were 0.3, 1.3, and 0.4 Å, respectively. All the native contacts were successfully reproduced. When protein structures in the apo forms were used, ColDock successfully predicted three out of four cases (Fig.3). For BPP, the ligand binding site of the protein in the apo form is closed (Fig.4) and was unable to open within 100 ns. The combination with a pocket expansion technique is required for such targets and is currently under investigation. Since ColDock uses standard MD simulations with an extra repulsive force, it can be easily combined with any method.

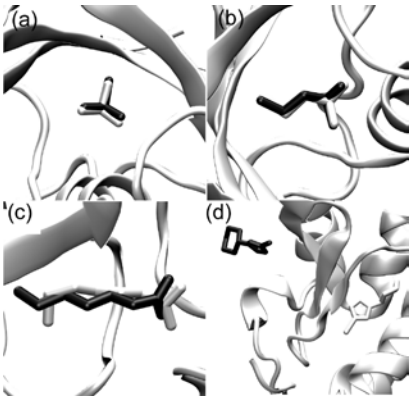

Fig.3 Predicted (black) and crystal (white) structures of ligands in (a) DMS, (b) DSS, (c) ACA, and (d) BPP.

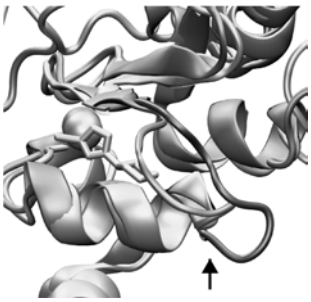

Fig.4 Structures of the X-linked inhibitor of apoptosis protein in the crystal holo (dark) and apo (light) forms. The arrow indicates the loop which closes the binding pocket in the apo form.

Elucidation of binding and unbinding processes of a ligand to a protein using a hybrid of the manifold theory and the Markov state model

Takashi YOSHIDOME

Department of Applied Physics,

Tohoku University, 6-6-05, Aoba, Aramaki, Aoba-ku, Sendai 980-8579

To construct an in-silico drug-design protocol, an accurate computation of the dissociation rate for protein-ligand systems is required. However, the computation is impossible with the molecular dynamics (MD) simulations because the time scale of the dissociation is second and is too long to perform the conventional MD for dissociation. A solution is to employ the Markov-state model (MSM). The model is constructed through the following steps: (i) Classify conformations into major states; (ii) Calculate the transition probabilities between the states, and; (iii) Compute physical quantities. We have recently proposed that an accurate computation of a physical quantity is possible when a manifold-learning technique employed for the classification [1].

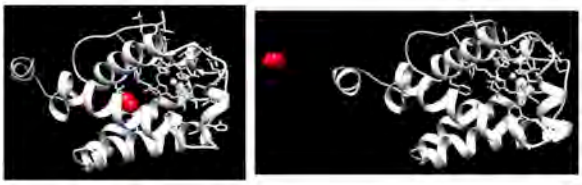

Fig. 1: The snapshots of the initial (left) and final (right) MD steps. Spheres are the O_2.

Here, we performed MD simulations of hemoglobin-O_2 system to demonstrate that the dissociation rate can accurately compute using MSM. The program AMBER16 [3] was used for the MDs. The calculations were primarily performed using L4cpu and L2fat. To investigate whether accurate computation of the dissociation rate is possible, its correct answer is required. To obtain the answer, dissociation should occur within the time scale (t_{MD}) that MD can be performed. As shown in Fig. 1, The dissociation of O_2 was successfully reproduced within t_{MD}.

References

[1] R. Ito and T. Yoshidome, Chem. Phys. Lett., **691**, 22 (2018).

[2] D.A. Case, *et al*., AMBER 2016, University of California, San Francisco (2016).

Accurate computation of the free-energy change of apoplastocyanin using the end-points method

Takashi YOSHIDOME

Department of Applied Physics,

Tohoku University, 6-6-05, Aoba, Aramaki, Aoba-ku, Sendai 980-8579

To elucidate the mechanism for a variety of biophysical processes such as protein folding and aggregation and binding of drug molecules, accurate and efficient computation of the free energy of proteins is inevitable. The standard methods enable us to exactly compute the free energy of proteins within a force field used. However, molecular dynamics (MD) simulations of many intermediate states connecting the initial (reference system containing only water molecules) and final (solution system consisting of water and solute) states are required. On the other hand, we have recently proposed accurate computation methods for the hydration-free energy [1] and for the configurational entropy [2]. These methods enable us to compute those quantities using the MD simulation data for the initial and final states. Thus, our computational method, referred to as "end-point method", is more efficient than the standard method.

To demonstrate the usefulness of the end-point method through an accurate computation of the free-energy change of protein folding, we applied the method to the protein folding of apoplastocyanin. We first performed a replica-exchange MD (REMD) simulation to sample the conformations including the native and unfolded states. The program AMBER16 [3] was used for the REMD, and generalized Born model was employed for the implicit solvent model. We then calculated the entropy change upon folding of apoplastocyanin using the end-point method and the morphometric approach [4]. The calculations were primarily performed using the L36cpu. The result was 1.7 kcal/mol, and experimental value was ~ 0 kcal/mol. A reason of discrepancy would be the force field for proteins.

References

[1] T. Yoshidome, T. Ekimoto, N. Matubayasi, Y. Harano, M. Kinoshita, and M. Ikeguchi, J. Chem. Phys., **142**, 175101 (2015).

[2] S. Hikiri, T. Yoshidome, and M. Ikeguchi, J. Chem. Theory Compt., **12**, 5990 (2016).

[3] D.A. Case, *et al*., AMBER 2016, University of California, San Francisco (2016).

[4] R. Roth, Y. Harano, and M. Kinoshita, Phys. Rev. Lett., **97**, 078101 (2006).

Physical Property Analysis of Macromolecular Self-Assembly using Quantitative Coarse-Grained Molecular Model

Wataru Shinoda
Department of Materials Chemistry, Nagoya University
Furo-cho, Chikusa-ku, Nagoya 464-8653

Coarse grained (CG) model has been widely used in macromolecular and biological simulations. To investigate molecular processes at the meso- and macroscopic scales, "phenomenological" CG models have mostly been used. However, chemical details often significantly affect the physical properties of molecular assembly, suggesting the need of a quantitative CG model that can reflect the difference of molecular species at an appropriate resolution. Our CG model is one of these trials to conduct a quantitative simulation particularly focusing on the interfacial problems in soft materials. Thus, we have been developing a CG model that can capture the interfacial thermodynamic properties of molecular assembly correctly.[1] The CG model is often called the SDK (Shinoda-Devane-Klein) model.[2] Based on the SDK approach, we are developing a new CG model for polymers and biological macromolecules. In this report, we write specifically a polymer CG model for perfluoro sulfornic acid (PFSA) membranes.[4]

In our CG approach, we use experimental and computational data as references for the parameter optimization of the CG model. As shown in Fig. 1, we define a single CG site to represent a group of about 10 atoms. The computational data is usually obtained by a series of all-atom molecular dynamics (AA-MD) simulations of relatively small systems. Using the supercomputer at ISSP, we can conduct a large-scale simulation of PFSA membrane

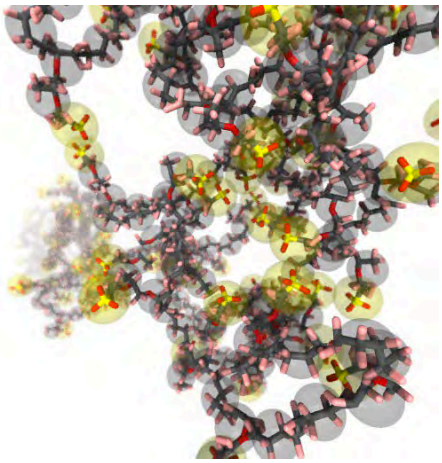

Figure 1: The CG mapping of PSFA ionomer. All-atom representation is given in stick and CG representation is given in transparent particle.

even with the all-atomic force field. 100ns-long AA-MDs of PSFA system containing 200,000 atoms have been routinely conducted, which produces well converged results for structural properties for relatively short chained polymers (connected 10 monomer units). This produces a reliable reference data for structural properties of PSFA membranes. However, polymers that are experimentally used for the electrolyte purpose have much higher molecular weight typically, so we need to handle the longer polymer chains including more than a hundred of monomer units to simulate the experimentally relevant system. This is

prohibitively difficult for AA-MD, so we need a quantitative CG model at least to reproduce the morphology made by PFSA including some amount of water. Thus, we extended the SDK model to simulate the PSFA membranes. One finding is that, in order to reproduce the interfacial properties as well as rather fine structure, a hybridization of the SDK and IBI (Iterative Boltzmann Inversion) models could be useful.[4] The hybrid SDK/IBI CG model was confirmed to successfully reproduce the structural properties from AA-MD. This also enables us to simulate reasonable target membrane systems including long polymer chains with the realistic length. We have run a large scale CG-MD of PFSA membrane containing 0.3 million CG particles, which represents about three million atom system. We successfully equilibrated the CG system after a series of annealing simulations, and then, generated the corresponding all-atom configuration using a reverse-mapping technique. In this way, we generated a reasonable all-atom configuration for the glass polymer membrane, and a relatively short equilibration MD simulation was just required to prepare a large-scale polymer membrane system, thanks to the pre-equilibrated structure produced by the quantitative CG-MD simulation. Here we used the LAMMPS and GROMACS softwares for CG and AA-MD simulations, respectively. Both of these simulation were significantly accelerated by GPU. The obtained well-equilibrated all-atom structure (Fig. 2) should be useful for the mechanical and ion conductivity examination of the polyelectrolyte membrane.

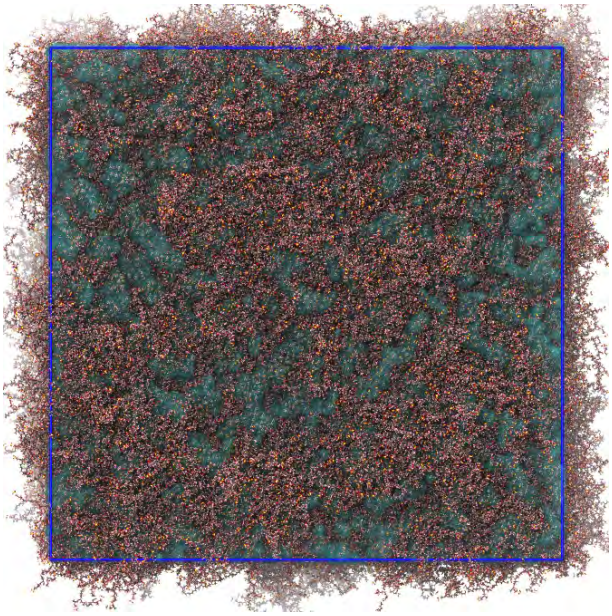

Figure 2: A snapshot from a large-scale all-atom MD simulation of the PFSA membrane system including three million atoms. This system was first generated and equilibrated by a CG-MD, and then was converted to atomic representation by the reverse mapping, then finally, again equilibrated by a short (30 ns) all-atom MD simulation. PFSA ionomers are represented by lines and water are drawn by cyan continuum volume.

References

[1] W. Shinoda, R. DeVane, and M. L. Klein: Mol. Simul. **33** (2007) 27.

[2] W. Shinoda, R. DeVane, and M. L. Klein: Curr. Opin. Struct. Biol. **22** (2012) 175.

[3] A. Kuo, A. Tanaka, J. Irisawa, W. Shinoda, and S. Okazaki: J. Phys. Chem. C **121** (2017) 21374.

[4] A. Kuo, S. Okazaki, and W. Shinoda: J. Chem. Phys. **147** (2017) 094904.

Numerical study on low-energy states of quantum spin systems

Hiroki NAKANO
Graduate School of Material Science, University of Hyogo
3-2-1 Kouto, Kamigori-cho, Ako-gun, Hyogo 678-1297, Japan

In condensed matter physics, generally, it is very di cult to estimate physical quantities precisely in systems of many-body problems. For such systems, therefore, numerical approaches have widely been used as effective ones. From this motivation, many researchers have carried out a lot of computational studies, which contribute much to our deeper understanding of quantum spin systems. Even for the situation, numerical studies are particularly di cult when spatial dimensions of target systems with frustrations are larger than one. This di culty occurs under the situation that applicable numerical methods are limited. It is well known that such systems cannot be treated by the quantum Monte Carlo simulations and the density matrix renormalization group calculations. Only the numerical diagonalization method based on the Lanczos algorithm is generally applicable when a target system includes frustrations and when the spatial dimension of the system is larger than one. At the same time, this method also has a serious weak point. Only very small system sizes can be treated by this method. We then succeeded in developing a hybrid-type parallelized code of Lanczos diagonalization[1] to overcome this disadvantage. Using this Lanczos-diagonalization code that we developed, we examine various quantum spin systems as a primary approach.

The primary study of this year in the present project examines the $S = 1/2$ Heisenberg antiferromagnet on the triangular lattice with next-nearest-neighbor interactions under the magnetic eld[2]. The amplitude of the nearest-neighbor interactions and the next-nearest-neighbor interactions are denoted by J_1 and J_2, respectively. It is widely known that the system shows the magnetiztaion plateau at one-third height of the saturation in the magnetization curve when $J_2 = 0$. On the other hand, when J_2 is in nitely larger than J_1, the system is reduced to three isolated systems, each of which is the triangular-lattice antiferromagnet with only the nearest-neighbor interaction with its amplitude J_2. Therefore, the one-third-height plateau exists for $J_2 \gg J_1$. The primary question of our study is what happens in the case of intermediate J_2. We examine whether or not the plateau of this height disappears. We carry out Lanczos diagonalizations and obtain the magnetization curves for 27 and 36-site clusters. Our calculations clarify that the plateau at this height closes ar around $J_2/J_1 = 0.2$, that the plateau disappears at least until $J_2/J_1 = 0.7$, and that the plateau opens again for even larger J_2. The clari ed behavior becomes a fundamental information concerning the triangular-lattice antiferromagnet.

Since 2016, our project also treats the case when the triangular-lattice antiferromagnet includes the distortion of the $\sqrt{3}$ $\sqrt{3}$ type. Note here that this distortion links the two cases of the triangular and dice lattices. Our calculations clari ed that there exists an intermediate region where the ground state shows continuously increasing spontaneous magnetization[3]. In 2017, the thermodynamic properties such as the speci c heat and the susceptibility are also studied around the phase boundaries of the intermediate phase[4, 5].

Our studies contribute to our understandings of the triangular-lattice antiferromagnet and the nontrivial e ect of frustration in mag-

netic materials.

References

[1] H. Nakano and A. Terai: J. Phys. Soc. Jpn. **78** (2009) 014003.

[2] H. Nakano and T. Sakai: J. Phys. Soc. Jpn. **86** (2017) 114705.

[3] H. Nakano and T. Sakai: J. Phys. Soc. Jpn. **86** (2017) 063702.

[4] A. Shimada, H. Nakano, T. Sakai, and K. Yoshimura: J. Phys. Soc. Jpn. **87** (2018) 034706.

[5] A. Shimada, H. Nakano, T. Sakai, and K. Yoshimura: J. Jpn. Soc. Powder Powder Metallurgy **65** (2018) 3.

Numerical study of non-equilibrium systems

Kenji HARADA
Graduate School of Informatics, Kyoto University, Kyoto 606-8501, Japan

Many systems in Nature are open systems coupled to external reservoirs. Sometimes the systems in the microscopic level break a detailed balance condition between microstates. This type of systems shows non-equilibrium behavior. In particular, the interesting phenomena in a non-equilibrium system is a phase transition. In the last decades, our understanding for a phase transition of non-equilibrium systems makes the remarkable progress. A highlight is a universality in a continuous phase transition of directed percolation (DP) problem[1]. If we regard an allowed direction of percolation in a DP problem as a time, a $(d+1)$-dimensional DP problem describes a d-dimensional time evolutional system as a reaction-diffusion model, or a d-dimensional quantum system defined by a non-Hermitian Hamiltonian. If there is no active element in a system at a time, the time evolution of the system freezes. Since a system cannot escape from the state, it is called an absorbing state. Increasing a local percolation probability, a phase transition occurs at which a convergence into the absorbing state disappear. For various DP problems, the density of active sites continuously appears at the phase transition point which is called an absorbing phase transition. Interestingly, it shows a criticality as like a conventional continuous phase transition of equilibrium systems. Many previous studies confirmed the universality of continuous absorbing phase transiton. The idea of universality in equilibrium systems was generalized into non-equilibrium systems.

To study this problem, we tried to use a tensor network scheme. There are two approaches in a tensor network for this problem. Because the temporal evolution of a system is described a master equation of a state probability distribution, the first method is a time-evolution of a state probability distribution in which the state probability distribution is defined as a tensor network. The second method is a renormalization of a time-evolutional operator in a master equation.

We applied the first method to the one-dimensional DP problem. A promised tensor network of a state probability distribution, in this case, is a matrix product state. In particular, we find a better performance of a specialized matrix product form to keep a precision in a time-evolution of a state probability distribution. It is a canonical form. Because a time evolutional operator of DP problem is a tensor network of local time evolutional operators, the standard SVD approximation for multiplication of a local time evolutional tensor in a part of a canonical form satisfies a global optimization condition. The precision of a canonical form calculation can be compared with that of a standard Monte Carlo simulation.

For the second method, we consider a key feature of many tensor network renormalization techniques. Then, we introduce an entanglement branching operator to split a composite entanglement flow in a tensor network[2]. The entanglement branching is a new useful operation to manipulate a tensor network. For example, finding a particular entanglement structure by an entanglement branching operator, we can improve a conventional tensor renormalization method to catch a proper renormalization flow in a tensor network space.

[1] M. Henkel, H. Hinrichsen, and S. Lübeck, "Non-Equilibrium Phase Transitions. Volume 1: Absorbing Phase Transitions" (Springer, 2008).

[2] K. Harada, "Entanglement branching operator", Phys Rev B **97** (2018) 045124.

Designing Thermal Functional Materials via Materials Informatics

Junichiro SHIOMI

Department of Mechanical Engineering, The University of Tokyo

7-3-1 Hongo, Bunkyo, 113-8656

Materials informatics (MI), which has been considered as the fourth paradigm of science in addition to theory, simulation, and experiment, is now gaining a great attention in the field of heat transfer as a powerful and efficient tool to accelerate the discovery and design of materials with desired thermal property. This year, we focused on designing nanostructures for thermal functional materials via MI.

The first main part of last year work is about multifunctional structural design of graphene thermoelectrics by Bayesian optimization (BO). We have applied BO to design nanostructures with optimal thermal transport before [1]. This year, we extend the BO to consider multi-evaluation (phonon and electron) during the designing [2]. We consider two different models as shown in Fig. 1: periodically nanostructured GNR (Model A) and antidot GNR (Model B).

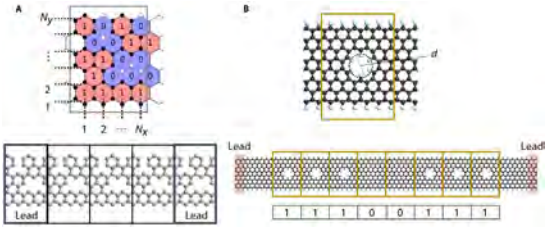

Figure 1: Nanostructured thermoelectric graphene nanoribbons (GNRs). (A) Periodically nanostructured GNR (Model A) and (B) antidot GNR (Model B).

Figure 2A shows average, maximum and minimum ZT of Model A with different numbers of vacancies. The Bayesian search accelerates the exploration of high *ZT* structures in all cases as shown in Fig. 2B. In most cases, top-0.5% of the structures can be found by the Bayesian search with half the calculations for the random search.

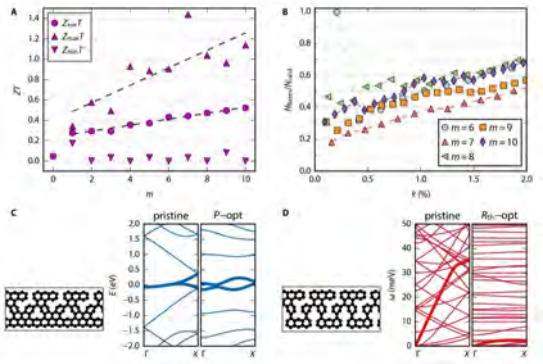

Figure 2: (A) The maximum, minimum, and average *ZT* of all candidates. Dashed lines show the linear fitting. (B) Efficiency of Bayesian optimization. (C)/(D) show the optimal structure and electron/phonon band structure.

Figures 2C and 2D show GNR structures that have the largest power factor and thermal resistance. As for the structure with optimized power factor,

vacancies are introduced over the entire area of GNR except for the hexagonal lattices along an edge. The structural optimization leads to strong flattening of electronic bands around energy levels of the edge state and eventually band gaps are generated. Nanostructuring in middle areas of zigzag GNRs leads to phonon scattering without a significant change of the edge state and enhances the thermoelectric performance.

Figure 3A compares thermoelectric properties of the pristine structure, the periodic antidot structure, and the optimal structure, the last two of which are shown in Fig. 3B. The optimal structure has an aperiodic array of antidots, which increases *ZT* by 11 times. It is interesting to note that simply arranging the antidot periodically increases *ZT* by 5.0 times compared with the pristine structure, yet the remaining 2.1 times does require the optimization. This indicates that the optimization of the arrangement of antidots can effectively improve thermal and electronic properties, simultaneously.

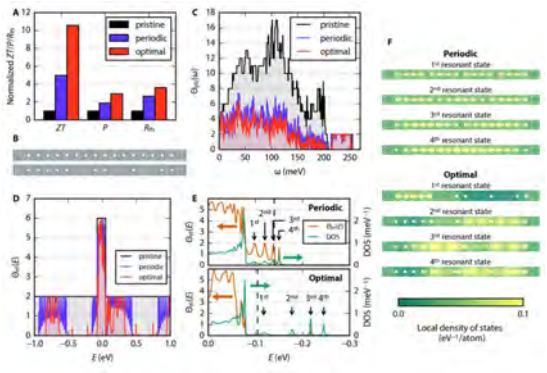

Figure 3: Optimization of antidot GNR structure. (A) Thermoelectric properties of representative structures. (B) Periodic and optimal aperiodic structures. (C)/(D) Phonon/Electron transmission functions. (E) Electron transmission functions and density of states periodic/optimal structures. (F) Local DOS distribution of resonant states of periodic/optimal structures.

Figure 3C shows the phonon transmission functions of the pristine, periodic, and optimal aperiodic structures. The phonon transmission decreases significantly by introducing the periodic antidots and hence thermal resistance increases. Electron transmission functions of representative structures are compared in Fig. 3D. Unlike pristine GNRs that have low Seebeck coefficient due to the absence of the band gap, periodic antidot GNRs have higher Seebeck coefficient because of the presence of transport gaps, corresponding to energy gaps of an infinite periodic antidot GNR. The introduction of periodic antidots, therefore, can enhance the thermoelectric performance. The optimal antidot arrangement can suppress resonant peaks. In Fig. 3E, the electron transmission functions and density of states (DOS) show that although resonant states exist near the edge state in both the periodic and optimal structures, their electron transmission functions are strongly suppressed in the optimal structure. The local density of states (LDOS) at the resonant energy mapped onto each atom are shown in Fig. 3F. LDOS in the finite periodic structure spreads over the whole nanostructured region while the optimal aperiodic structure clearly leads to the localization of states in limited areas. It is intuitively

comprehensible that the widely-spreading states, which can be regarded as Bloch states, contribute to electron transport while the strong localization generates the region with extremely low DOS and suppresses the electron transport as shown in Fig. 3E.

The second main part of last year work is about the development of Monte Carlo tree search method. The Bayesian optimization is very effective and accurate when the total number of candidate is around several hundred thousand. However, when dealing with cases with huge or even unlimited number of candidates, it becomes very difficult. Here, we introduce our developed another effective method named Monte Carlo Tree Search (MCTS) [3], which combines the generality of random simulation with precision tree search. Tree search is a popular method for making optimal decisions in artificial intelligence (AI) problems, such as Go games.

The MCTS algorithm is based on a search tree built node by node according to the evaluation of each simulated case, as shown in Fig. 4. Each node contains two important information: an estimated value based on simulation results and the number of times it has been visited. The process of MCTS is composed of four steps: selection, expansion, simulation, and backpropagation. (i) Selection: Starting at root node R, recursively select optimal child nodes according to larger or small upper confidence bound (UCB) score until a leaf node L is reached. (ii) Expansion: If the leaf node L is a not a terminal node then creates one or more child nodes and select one C. (iii) Simulation: Randomly select one playout from C and do the conductance calculation. (iv) Backpropagation: Use the calculated thermal conductance value to update the node information on the path back from C to R. It has to be mentioned that MCTS does not guarantee finding global optimal structure, and instead it offers structure close to the global optimal one with high efficiency.

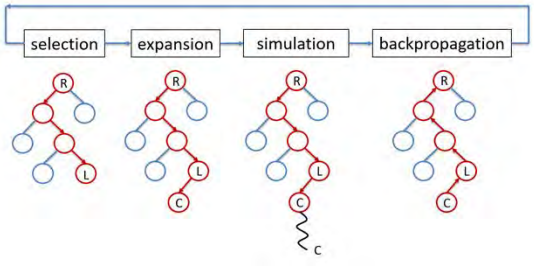

Figure 4: Schematics of Monte Carlo tree search method.

To test the performance Monte Carlo tree search, we applied MCTS to design the Si/Ge alloy interfacial structure to tune heat conduction across the Si-Si and Si-Ge interfaces. The convergence of MCTS shown in Fig. 5 is slower compared with BO [1]. Not all the 10 rounds of optimization can target the global optimal structures with the same number of calculated candidate structures as BO, however they are approaching the global optimal conductance. The advantage of MCTS is that it can deal with optimization cases with unlimited or huge number of candidates that BO cannot deal with. With the increase of number of candidates, the consumed time for selection of next candidate in BO will increase quickly,

which make the BO optimization rather time consuming, while the MCTS is able to obtain the quasi-optimal structures with high efficiency.

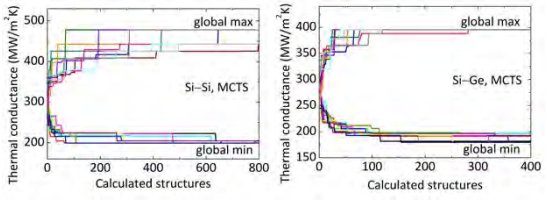

Figure 5: Performance test of Monte Carlo tree search for Si-Si and Si-Ge alloy interface.

In summary: (1) By taking graphene nanoribbons (GNRs) as a representative thermoelectric material, we carried out structural optimization by alternating multifunctional (phonon and electron) transport calculations and the Bayesian optimization to overcome the trade-off. We achieved multifunctional structural optimization with efficiency more than five times that of the random search. The obtained GNRs with optimized antidots significantly enhance the thermoelectric figure of merit (ZT) up to 11 times that of the pristine GNR. The knowledge of the optimal structure further provides new physical insights that independent tuning of electron and phonon transport properties can be realized by making uses of the zigzag edge states and aperiodic nanostructuring. (2) We have designed Monte Carlo tree search method which can provide approaching global optimal structures with high efficiency and it can be applied to optimal/design cases with unlimited number of candidates that Bayesian optimization cannot deal with.

References

[1] S. Ju, T. Shiga, L. Feng, Z. Hou, K. Tsuda, J. Shiomi: Physical Review X **7** (2017) 021024.

[2] M. Yamawaki, M. Ohnishi, S. Ju, J. Shiomi: Science Advances (under revision).

[3] T. M. Dieb, S. Ju, K. Yoshizoe, Z. Hou, J. Shiomi, K. Tsuda: Science and Technology of Advanced Materials 18 (2017) 498.

Control of Phonon and Electron Transport Properties Using Mechanical Strain

Masato OHNISHI and Junichiro SHIOMI

Department of Mechanical Engineering,

The University of Tokyo, Hongo, Bunkyo-ku, Tokyo 113-8656

A recent advance of nanotechnology allows us to design materials in nanoscale. When the length scale of nanostructures in materials reaches in the order of phonon wavelength, wave nature is expected to dominate their thermal transport properties. Despite many attempts to observe such coherent wave nature of phonons in experiments, coherent phonons had been observed only except for at low temperature (< 10 K) [1] or low frequency (< 1 THz) [2] because phonons easily lose their phase information during scattering processes. Recently, Kodama *et al*. [3] have revealed that thermal conductivity of carbon nanotubes (CNTs) decreases by ≈ 60% at room temperature and peak temperature of temperature dependent thermal conductivity decreases by ≈ 50 K due to encapsulation of fullerenes. These results indicate that the encapsulated fullerenes do not act as simple phonon scatters like impurities but modulate phonon dispersion of outer single-walled CNTs (SWNTs).

Observation of carbon nanopeapods with transmission electron microscope has shown that the fullerene encapsulation induces radial expansion in outer SWNTs [3]. We, therefore, have attempted to reveal effects of fullerene encapsulation. We analyzed phonon dispersion of SWNTs and peapods based on spectral energy density (SED) analysis.

We found that the radial expansion leads to softening and hardening of axial and radial modes, respectively, which should be caused by variation of force constants due to the induced strain. Moreover, the periodic strain leads to zone-folding effect of phonon modes in outer SWNT and encapsulated fullerenes. Zone-folding effect leads to reduction of group velocity. Figure 1 shows that magnitude of reduction of thermal conductivity along radial direction due to relaxation time and group velocity. This figure clearly shows that thermal conductivity decreases due to the decrease in phonon group velocity.

Our simulations reveal that the encapsulation-induced periodic strain makes an artificial superlattice of CNTs, which provides a new concept of tuning of microscopic thermal transport and strain-thermal engineering. We believe that experimantal study based on our simulations can realize use of coherece wave nature for advanced thermal devices such as thermal rectification and thermal cloaking.

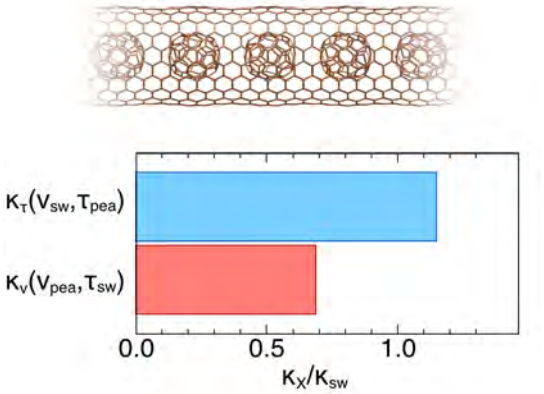

Fig. 1. Suppression of thermal conductivity along radial direction. Decrease in group velocity dominates the suppression of thermal conductivity.

References

[1] J. Maire, *et al*., Science Advances 3, e1700027 (2017).

[2] M. R. Wagner, *et al*., Nano Letters 16, 5661 (2016).

[3] T. Kodama, *et al.*, Nat. Mater. 295, 828 (2017)

Magnetic excitation and spin transport in frustrated quantum spin chain

Hiroaki ONISHI
Advanced Science Research Center, Japan Atomic Energy Agency, Tokai, Ibaraki 319-1195

In ordinary magnetic insulators, elementary excitation is described by magnon and the flow of magnons causes spin current and thermal current. In contrast, frustrated magnets often show nontrivial ground states and elementary excitations. Thus we expect that novel types of carriers would contribute to spin and thermal transport phenomena. Here we focus on a spin nematic state in a spin-1/2 J_1-J_2 chain with ferromagnetic J_1 and antiferromagnetic J_2 in a magnetic field. As for magnetic excitations, we have found gapless quadrupole excitations [1] as well as gapless longitudinal and gapped transverse spin excitations [2]. These indicate that bound magnons can be created without energy cost and contribute to transport.

In the present work, to gain an insight into bound-magnon-mediated transport, we study temperature and field dependencies of spin and thermal Drude weights. For this purpose, we perform exact diagonalization calculations to obtain all eigenvalues and eigenvectors of the Hamiltonian, using ScaLAPACK designed for distributed memory parallel computers, and evaluate thermal expectation values. Utilizing the total magnetization and the momentum as conserved quantities, the maximum dimension is 9252 for 20 sites, which can be handled with workstations. It grows to 112720 for 24 sites, accessible due to MPI parallel simulations on the system B of the ISSP supercomputer.

Figure 1 shows the temperature dependence of the Drude weights at zero field. Note that the system size dependence is large even with

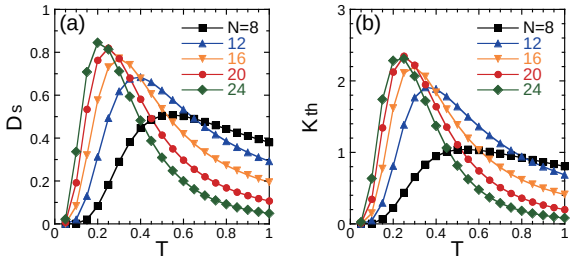

Figure 1: Temperature dependence of (a) spin and (b) thermal Drude weights at zero field for $J_1 = -1$ and $J_2 = 1$.

24 sites, and results with up to 24 sites are not enough to obtain a conclusive statement about the behavior in the thermodynamic limit. We find a peak structure, since the Drude weights drop to zero as the temperature goes to zero due to the finite-size effect. As the system size increases, the Drude weights become large at low temperature, while they become small at high temperature. For the spin Drude weight, the peak seems to approach zero temperature, indicating that the spin Drude weight is zero at finite temperature, i.e., the spin transport is diffusive. Analyses on the magneto-thermal effect in the magnetic field are in progress.

References

[1] H. Onishi, Physica B (in press).

[2] H. Onishi, J. Phys. Soc. Jpn. **84**, 083702 (2015); J. Phys.: Conf. Ser. **592**, 012109 (2015).

Phase diagrams of random topological matters

TOMI OHTSUKI[1]
TOHRU KAWARABAYASHI[2]
KEITH SLEVIN[3]
KOJI KOBAYASHI[4]
1) Dept. Phys., Sophia University, Chiyoda-ku, Tokyo 102-8554, Japan
2) Dept. Phys., Toho University, Miyama 2-2-1, Funabashi 274-8510, Japan
3) Dept. Phys., Osaka University, Toyonaka, Osaka 560-0043, Japan
4) IMR, Tohoku University, Sendai 980-8577, Japan

Recent discoveries of two-dimensional quantum spin Hall states and three-dimensional (3D) topological insulators (TIs) have inspired extensive research of these novel topological materials. Here we have studied disordered topological insulators as well as Weyl semimetals (WSM), which are constructed by stacking 2D Chern insulator (CI) layers.

Based on the renormalization group analysis, we have proposed the scaling theory near the multicritical point of WSM-CI-Metal, and have verified the scaling behavior numerically [1]. We have shown that the Anderson localized phase appears between CI-Metal, while the transition is direct for WSM-Metal and CI-WSM. We have also discussed novel scaling behavior of CI-WSM transition [2].

We have demonstrated that the image recognition based on multilayer convolutional neural network (so called deep learning) works well for drawing the phase diagram of disordered topological insulators and Weyl semimetals [3,4]. In addition, we have applied 3D image recognition to analyze entire 3D wave functions. We have shown that a full phase diagram of the disorder-energy plane is obtained once the 3D convolutional neural network has been trained at the band center (Fig. 1). We have further demonstrated that the full phase diagram for 3D quantum bond and site percolations (which are topologically disordered systems) can be drawn by training the 3D Anderson model at the band center [5].

References

1. X. Luo, B. Xu, T. Ohtsuki, R. Shindou: Physical Reivew B **97**, 045129 (2018).
2. X. Luo, T. Ohtsuki, R. Shindou: arXiv:1803.09051.
3. T. Ohtsuki, T. Ohtsuki: Journal of the Physical Society of Japan **85**, 123706 (2016).
4. T. Ohtsuki, T. Ohtsuki: Journal of the Physical Society of Japan **86**, 044708 (2017).
5. T. Mano, T. Ohtsuki: Journal of the Physical Society of Japan **86**, 113704 (2017).

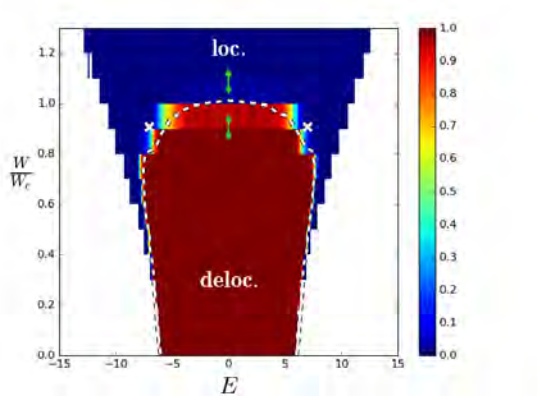

Figure 1: Color map of the intensity P_{deloc} (probability that the system is a metal) for all the energy spectrum of 3D Anderson model. An average over 5 samples was performed. The two green arrows indicate the region where the neural network is trained. Dashed line and the cross are the phase boundaries derived by other methods. Taken from [5].

Liquid–gas spinodal of the modified Lennard-Jones fluid: A preliminary study

Kazuhiro Fuchizaki and Kei Watanabe
Department of Physics, Ehime University, Matsuyama 790-8577
Hiroshi Noguchi
The Institute for Solid State Physics, The University of Tokyo, Kashiwa 277-8581

Spinodal line shows a boundary beyond which a thermodynamic phase no longer stably exists. The name reminds us of the mean-field (classical) spinodal derived from ϕ^4 theory. When fluctuations of a system are taken into consideration, the location of the lines would change. As for the location of the spinodal lines, the research was already performed for a 3D Ising system. The spinodal line was shown to approach the magnetization curve when $L \gg \xi$ [1], where L and ξ denote the linear dimension of a cell, obtained by dividing the system, and the correlation length, respectively. Because a fluid system is believed to belong to the same universality class as that of the Ising system, a similar behavior is expected regarding the spinodal and binodal lines. However, this expectation has never been proved yet. The present research is to try to demonstrate that the liquid–gas spinodal line is gradually proximity to the binodal line for $L \gg \xi$. As a fluid system, the modified Lennard-Jones (mLJ) system was employed because its thermodynamic behavior is precisely known [2]. We also make comments on the validity of the equation of state (EOS), recently proposed for dense fluids [3] based on a new cluster expansion.

Here and after, all quantities are expressed in units of σ and ϵ, which are the length and energy scales of the mLJ potential function, respectively. A cubic system with a side of $N = 35.22$ was employed. Periodic boundary conditions were imposed on the system, in which 16384 particles were contained. The number density was $\rho = 0.375$, which is slightly larger than the critical density, $\rho_c = 0.331(3)$ [4]. The isothermal molecular dynamics simulation was conducted. After sufficient equilibration at a temperature T below the critical temperature $T_c = 1.0762(2)$ [4], the system was divided into cubic cells with a side L, and the probability, $P_L^{(2)}(\rho_1, \rho_2)$, of finding simultaneously the densities, ρ_1 and ρ_2, in the adjacent cell was evaluated during subsequent production runs. We expect that $-\ln P_L^{(2)}(\rho_1, \rho_2)\Big|_{\rho_1=\rho_2=\rho} = -\ln P(\rho)$ behaves as the coarse-grained free energy, which cannot be calculated directly. In this preliminary study, we focused on low-temperature behaviors at $T/T_c = 0.7, 0.8$, and 0.9. Three lengths, 5.87, 7.044, and 8.805, were chosen for the side L. To assess the location of the binodal lines, the EOS [3] was used as a guide.

Figure 1 shows snapshots of the system after equilibration, i.e., after separation into liquid and gas phases, at those temperatures. A flat interface resulted in at the lowest temperature examined. Because the temperatures were well below T_c, the correlation length ξ was not assessed from the critical parameters [4], but were directly evaluated by fitting the density profile in x-direction around the interface to a function, $\sim \tanh[(x - x_0)/\xi]$, where x_0 denotes the interface position.

The binodal and spinodal densities are de-

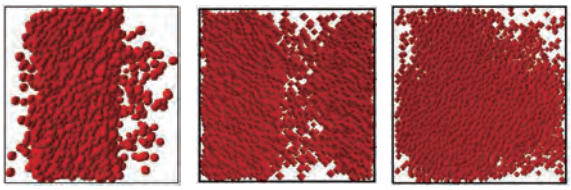

Figure 1: Snapshots showing liquid–gas coexistence at $T/T_c = 0.7, 0.8$, and 0.9 (from left to right).

noted by ρ_b and ρ_s, respectively (and their gas branches are denoted by ρ_b^g and ρ_s^g upon necessary). Those densities correspond to the minima and the inflection points of the coarse-grained free energy, respectively. The resulting $P(\rho)$ had indeed two peaks centered around the binodal densities.

To discuss the universal behavior, from which the dependence of the relationship between ρ_b and ρ_s on L/ξ is to be extracted, we invoke the Ising–fluid correspondence regarding criticality. That is, the order parameter, the magnetization, and the spinodal magnetization of the Ising system are regarded as ρ, $|\rho_b - \rho_c|$, and $|\rho_s - \rho_c|$, respectively. The interface free energy per cell volume, $\Delta f \sim (R/\xi)^{d-1}/L^d$, is expressible in terms of the change in density upon condensation $\Delta\rho \sim (R/L)^d\rho \sim (R/L)^d(\rho_c - \rho_b^g)$, as

$$\Delta f \sim \left(\frac{\Delta\rho}{\rho_c - \rho_b^g}\right)^{1-\frac{1}{d}} \frac{\xi}{L}\xi^{-d}.$$

The interface free energy is also evaluated as the free-energy barrier between the two minima:

$$\Delta f \sim \frac{k_B T}{L^d} \sim (\Delta\rho)^2\chi^{-1}.$$

Equating these two relations, we obtain

$$\frac{\Delta\rho}{\rho_c - \rho_b^g} \sim 1 - \frac{\rho_c - \rho_s^g}{\rho_c - \rho_b^g} \sim \left(\frac{\xi}{L}\right)^{\frac{1}{1+d^{-1}}}.$$

The left-hand side, $1 - \frac{\rho_c - \rho_s^g}{\rho_c - \rho_b^g}$, evaluated at the temperatures are plotted against $(L/\xi)^{-3/4}$ in Fig. 2. (The points recently obtained at $T = 0.7T_c$ are also included.) The points seem

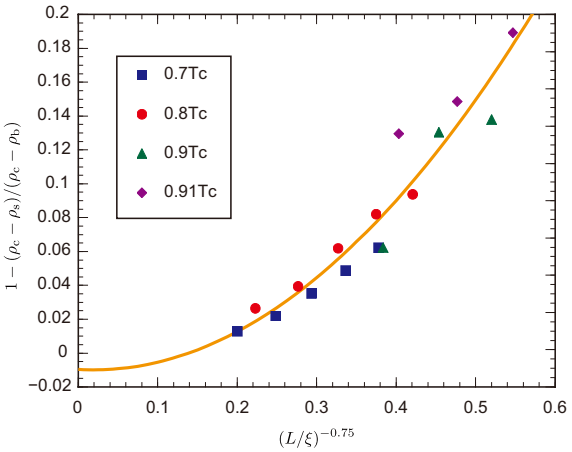

Figure 2: $\Delta\rho/(\rho_c - \rho_b^g)$ at four temperatures indicated are plotted against $(L/\xi)^{-3/4}$.

to fall into a single curve delineated by an orange line, showing a universal behavior. Moreover, the points seem to approach asymptotically the origin in the limit $L/\xi \to \infty$. Indeed, when the points are naively fitted to a quadratic function of $(L/\xi)^{-3/4}$, the function intercepts the ordinate at -0.0097, which is regarded virtually as zero under the statistics of the present data.

As consistent with the consequences obtained from the Ising model [1], the location of effective spinodal curve changes with the coarse-graining size. Furthermore, it asymptotically approaches the binodal curve in the thermodynamic limit. Finally, it should be recorded that Ushcats' EOS [3] overestimates the pressure of the mLJ fluid for the temperature range investigated.

References

[1] K. Kaski, K. Binder, and J. D. Gunton, Phys. Rev. B **29**, 3996 (1984).

[2] Y. Asano and K. Fuchizaki, J. Chem. Phys. **137**, 174502 (2012).

[3] M. V. Ushcats, J. Chem. Phys. **141**, 101103 (2014).

[4] K. Okamoto and K. Fuchizaki, J. Phys. Soc. Jpn. **86**, 034006 (2017).

SIMD Vectorization of Force Calculation with AVX-512 instructions

Hiroshi Watanabe
Institute for Solid State Physics, University of Tokyo
Kashiwa-no-ha, Kashiwa, Chiba 277–8581

The recent increase in computational power is mainly due to an increase in the number of CPU-cores and the width of registres. Therefore, the SIMD vectorization is unavoidable to make full use of the computational power. The CPU architecture of System C at ISSP is Intel Skylake, which supports AVX-512 instructions. In this report, we describe the effect of optimizations with AVX-512 instructions for calculating the force of Lennard-Jones potential. The AVX-512 instruction set uses registers with 512-bit width. Each register can treat eight 64-bit double-precision floating point numbers simultaneously. The AVX-512 instruction sets include gather, scatter, and mask operations which are useful for the vectorization of loop involving indirect accesses. While the auto-vectorized codes by Intel compiler work efficiently, there is still room for optimization. We have tried the following optimization techniques. Collision Detection Elimination (CDE); The compiler produces the code which checks the conflicts between the indices of j-atoms. Since there are no conflicts, the check code can be eliminated. Remainder Loop Elimination (RLE); Since the number of loop count is not so large, the computational time to process the remainder loop can be significant. Therefore, we eliminate the remainder loop by using mask operations. Software Pipelining (SWP); We adopt the software pipelining technique for the vectorized kernel. SWP is one of the loop optimization techniques to increase the number of instructions which can be executed simultaneously. In order to evaluate the effects of optimizations, we performed benchmark simulations. We observe the time to perform force calculation of Lennard Jones potential 100 times. The number of atoms is 119164. The cutoff length is 3.0 σ. The results are shown in Fig. 1. A sample code is available online [1]. The vectorized codes with AVX-512 was 78% faster than the codes automatically vectorized by the compiler. However, we find that the code vectorized with AVX2 is slightly faster than the code vectorized with AVX-512.

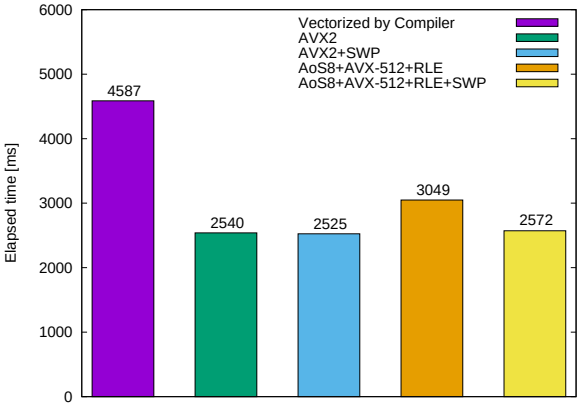

Figure 1: Improvements by optimization techniques.g

References

[1] `https://github.com/kaityo256/lj_simdstep`

Magnetization plateaus in the spin-1/2 Heisenberg model with kagome structures

Takami TOHYAMA
Department of Applied Physics, Tokyo University of Science, Tokyo 125-8585

Frustrated quantum spin systems containing kagome-type structures give rise to novel quantum states. Magnetization plateaus provide a good playground for such novel quantum states. It is, therefore, interesting to investigate magnetization plateaus in spin-1/2 frustrated Heisenberg models with kagome-type structures .

In this project, we have examined magnetization plateaus of two kagome-based lattices, i.e., a kagome-strip chain [1] and a square-kagome lattice [2], as shown in Fig. 1. Both lattices have with three nonequivalent antiferromagnetic exchange interactions whose Hamiltonian in the magnetic field is defined as $H = \sum_{\langle i,j \rangle} J_{i,j} \mathbf{S}_i \cdot \mathbf{S}_j - h \sum_i S_i^z$, where $\mathbf{S}_i$ is the spin-$\frac{1}{2}$ operator at site i, $\langle i,j \rangle$ runs over the nearest-neighbor spin pairs, $J_{i,j}$ corresponds to one of J_1, J_2, and J_3 shown in Fig. 1, and h is the magnitude of the magnetic field in the z-direction.

We use the density-matrix renormalization-group (DMRG) for the kagome-strip chain up to system size $N = 5 \times 65$ in the open boundary condition [1]. The number of states kept in DMRG is $m = 400$ and truncation error is less than 5×10^{-7}. We accurately determine the magnetic structures in a certain parameter range, and we find various types of plateaus. In total, we identify twelve kinds of magnetization plateaus, nine of which have magnetic structures that break translational and/or reflection symmetry spontaneously. The structures are classified by an array of five-site unit cells with specific bond-spin correlations.

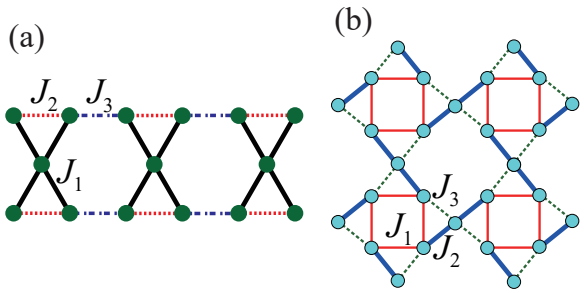

Figure 1: (a) Kagome-strip chain and (b) square-kagome lattice with three nonequivalent exchange interactions.

Among the plateaus, we find a nontrivial 3/10 plateau, whose magnetic structure consists of a period of four unit cells. Such long-period magnetic structure has not been reported before in one-dimensional quantum spin systems.

We perform the Lanczos-type exact diagonalization calculations for the square-kagome lattice with $N = 18$, 24, 30, and 36 under the periodic boundary conditions [2]. We obtain magnetic phase diagrams at $h = 0$ and finite h inducing 1/3 and 2/3 plateaus. We find a new 2/3 plateau that breaks four-fold rotational symmetry spontaneously. The origin of the plateau is attributed to the presence of the three nonequivalent exchange interactions.

References

[1] K. Morita *et al.*: Phys. Rev. B **97** (2018) 014412.

[2] K. Morita and T. Tohyama: J. Phys. Soc. Jpn. **87** (2018) 043704.

Speeding up of the effective physical model estimation by machine learning

Ryo TAMURA
International Center for Materials Nanoarchitectonics,
National Institute for Materials Science
1-1 Namiki, Tsukuba, Ibaraki, 305-0044

The importance of data-driven techniques using machine learning is recognized in materials science[1, 2]. Using machine learning, we are currently developing a generic effective physical model estimation method from experimentally measured data[3]. In the estimation method, plausible model parameters that explain the given measured data are determined by maximizing the posterior distribution. Thus, in each effective physical model estimation, we should search the maximizer of the posterior distribution, which is the computationally extensive probability distribution.

To accelerate an estimation of effective physical model, an efficient method for finding a better maximizer of computationally extensive probability distributions is proposed on the basis of a Bayesian optimization technique. Bayesian optimization has recently attracted much attention as a method to search the maximizer/minimizer of a black-box function in informatics and materials science[4]. In this method, the black-box function is interpolated by Gaussian processes, and the interpolated function is used to predict the maximizer/minimizer of the black-box function. A key idea of the proposed method is to use extreme values of acquisition functions by Gaussian processes for the next training phase, which should be located near a local maximum or a global maximum of the probability distribution.

Our Bayesian optimization technique is applied to the posterior distribution in the effective physical model estimation[5]. Here, instead of searching the maximizer of posterior distribution (P), the minimizer of energy function defined by $E = -\log P$ is searched. Even when the number of sampling points on the posterior distributions is fixed to be small, the Bayesian optimization provides a better minimizer of the energy function in comparison to those by the random search method, the steepest descent method, or the Monte Carlo method(Figure 1). In this demonstration, the quantum Heisenberg model is used as the target Hamiltonian and the temperature dependence of specific heat is inputted. Furthermore, the Bayesian optimization improves the results efficiently by combining the steepest descent method and thus it is a powerful tool to search for a better maximizer of computationally extensive probability distributions. Because the maximizer of a probability distribution is searched in many scientific fields, our method will play an important role in the promotion of science.

References

[1] T. Suzuki, R. Tamura, and T. Miyazaki, Int. J. Quantum Chem. **117**, 33 (2017).

[2] K. Shiba, R. Tamura, G. Imamura, and G. Yoshikawa, Sci. Rep. **7**, 3661 (2017).

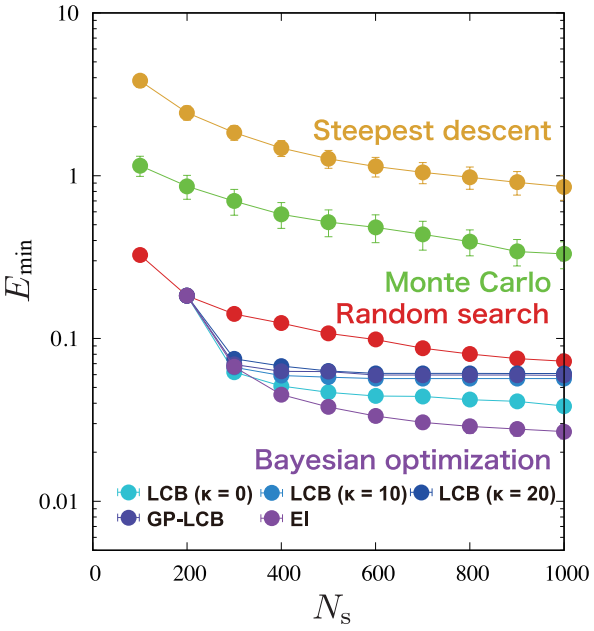

Figure 1: Obtained minimum value of the energy function ($E_{\min}$) depending on the number of sampling points (N_s) by some methods.

[3] R. Tamura and K. Hukushima, Phys. Rev. B **95** 064407 (2017).

[4] T. Ueno, T. D. Rhone, Z. Hou, T. Mizoguchi, and K. Tsuda, Materials Discovery **4**, 18 (2016).

[5] R. Tamura and K. Hukushima, PLoS ONE **13**, e0193785 (2018).

Direct numerical method for quantum response and quantum dynamics

Seiji MIYASHITA
Department of Physics, University of Tokyo
Hongo, Bunkyo-ku, Tokyo 113-0033

We studied the following topics related to our subject.

1. Optical bistability (OB) in the strong coupled quantum region

We studies the microscopic mechanism of the optical bistability by making use of an extended parallel algorithm. In particular, we pointed out OB takes place in the so-called quantum region where the number of atoms is larger than that of photons. We found the distribution of photon number in a cavity and the futures of bistability from the view point of dynamical first order phase transition and the transmission spectrum for the detuning frequency. We also study the properties of metastability including the hysteresis behavior, in particular, the size dependence of the relaxation time[1]

2. Population dynamics of the quantum Storner-Wohlfarh model

Dynamics under external sweeping field is also studied. The size(S)- and sweeping velocity-dependences of scattered population distribution of the quantum Stoner-Wohlfarth model was studied and it is found that a sharp change of the distribution occur after the SW point with a delay which persist in the large S. Dissipation effects on the quantum beating was also clarified by making use of a quantum master equation[2].

3. Shortcuts to Adiabaticity

If we sweep the external field very slowly, the system exhibits the adiabatic motion. In order to realize the adiabatic state in a finite time, the so-called counter adiabatic method has been proposed. But it is generally has a complicated form. We proposed an approximated counter adiabatic method and demonstrated that it practically works well to create the cat state in a Bose-Einstain condensate[3].

4. Quantum responses with the spin-orbit coupling (SOC)

We studied how the synergetic effect of spin-orbit coupling (SOC) and Zeeman splitting (ZS) affects the optical conductivity in the one-dimensional Hubbard model using the Kubo formula[4]: the dependences of resonance (EDSR) in the metallic regime and the optical conductivity in the Mott-insulating phase on the relative angle between the SOC vector and the magnetic field direction. The effect of U was also studied. We studied a mechanism of a sub-gap optical conductivity through virtual hopping of the electron. Motivated by recent terahertz absorption measurements in α-RuCl3, we developed a theory for the electromagnetic absorption of materials described by the Kitaev model on the honeycomb lattice using the formulation in terms of Majorana fermions[5].

5. Structure of an impurity-induced effective spin

We also studied properties of induced effective spin due to inhomogeneous structures in one dimensional spin chaines. e.g. the AKLT model and the alternate-bond antiferromag-

netic Heisenberg model. We found that with an appropriate magnetic field the induced effective spins can be operated independently, and also found there are two scales of length, i.e., that of magnetization profile and that of structure of the matrix product wavefunction for the state.[6]

6. New types of phase diagram in the spin-crossover material

We also found a specific phase diagram with a horn structure in spin-crossover systems exhibiting an internal temperature phase. We also studied the dynamis of transition in 3D. Moreover we study dynamics of transitions after photo-irradiation and analyzed the so-called elastic expansion before the thermal one[7].

Study on permanent magnets

We have studied microscopic mechanisms of the coercive force of permanent magnets at finite temperatures[8]. We have studied magnetic properties of $Nd_2Fe_{14}B$ in a realistic atomic scale at finite temperatures. For the purpose, we developed numerical methods such as Monte Carlo (MC) methods for the free energy landscape by making use of the Wang-Landau method, with which temperature dependence of the coercive force was obtained.

In parmanent magnets, the dipole-dipole interaction plays important roles. To perform MC simulation, we developed a new algorithm extending the idea of the stochastic cutoff method and the Fukui-Todo $O(N)$ method, and found that the anisotropy of the Fe atom which has been considered to be weak has an important role to maintain coercivity at relaviely high temperatures.[9]. We also studied peculiar properties of the ferromagnetic resonance of the $Nd_2Fe_{14}B$ magnet which has a tilted magnetization from the c axis at low temperatures by making use of the LLG method.

References

[1] Tatsuhiko Shirai, Synge Todo, Hans de Raedt, and Seiji Miyashita, in preparation.

[2] Takuya Hatomura, Bernard Barbara, and Seiji Miyashita, Phys. Rev. B **96**, 134309 (2017).

[3] T. Hatomura, J. Phys. Soc. Jpn. 86, 094002 (2017). T. Hatomura, New J. Phys. 20, 015010 (2018); Invited paper for the special issue “Focus on Shortcuts to Adiabaticity”.

[4] Adrien Bolens, Hosho Katsura, Masao Ogata, and Seiji Miyashita, Phys. Rev. B **95**, 235115 (2017).

[5] Adrien Bolens, Hosho Katsura, Masao Ogata, and Seiji Miyashita, Phys. Rev. B **97**, 161108 (2018).

[6] Hayate Nakano and Seiji Miyashita, in preparation.

[7] Masamichi Nishino, Seiji Miyashita, and Per Arne Rikvold, Phys. Rev. B **96**, 144425 (2017). Cristian Enachescu, et al. Laurentiu Stoleriu, Masamichi Nishino, Seiji Miyashita, Alexandru Stancu, Maciej Lorenc, Roman Bertoni, Herve Cailleau, and Eric Collet, Phys. Rev. B **95**, 224107 (2017).

[8] Satoshi Hirosawa, Masamichi Nishino and Seiji Miyashita, Adv. Nat. Sci.: Nanosci. Nanotechnol.**8**, 013002, (2017).

[9] Taichi Hinokihara, Masamichi Nishino, Yuta Toga, and Seiji Miyashita, Phys. Rev. B 97, 104427 (2018).

Pressure dependence of electronic structure and superconductivity in intercalated FeSe

Harald O. Jeschke
Research Institute for Interdisciplinary Science, Okayama University
Kita-ku, Okayama, Okayama 700-8530

Iron based superconductors are among the most intensively studied class of materials of the past decade. Significant insight into unconventional superconductivity was precipitated by the discovery of the first large family of high temperature superconductors since the discovery of the cuprates. At present, FeSe which belongs to the iron chalcogenide class of materials is at the forefront of theoretical and experimental efforts. In particular, the exceptionally large nematic region, the peculiar magnetism and the strong sensitivity to pressure are hot topics in this field. Among iron chalcogenide superconductors, FeS can be viewed as a simple, highly compressed relative of FeSe without nematic phase and with smaller electronic correlations. However, under pressure, the superconductivity of stoichiometric FeS disappears and reappears, forming two domes [1].

We perform electronic structure and spin fluctuation theory calculations for tetragonal FeS in order to analyze the nature of the superconducting order parameter. In random phase approximation we find a gap function with d wave symmetry at ambient pressure, in agreement with several reports of a nodal superconducting order parameter in FeS.

Our calculations show that as function of pressure, the superconducting pairing strength decreases until at 4.6 GPa, a Lifshitz transition happens in the electronic structure. Due to an additional hole like Fermi surface sheet, the pairing symmetry changes to sign changing s wave, and the pairing strength increases to a new maximum at 5.5 GPa as shown in Fig 1. Thus, the occurrence of two domes in the superconducting transition temperature can be linked to the occurrence of a Lifshitz transition in pressurized FeS [2].

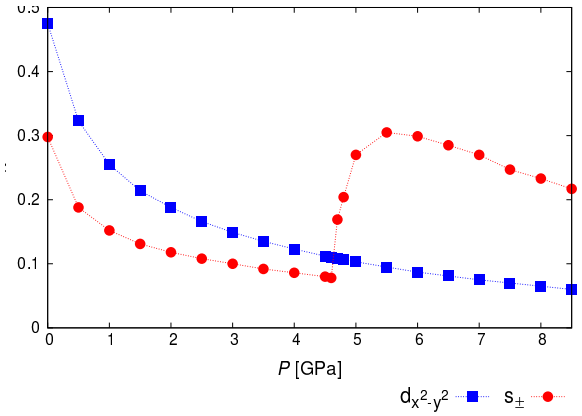

Figure 1: Pressure dependence of pairing eigenvalues λ in tetragonal FeS

References

[1] J. Zhang, F. L. Liu, T. P. Ying, N. N. Li, Y. Xu, L. P. He, X. C. Hong, Y. J. Yu, M. X. Wang, J. Shen, W. G. Yang, and S. Y. Li, npj Quantum Materials **2**, (2017) 49.

[2] M. Shimizu, N. Takemori, D. Guterding, and H. O. Jeschke: in preparation.

Emergent particles at deconfined quantum criticality

Hidemaro Suwa
Department of Physics, University of Tokyo
7-3-1 Hongo Bunkyo, Tokyo 113-0033

Many phase transitions are well described in the picture of the Landau-Ginzburg-Wilson (LGW) paradigm, where an effective action is expanded in powers of an order parameter and its derivatives. This paradigm is very powerful for understanding a generic phase transition and experimental results. Deconfined quantum criticality (DQC) is a non-trivial phenomenon beyond the LGW paradigm: an effective action in the low-energy limit is described by internal degrees of freedom or fractional excitations rather than the original degrees of freedom in a Hamiltonian. It is expected to appear at the quantum phase transition point between the Néel and the valence-bond-solid (VBS) phases. In terms of quantum spins, fractional excitations are spinons; while confined in the VBS phase, they are deconfined at the quantum critical point. Several numerical studies have reported evidence of a continuous phase transition and validity of DQC scenario at the phase transition points of the quantum spin systems, the classical loop model, the fermionic system coupled to Z_2 gauge fields, and so on. Moreover, the DQC can emerge on the surface of symmetry protected topological phases, which may be experimentally observed in the near future.

We numerically studied the criticality in the two-dimensional quantum spin system, namely the SU(2) J-Q model, in the use of the system B as a class C project (ID: H29-Ca-0097). Dynamical quantities were calculated using the worldline quantum Monte Carlo method with the generalized moment method and the analytic continuation. Independent worldline quantum Monte Carlo simulations with the single loop update were efficiently run by MPI parallelization.

If spinons are deconfined, the lowest singlet and triplet excited energies cost by two spinons should be identical in the thermodynamic limit. We tested this necessary condition estimating the singlet and triplet energy gaps at several wavevectors. Our simulations clarified that the singlet and triplet dispersions indeed converge to the same form and spinons are linearly dispersing around $k = (0, 0)$, $(\pi, 0)$, $(0, \pi)$, and (π, π) for the square lattice. Moreover, we showed that the velocity around these gapless points is unique, which is another strong evidence of spinon deconfinement.

In the meantime, the DQC theory predicts another emergent particle, a Higgs boson, around the transition point in a similar way to the Standard Model. It is intriguing to identify such an emergent particle in a material as well as the universe, which would show a universal mechanism working for both particle physics and condensed matter physics. To capture a hidden excitation, we studied the dynamical spin structure factor using the numerical analytic continuation. We found a nontrivial quasi particle excitation appearing both in the singlet and triplet sectors. Nevertheless, the identification has not been conclusive because of relatively large statistical noise. We will continue to run simulations for longer time and larger system sizes aiming at clear identification.

Rotational dynamics in $[C_n mim][PF_6]$ ionic liquids

Hailong PENG and Hayato SHIBA
Institute for Materials Research, Tohoku University
2-1-1, Katahira, Sendai 980-8577

We performed classical molecular dynamics simulation on 1-alkyl-3-methylimidazolium hexafluorophosphate ionic liquids (ILs). The bonded parameters of potential are based on OPLS-AA force field, and nonbonded parameters utilize Lennard-Jones formula with the Lorentz-Berthelot combining rules for different atomic pairs. All the force field parameters are taken from Zhong *et al.*,[1] where the hydrogens on the alkyl chain are incorporated within the carbon but the ones on the imidazolium ring are sustained. All the computer simulations are conducted by open source code package LAMMPS [2]. The simulated systems include 1000 ionic pairs, which are contained in a cubic box.

Important relaxation modes in these ILs include the transitional dynamics of the center of mass, rotational dynamics of the immidiazolum ring, and orientational dynamics of the alkyl chain. In our simulation study, we found the orientational dynamics of the alkyl chain is the slowest relaxation mode in the ILs with long alkyl chain, and accounts for the slow structural relaxation in the liquid. In order to highlight the role played by the rotational dynamics of the alkyl chain, we change the alkyl-chain length, i.e., in $[C_n mim][PF_6]$ (n =2, 4, 6, 8, 10, 12) ILs.

Upon cooling down the $[C_n mim][PF_6]$ ILs, structural relaxation time drastically increases with temperature decreasing. At the same temperature, the structural relaxation time also increases with alkyl-chain length. Transport coefficients, including self diffusion coefficient and shear viscosity, are calculated at different temperatures with the variation of alkyl chain. Stokes-Einstein relation, which connects diffusivity and viscosity in liquids, found to be broken down at low temperatures. The critical temperature points for the onset of the breakdown is found to decrease with the increment of alkyl chain length.

In order to reveal the coupling and decoupling behavior between the translational and rotational dynamics in these ILs. We measured the characteristic time for the translational dynamics via self-intermediate scattering function, and the time scale for rotational dynamics via self-correlation function of rotational vectors in terms of second Legendre polynomial.

At hight temperatures, the translational and rotational dynamics couple with each other. But they decouple with each other at low temperatures. The critical temperatures for the decoupling behavior is found to decrease with the alkyl-chain length. This decoupling behavior can possibly be connected with the breakdown of Stokes-Einstein relation. Further analysis is required to reveal the underlying mechanism.

References

[1] X. J. Zhong, Z. P. Liu, and D. P. Cao: J. Phys. Chem. B **115** (2011) 10027.

[2] S. Plimpton: J. Comput. Phys. **117** (1995) 1.

Majorana stripe order

Yoshitomo. Kamiya
RIKEN
Hirosawa, Wako, Saitama 351-0198

We studied a system of interacting Majorana fermions on a square lattice that may be realized on the surface of a three-dimensional topological insulator subject to a superconducting proximity effect and an external magnetic field. Specifically, we looked into the strong coupling limit of this problem (corresponding to the so-called neutrality condition [1]), which can be faithfully mapped to a quantum spin model with only local interactions. This spin model comprises four-spin interactions and two-spin interactions, some of which do not commute with each other. Most importantly, from a methodological viewpoint, this spin model can be studied with a quantum Monte Carlo simulation free from a negative sign problem. We employed the directed-loop algorithm and simulated the clusters of different system sizes with $L \times L$ up to $L = 60$ by using the resource of the Supercomputer Center, the Institute for Solid State Physics, the University of Tokyo. Such a cluster corresponds to $L \times (2L - 1)$ Majorana fermion modes, and the one for $L = 60$ is significantly larger than the system size in the the previous exact diagonalization study with only 60 Majorana fermion modes [1]. We found that the interacting Majorana fermions on the square lattice spontaneously breaks translational and rotational symmetries of the lattice, ordering into a novel state that we call a Majorana stripe state [2]. This corresponds to a fourfold degenerate ground state (modulo some one-dimensional gauge-like symmetries, which are not broken), inducing a finite-temperature phase transition. Our conclusion based on the much larger-scale quantum Monte Carlo simulations was in fact able to modify the one in the previous work [1], where a peculiar quantum critical behavior was conjectured based on the exact diagonalization study on a small cluster.

References

[1] C.-K. Chiu, D. I. Pikulin, and M. Franz: Phys. Rev. B **91** (2015) 165402.

[2] Y. Kamiya, A. Furusaki, J. C. Y. Teo, and G.-W. Chern: arXiv:1711.03632 (under review).

Numerical studies of bulk-edge correspondence in topological phases

Y. Hatsugai
Department of Physics, University of Tsukuba
1-1-1 Tennodai, Tsukuba 305-8571, Ibaraki, Japan

Bulk-edge correspondence[1] is a basic feature of topological phases, which has been intensively studied recently. Apart from the symmetry breaking, phases of matter can be distinguished based on the topology. Although topology is an abstract concept of mathematics, it is useful to classify phases of matter. It gives a new way of understanding of the phases and the novel class of the phase transition. Typical examples are the quantum Hall effects and Haldane phases of the 1D quantum spin chains of spin integers. "Topology" gives a new classification scheme of the phases, at least, theoretically. However in most cases, the topology is hidden, in a sense, they can not be observed directly. Also the system is (mostly) gapped and there is no low energy excitation. This feature is for the bulk. On the other hand, if the system is with boundaries or some geometrical perturbation as impurities, there exists low energy excitation which characterizes the topological phases. This is the bulk-edge correspondence. The bulk is characterized by the edge states and the localized states near the boundaries are governed by the non trivial bulk. Hidden topological feature of the bulk is directly observed through the edge states. Boundary (edge) currents of the quantum Hall states and the fractionalized (1/2) spins near the boundaries of the Haldane (integer) spin chain (Kennedy triplets) are the edge states governed by the principle. Also surface states of topological insulators observed by the ARPES is another recent typical example.

Although the bulk-edge correspondence has been mainly discussed for quantum systems, it is valid also for classical systems such as photonic crystals governed by the Maxwell equation and even mechanical systems obeying the Newton's law.

To establish the universal feature of the bulk-edge correspondence, we have performed several numerical studies. For the formation of the energy gap as a topological non-trivial vacuum, periodic structure due to lattice is useful. Then to investigate many body physics for the topological phases, we have constructed pseudo-potentials on various lattices[2] (See Fig.1)) and demonstrated its validity by showing topological quantum phase transition on a honeycomb lattice[3]. Also novel topological numbers associated with the entanglement hamiltonian is discussed in three dimension[4], which can be useful with interaction in principle. A classical analogue of diamond as the mechanical diamond is considered in relation to the chiral symmetry breaking and the Weyl points and the classical analogue of the Fermi arcs are discussed[5] (See Fig.2)).

References

[1] Y. Hatsugai, "Chern Number and Edge States in the Integer Quantum Hall effect", Phys. Rev. Lett. 71, 3697 (1993). DOI:10.1103/PhysRevLett.71.3697

[2] K. Kudo and Yasuhiro Hatsugai, "Many-Body Chern Numbers of $\nu = \frac{1}{3}$ and $\frac{1}{2}$ States on Various Lattices", J. Phys. Soc. Jpn. 86, 103701 (2017). DOI: 10.7566/JPSJ.86.103701

[3] K. Kudo and Y. Hatsugai, "Fractional Quantum Hall Effect in n = 0 Landau Band of Graphene with Chern Number Matrix", J. Phys. Soc. Jpn. to appear, arXiv:1803.09978.

[4] H. Araki, T. Fukui, and Y. Hatsugai, "Entanglement Chern number for three-dimensional topological insulators: Characterization by Weyl points of entanglement HamiltoniansMechanics", Phys. Rev. B 96, 165139 (1-8) (2017). DOI: 10.1103/PhysRevB.96.165139

[5] Y. Takahashi, T. Kariyado and Y. Hatsugai, "Weyl points of mechanical diamond", arXiv:1801.06784.

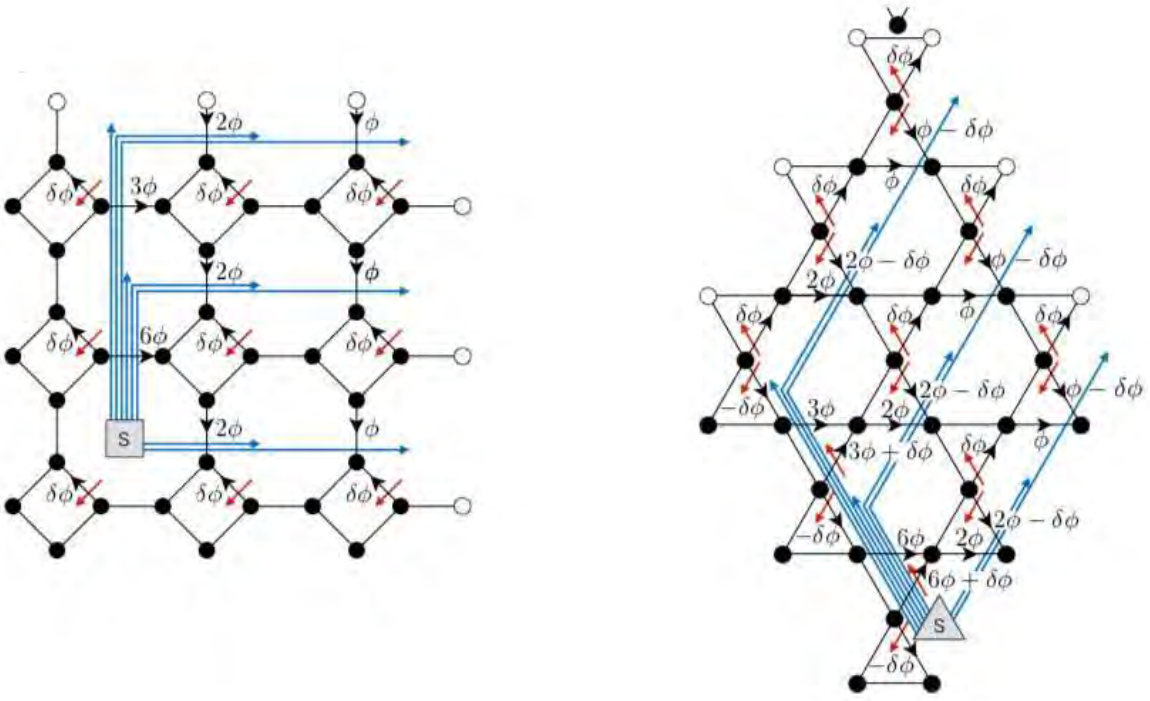

Figure 1: String gauges for square-octagon (left) and kagome (right) lattices [2].

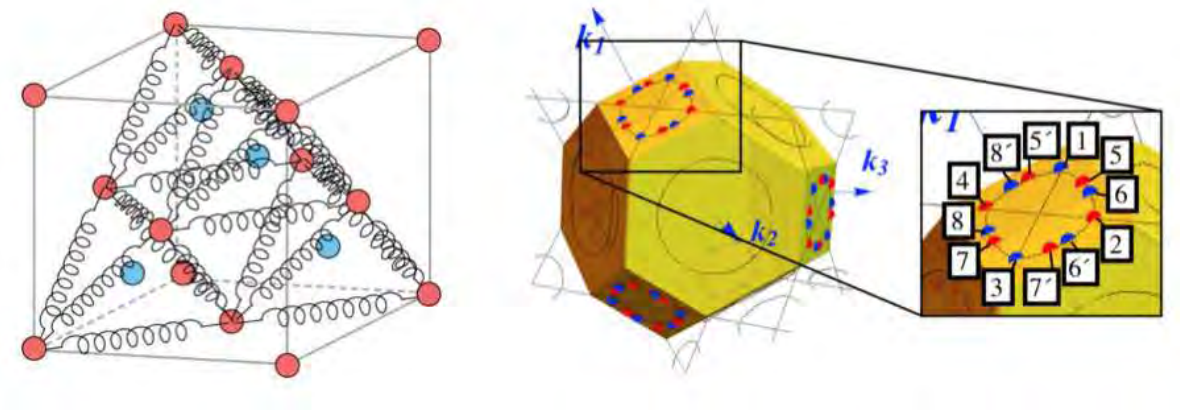

Figure 2: Mechanical diamond with next neighbor interaction (left) and its Weyl points(right) [5].

Molecular Dynamics Simulation Study of Crystal Nucleation Mechanism of Hydroxyapatite via Formation of Pre-Nucleation Clusters

Hiroki NADA

National Institute of Advanced Industrial Science and Technology (AIST),

16-1 Onogawa, Tsukuba, Ibaraki 305-8569

The crystal nucleation mechanism of hydroxyapatite (HAP) is an important research subject in connection with the development of biomaterials and water treatment materials. The nucleation of HAP crystals occurs via the formation of amorphous calcium phosphate (ACP), and the formation of ACP occurs via the formation of pre-nucleation clusters. Thus, it is important for understanding the mechanism of HAP crystal nucleation to elucidate a transition process from the structure of the clusters to that of ACP, in addition to a transition process from the structure of ACP to that of HAP.

However, the structure of the clusters is still poorly understood. This is because it is difficult to observe the clusters by experimental means. Therefore, molecular dynamics (MD) simulation was used for elucidating the structure of the clusters in this study.

The simulation was performed for three different clusters, $Ca_3(PO_4)_2\ 10H_2O$, $Ca_9(PO_4)_6\ 20H_2O$, and $Ca_9(PO_4)_6\ 30H_2O$ (hereafter, clusters A, B, and C, respectively). Simulation results suggested that the structures of clusters B (Figure 1) and C are more stable than the structure of cluster A. This result is consistent with a recent X-ray diffraction study, which suggested that cluster C may be a structural unit of ACP [2].

In addition, a large-scale MD simulation of bulk ACC was also performed. Simulation results indicated the existence of crystal-like short-range order in the atomic arrangement of the ACC [1]. However, more detailed studies are needed to elucidate whether the ordered atomic arrangement in the ACC is the same as that of cluster C (or cluster B).

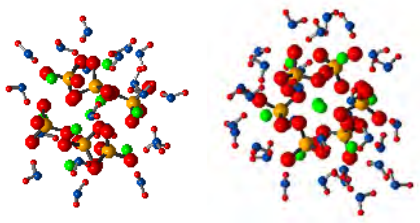

Fig. 1: The structures of clusters B (left-hand panel) and C (right-hand panel).

References

[1] L.-W. Du et al.: Cryst. Growth. Des. **13** (2013) 3103.

Analysis of magnetization reversal process based on atomistic models

Taichi HINOKIHARA

Graduate School of Science, The University of Tokyo, 7-3-1 Hongo, Bunyo-ku, Tokyo 113-8656, Japan

Analyzing the origin of the coercivity is important for developing high-performance permanent magnets. Recently, it has been reported that the physical properties, such as magnetization and anisotropy, have been successfully reproduced using an atomistic spin model derived from the first-principle calculations [1]. However, it is known that the coercivity strongly depends on the grain size due to the dipole-dipole interactions (DDI). Since it is difficult to evaluate such the effect by using the atomistic spin model, efficient method to calculate the DDI and an efficient coarse-graining method to reduce the number of spins are required. This year, we have proposed a new efficient method to calculate the long-range interacting system without any approximations [2]. The new method is based on the stochastic cut-off (SCO) method. Although the SCO method becomes efficient when systems have a simple lattice structure, our method enables us to calculate efficiently even in amorphous systems. We have applied this method to the atomistic model for $Nd_2Fe_{14}B$ magnets, and have confirmed that present method is approximately three times faster than the SCO method above the room temperatures.

We have also developed the coarse-graining method with variable spin momentum length. We first derive the momentum distribution for coarse-grained spins by means of the Wang-Landau method at given temperatures. Then, the exchange couplings between the coarse-grained spins are evaluated by adjusting physical quantities, such as the spin-spin correlations in both the atomistic and coarse-grained systems. We have confirmed that the magnetization, anisotropy, and domain wall width calculated by the coarse-grained model correspond reasonably well with those calculated by the atomistic model.

References

[1] Y. Toga, M. Matsumoto, S. Miyashita, H. Akai, S. Doi, T. Miyake, and A. Sakuma : Phys. Rev. B **94**, 174433 (2016).

[3] T. Hinokihara, M. Nishino, Y. Toga, and S. Miyashita: Phys. Rev. B **97,** 104427 (2018)

Deformation and fracture dynamics of crystalline polymers by large-scale coarse-grained molecular dynamics simulation

Yuji Higuchi
Institute for Solid State Physics, University of Tokyo
Kashiwa-no-ha, Kashiwa, Chiba 277-8581

We have studied fracture processes of polymers such as polyethylene [1, 2] and double-network gels [3] using coarse-grained molecular dynamics simulations. This year, we focused on fracture dynamics of the lamellar structure consisting of amorphous and crystalline layers in polyethylene. Tie chains and entanglements in amorphous layers connect solid crystalline layers, called as stress transmitters; however, their functions and differences are still unclear. Thus, their effects against the stretching is studied by large-scale coarse-grained molecular dynamics simulations on System B.

The stretching simulation of the lamellar structure consisting of 4×10^6 monomers (Fig. 1) is performed. Compression and voids are observed in amorphous layers, while crystalline layers are solid and not broken. To estimate local stress of stress transmitters, all forces are divided into two-body interaction and the stress is evenly divided into the monomers. Polymer chains in the amorphous layers are sorted into tie chains, entanglement, and so on. Then, the local stress for each types is estimated. The important results are as follows. (i) The local stress for tie chains and entanglements are almost equal against the stretching, whereas the stress for entanglements relaxes rapidly and is finally less than that for tie chains when the strain is fixed. (ii) The local stress for tie chains in each amorphous layer is equal although it was experimentally suggested that they are active and inactive [4]. (iii) The local stress for tie chains in the amorphous layers with defects becomes little larger than those without defects after voids are generated. This may correspond to the active and inactive states as suggested by the experiment. However, the difference appears only after the fracture, indicating the difficulty of the prediction of the broken layer.

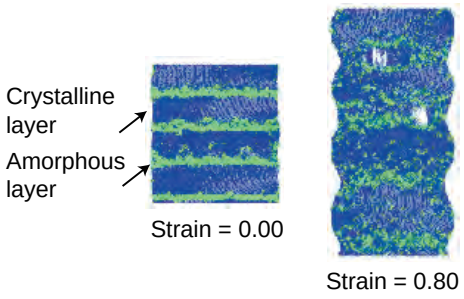

Figure 1: Deformation and fracture processes of lamellar structure in crystalline polymers.

References

[1] Y. Higuchi and M. Kubo: Macromolecules **50** (2017) 3690.

[2] Y. Higuchi: Polym. J. in press.

[3] Y. Higuchi, K. Saito, T. Sakai, J. P. Gong, and M. Kubo: Macromolecules in press.

[4] K. Nitta and M. Takayanagi: J. Macromol. Sci. B **42** (2003) 107.

Molecular Dynamics Simulation of Ferroelectrics Using a Shell Model III

T. Hashimoto

Research Center for Computational Design of Advanced Functional Materials (CD-FMat), National Institute of Advanced Industrial Science and Technology (AIST), Tsukuba Central 2, 1-1-1 Umezono, Tsukuba, Ibaraki 305-8568, Japan

(Ba,Sr)TiO_3 is a potential candidate for Pb free piezoelectric materials. $BaTiO_3$ undergoes phase transitions among, listing from high temperature to low temperature, cubic (C), tetragonal (T), orthorhombic (O), and rhombohedral (R) phases. (Ba,Sr)TiO_3 also undergoes phase transitions among the same phases, but the transition temperatures are shifted to the lower temperatures.

In this study, we performed molecular dynamics (MD) simulations using the shell model[1, 2]. We used an MD program developed by us. We used the smooth particle mesh Ewald method for computing the Coulomb interactions. We used MD cells made up with 12×12×12 unit cells. The cutoff length for the nonbonded interactions were 10.0 Å. We used the adiabatic method in which the shells are given a small mass. One MD step (Δt) was 0.1 fs. The Nosé-Hoover chain method and the Parrinello-Rahman method were used for generating constant temperature and constant pressure (NPT) ensembles. The externally applied pressure was set to 0 Pa.

The piezoelectric constants were calculated by[3] $d_{kij} = \frac{1}{k_B T} \langle \Delta M_k \Delta \eta_{ij} \rangle$. Here, $\eta_{ij} = \frac{1}{2}\left(H_0^{t-1} G H_0^{-1} - 1\right)$ is the strain tensor, where $G = H^t H$ with $H = \{\mathbf{a}, \mathbf{b}, \mathbf{c}\}$ representing the MD cell, and H_0 is the reference state of H. $\mathbf{M}$ is the total dipole moment of the MD cell. ΔX represents $X - \langle X \rangle$, where X is M_k or η_{ij}. The dielectric susceptibilities were calculated by $\chi_{\alpha\beta} \simeq \frac{1}{\varepsilon_0 < \Omega > k_B T} < \Delta M_\alpha \Delta M_\beta >$, where ε_0 and $< \Omega >$ are the permittivity of vacuum and the average of the volume of the MD cell, respectively.

First, we considered the x=0.25 system of $Ba_{1-x}Sr_xTiO_3$. The transition temperatures were shifted to the lower temperatures as shown by Tinte *et al.*[4], but the dielectric susceptibilities and the piezoelectric coefficients were not dramatically changed from the x=0 system for the x= 0.25 system. The detailed results will be published elsewhere.

References

[1] M. Sepliarsky, S. R. Phillpot, D. Wolf, M. G. Stachiotti, and R. L. Migoni, Appl. Phys. Lett. **76** (2000) 3986.

[2] T. Hashimoto and H. Moriwake, Mol. Simul. **41** (2015) 1074.

[3] A. García and D. Vanderbilt, Appl. Phys. Lett. **72** (1998) 2981.

[4] S. Tinte *et al.*, J. Phys.: Condens. Matter **16** (2004) 3495.

Quantum Annealing for Machine Learning

Shu TANAKA
Waseda Institute for Advanced Study, Waseda University
Nishi-waseda, Shinjuku, Tokyo, 169-8050

We have considered the performance of quantum annealing for machine learning. Quantum annealing is an algorithm to obtain better solutions of combinatorial optimization problem [1, 2]. This year, we focused on the following two topics.

(A) Simulated quantum annealing for clustering [3]

We proposed a scheme of simulated quantum annealing for machine learning previously [4, 5, 6]. In these studies, we considered the performance of hybrid quantum annealing for machine learning in which the temperature and quantum fluctuation decrease simultaneously by real-world data. In this project, to consider the performance of quantum annealing systematically, we compared the performance of simulated quantum annealing and that of simulated annealing for clustering by using artificially generated data. In addition, in order to determine the number of clusters, we used the concept of gap statistics. As a result, our calculation succeeded to obtain an appropriate clustering result which is consistent with the generated data.

This work was done in collaboration with Ryo Tamura (NIMS/The University of Tokyo).

(B) Dynamical properties of quantum annealing for singular value decomposition [7]

Hashizume et al. studied the framework of quantum annealing for singular value decomposition (SVD) previously [8]. In [8], they considered properties of quantum annealing for SVD in the adiabatic limit. In this project, we examined dynamic behavior of quantum annealing for SVD by solving the Schrödinger equation directly. As a result, we found that the setting of the initial gap is significant for the performance of quantum annealing for SVD.

This work was done in collaboration with Yoichiro Hashizume (Tokyo University of Science) and Ryo Tamura (NIMS/The University of Tokyo).

References

[1] T. Kadowaki and H. Nishimori: Phys. Rev. E **58** (1998) 5355.

[2] S. Tanaka, R. Tamura, and B. K. Chakrabarti: "Quantum Spin Glasses, Annealing and Computation" (Cambridge University Press, 2017).

[3] S. Tanaka and R. Tamura: in preparation.

[4] K. Kurihara, S. Tanaka, and S. Miyashita: Proceedings of the 25th Conference on Uncertainty in Artificial Intelligence (UAI2009).

[5] I. Sato, K. Kurihara, S. Tanaka, H. Nakagawa, and S. Miyashita: Proceedings of the 25th Conference on Uncertainty in Artificial Intelligence (UAI2009).

[6] I. Sato, S. Tanaka, K. Kurihara, S. Nakagawa, and H. Nakagawa: Neurocomputing, **121** (2013) 523.

[7] Y. Hashizume, R. Tamura, and S. Tanaka: in preparation.

[8] Y. Hashizume, T. Koizumi, K. Akitaya, T. Nakajima, S. Okamura, and M. Suzuki: Phys. Rev. E **92** (2015) 023302.

Investigation of Cell Elongation Effect on Collective Motion

Katsuyoshi Matsushita
Osaka University
Graduate School of Science, Toyonaka, Osaka 563-0043

The collective motion of cells is indispensable in the various biological processes. In this motion, cells align their polarities of movement (or their directions of cytoskeleton) in the same direction and directionally move with mechanically contacting with each other. The collective motion occurs on the based of the cell-cell communication through the cell-cell interaction. One of the important cell-cell interactions is the so-called contact inhibition of locomotion [1] and have intensively investigated in the researchers in the field of physics. This effect is regarded as an excluding volume effect associating with cell-cell adhesive contact between cells. This effect regulates cell polarities of movements and thereby drives the collective behavior of cells in their movement.

Excluding volume effect depends on the shape of cells and is possible to induce various collective behavior in the movement of cells. In particular, the elongated shape of cells has been investigad for suspended rigid bacteria in fluid and is known to crucially affect the order of movement [2]. In contrast, whereas a similar elongation has been well known in collective motions of cultured cells [3], the elongation effect on the order is not unclear today. Since the cultured cells can deform, the result in the rigid bacteria cannot be simply applied to them. Furthermore, the collective motion of cells in 2D culture medium largely differs from the bacteria swimming in fluid in their flocking mechanism because the cultured cells utilize the contact inhibition of locomotion in regulating the cell polarity of movement. These imply that the effect of excluding volume of elongated shape differs in the cases of bacterial and cultured cells. To clarify the effect on the cultured cells, the theoretical investigation based on thought experiment, which gives guidance information of the effect, is effective to design the experiment clarifying its effect because the corresponding experiment regulating the elongation is not so easy.

To investigate the effect of elongation in the case of cultured cells in medium, we consider in the cellular Potts model [4] with cell polarity of movements with feedback [5]. To do this, we assumed that the change in the elongation direction results in the elongation driven by the actin polymeraization. To the express the polymerization velocity $\dot{\rho}$ on the cellular Potts model, we introduce equivalent peripheral tension of cells, γ, as follows:

$$\gamma = \chi R \dot{\rho}, \tag{1}$$

where R is the reference radius of cell and χ is a certain constant representing response coefficient [6]. By considering the multipolar expansion along the polar angle of cell periphery [7, 8], we can derive both the propulsion force and the elongation force of cells, which are correlated with the cell polarity of movement. Furthermore, this formulation can express the softness of cell shape, in contrast to the previous investigation of rigid cell [9], because the elongation driven only by the tension in the present work differs from that driven by

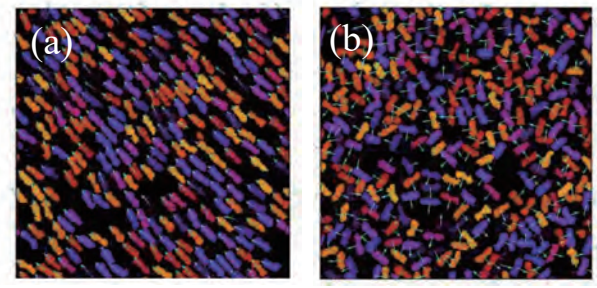

Figure 1: (a) unordering motion in cells elongated in the perpendicular direction of the cell polarity of movement and (b) ordering motion in cells elongated in the parallel direction of the cell polarity of movement.

rigidity energy from reference shape in the previous work.

By using this model, we examine the elongation direction dependence of the collective motion of cells. As a typical elongation, we consider the elongation in the perpendicular and parallel directions of the cell polarity of movement. The former and latter elongations are observed in wildtype and mutant of Dictyostelium Discoideum [10], respectively. As a result for same parameter sets excepting elongation directions, we observed the difference between their order of movement [11]: as shown in Fig. 1(a), we observed the order of movement and hence the collective motion for the cells perpendicularly elongated. Contrary to this, as shown in Fig 1(b), we did not observe the order of movement and individual diffusive motions. This result indicates that the elongation affects the formation of collective motion.

References

[1] R. Mayor and C. Carmona-Fontaine: Trends Cell Biol. . **12** (2010) 319.

[2] H. H. Wensink *et al.*: Proc. Natl. Acad. Sci. USA. **109** (2012) 14308.

[3] J. T. Bonner, *The Social Amoebae: The Biology of Cellular Slime Molds*, (Princeton University Press, 2008)

[4] J. A. Glazier and F. Graner Phys Rev, E **47** (1993) 2128; T. Hirashima *et al.*, Develop. Growth Differ. **59** (2017) 329.

[5] A Szabó *et al.*, Phys. Biol. **7** (2010) 046007.

[6] K. Matsushita, Proc. Sympo. Simul. Traffic Flow **22**, (2016) 5.

[7] K. Matsushita, Phys. Rev. E **95**, (2017) 032415.

[8] K. Matsushita, Phys. Rev. E **97**, (2018) 042413.

[9] R. M. H. Merks, *et al.*, Dev Biol. **289**, (2006) 44.

[10] Y. Asano *et al.*, Cytoskeleton **59**, (2004) 17.

[11] K. Matsushita, The abstract of the 55th Annual Meeting of the BSJ, (2017) 1Pos095.

Analysis on Structuring and Dynamics of Electrolyte Solutions Forming Electric Double Layer at Electrode Interfaces

Ken-ichi FUKUI

Department of Materials Engineering Science, Graduate School of Engineering Science, Osaka University, Machikaneyama, Toyonaka, Osaka 560-8531

Ionic liquids (ILs) are promising electrolytes for electrochemical devices such as secondary battery, capacitor, electric double layer (EDL)-FET, etc., due to their high chemical stability with negligible vaporization. Structuring and dynamics of the interfacial IL faced to a neutral graphite electrode or a negatively charged mica surface were analyzed by molecular dynamics (MD) calculations [1].

The MD simulations were performed with AMBER 11. The mica and graphite substrates consisted of unit cells of linear dimensions 73.9×68.3×20.0 Å^3 and 83.0×72.1 ×30.2 Å^3, respectively. For both systems, 800 BMIM-TFSI ion pairs (46000 atoms) were sandwiched between the substrates and a vacuum layer (> 4 nm). The systems were equilibrated at a constant volume for 100 ps, followed by a constant volume simulation for 5 ns with fixing all of the substrate atoms. The MD simulations were performed at 300, 350, 400, and 450 K.

As shown by the MD snapshot in Fig. 1, the density profile for both systems is modulated up to ~3 nm, but the analyses did not show apparent difference of the orientations and structures against the bulk liquid except for the first layer (z < 6 Å). The first layer was apparently more structured for the mica interface because of the larger interaction to the substrates. The two-dimensional arrangement of the first-layer ions are also specific to the substrates: two-dimensional ionic crystals for the mica substrate, and liquid or liquid crystals for the graphite substrate. Such structuring directly affects the mobility of ions at the interface These characteristic properties of the first layer are found to be consistent with the experimental results. Analyses of electrified (charged) interface for the graphite electrode are in progress.

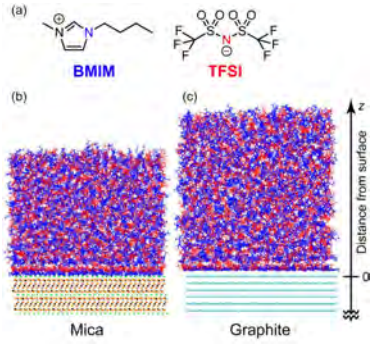

Fig. 1: (a) Ionic liquid (BMIM-TFSI) and (b)(c) MD snapshot for (b) mica and (c) graphite interfaces. BMIM cations and TFSI anions are represented by blue and red colors, respectively.

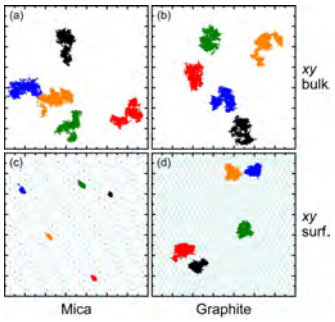

Fig. 2: XY contour maps (7×7 nm^2) for five BMIM cations during a 5 ns simulation (a)(b) at the bulk region and (c)(d) at the first layer (z < 6 Å); (a)(c) mica and (b)(d) graphite interfaces.

References

[1] Y. Yokota, H. Miyamoto, A. Imanishi, K. Inagaki, Y. Morikawa, K. Fukui, *Phys. Chem. Chem. Phys.* **20**, 6668-6676 (2018).

Design of organic structure-directing agents for the synthesis of zeolites with controlled active sites

Tatsuya Okubo
Department of Chemical System Engineering, The University of Tokyo
7-3-1 Hongo, Bunkyo-ku, Tokyo 113-8656

Syntheses of materials need to involve trial-and-error in time-consuming wet experiments. We have been working on the syntheses of zeolites with the aid of computational techniques to accelerate the speed of the material design. Zeolite is a class of crystalline microporous materials composed of tetrahedral atoms and oxygen atoms. Especially we focus on the crystal structures, chemical compositions, and atomic locations that are critical factors in the syntheses and applications of zeolites.

The site of Al in zeolite frameworks can influence the physicochemical properties of zeolites. It is of great interest to develop synthetic methods that allow for the siting Al into the specific tetrahedral sites (T-sites) within zeolite frameworks. The synthesis of zeolites with desired sites of Al, however, is very challenging mainly because of the unclarified formation mechanisms of zeolites and the limitation of analytical techniques. Thus far, some successes in controlling over the Al distribution in zeolite frameworks have been reported, but they have mainly relied on a trial-and-error approach by alteration of synthesis parameters such as types of organic structure-directing agents (OSDAs) and sources of Si and Al. Recently, computational calculations suggested that the placement of Al into the specific T-sites is not restricted as there exist thermodynamically favorable sites for Al in some zeolite frameworks[1, 2].

We synthesized IFR-type zeolite with controlled Al locations. The effects of OSDAs on the Al distribution were clarified by combining computational and experimental techniques. The molecular dynamics simulations on GULP suggested that the OSDAs are likely to be tightly fitted inside the zeolite cavities and can alter the relative stability of Al sites. IFR-type zeolites synthesized under an identical condition but with three different OSDAs were characterized by ^{27}Al solid-state NMR with the aid of DFT calculations using Quantum ESPRESSO. The results showed that the Al distribution of IFR-type zeolites can be tuned in accordance with energies derived from the zeolite–OSDA complexes. This combined computational and experimental approach provide a paramount step forward the rational synthesis of zeolites with controlled Al locations[3].

References

[1] K. Muraoka, W. Chaikittisilp, T. Okubo, Journal of the American Chemical Society, 2016, 51, 10718.

[2] M. D. Oleksiak, K. Muraoka, M.-F. Hsieh, M. T. Conato, A. Shimojima, T. Okubo, W. Chaikittisilp, J. D. Rimer, Angewandte Chemie International Edition, 2017, 56, 13366.

[3] K. Muraoka, W. Chaikittisilp, Y. Yanaba, T. Yoshikawa, T. Okubo, Angewandte Chemie International Edition, 2018, 57, 3742.

Dynamics of isolated quantum many-body spin systems

Takashi Mori
Department of Physics, University of Tokyo
Bunkyo-ku, Tokyo 113-0033, Japan

The adiabatic theorem in quantum mechanics tells us that if we change the parameter of the Hamiltonian infinitely slowly, the quantum system evolves without showing any excitation. However, an infinitely slow modulation of the Hamiltonian requires an infinitely long operation time. Since the coherence of a quantum system is destroyed due to the coupling to an external dissipative environment, a fast adiabatic control of the quantum system is desired.

Recently, theory of shortcuts to adiabaticity has been developed as a strategy to achieve adiabatic dynamics within a finite time [1, 2]. In this theory, non-adiabatic excitations are canceled out by applying the counter-diabatic driving field to the system [3]. A major difficulty of this method is that the Hamiltonian representing the counter-diabatic driving field is usually nonlocal and many-body operator, and therefore it is practically very difficult to implement such a driving field in experiment.

We have studied shortcuts to adiabaticity in many-body systems, and have found that shortcuts to adiabaticity tracking the instantaneous stationary states is possible by applying rather simple counter-diabatic fields, which is expressed by local magnetic fields, in *classical* spin systems [4]. In order to test this theory, I have performed numerical calculations of many-body dynamics in classical spin systems under the counter-diabatic driving. Since the theory requires a randomness in the counter-diabatic driving field, the ensemble average is calculated by performing parallel computations. As a result, it has been shown that the theory works very well, and we can realize the adiabatic tracking of the instantaneous stationary states within a finite time.

Our original motivation was to control adiabatic dynamics in many-body *quantum* systems. Although our proposal to achieve a shortcut to adiabaticity by a simple driving field is only applicable to classical spin systems, it is expected that we can obtain an approximate counter-diabatic driving field in quantum systems by considering the quantization of the classical counter-diabatic driving field [5]. It is a future problem to construct a good approximation of shortcuts to adiabaticity in quantum systems.

References

[1] M. Demirplak and S. A. Rice, J. Phys. Chem. A **107** (2003) 9937.

[2] M. V. Berry, J. Phys. A: Math. Theor. **42** (2009) 365303.

[3] A. del Campo, Phys. Rev. Lett. **111** (2013) 100502.

[4] T. Hatomura and T. Mori, in preparation.

[5] C. Jarzynski, Phys. Rev. E **95** (2017) 032122.

Effects of Z_3 anisotropy in antiferromagnetic XY model in a simple cubic lattice

Kazumasa HATTORI
Dept. of Physics, Tokyo Metropolitan University
Minami-Oosawa, Hachioji, Tokyo 192-0397

Antiferro 3-state Potts model in three-dimensional bipartite lattice is known to exhibit one (or two) phase transition(s) at finite temperature, while, at zero temperature, macroscopic degeneracy still remains due to the strong frustration[1, 2]. The nature of the partial-ordered state at finite temperature depends on the details of the lattice structure. For example, in a cubic or bcc lattices, the broken sublattice symmetry state is realized and for a diamond structure, permutationally symmetric sublattices state is favored.[3]

Recently, we have studied antiferro-quadrupole systems in a diamond structure on the basis of classical Monte Carlo simulations[4, 5], where we have analyzed an XY model with Z_3 single-ion anisotropy, which is a simple generalization of the 3-state Potts model. The macroscopic degeneracy in the 3-state Potts model at zero temperature is lifted in this model and the antiferro orders posses only 3 domains. Thus, it is interesting to examine how 3-state Potts model and the XY model with Z_3 anisotropy are related as a function of the anisotropy parameter.

In this study we have studied an antiferromagnetic XY model with Z_3 anisotropy $\sim \gamma \int d^3x \cos 3\theta(x)$ in a simple cubic lattice by using classical Monte Carlo simulations. We have mainly used the System-B F144 job for (up to) 888 parallelizations in order to obtain the data accuracy for low-temperature calculations. We find that there are two transitions for finite γ. One is the known 3d-XY type second-order transition and the other is the first-order at low temperature T^*. The existence of the second transition at T^* is clearly different from the case for the diamond structure model, where there is no such transition.[5] It turns out that T^* decreases as γ increases from the data for the system size up to 32^3. At the present status of the research, it is still insufficient to conclude the fate of T^* for $\gamma \to \infty$, and we need further efforts to analyze this system with larger system size and larger γ.

References

[1] J. R. Banavar, G. S. Grest, and D. Jasnow, Phys. Rev. Lett. **45**, 1424 (1980).

[2] A. Rosengren and S. Lapinskas, Phys. Rev. Lett. **71**, 165 (1993).

[3] S. Lapinskas and A. Rosengren: Phys. Rev. Lett. **81**, 1302 (1998).

[4] K. Hattori and H. Tsunetsugu: J. Phys. Soc. Jpn. **83**, 034709 (2014).

[5] K. Hattori and H. Tsunetsugu: J. Phys. Soc. Jpn. **85**, 094001 (2016).

Analysis of Glassy State of Bead-Spring Chains

Takahiro MURASHIMA
Shogo ASO
Department of Physics, Tohoku University,
Aramaki-Aza-Aoba, Aoba-Ward, Sendai, Miyagi 980-8578

We have studied a glassy polymer melt at high density using coarse-grained molecular dynamics simulation. The Kremer-Grest model [1] was used to represent a melt state of polymer chains. We used OCTA-COGNAC [2] to perform the molecular dynamics simulation. We have investigated the auto-correlation function of the stress and the radial distribution function in equilibrium state. The results are summarized in SA's thesis [3].

References

[1] K. Kremer, G. S. Grest: J. Chem. Phys. **92** (1990) 5057.
[2] http://octa.jp
[3] S. Aso: Master's Thesis (2018).

Structure and dynamics of tetrahedral liquids

Rui Shi and Hajime Tanaka
Department of Fundamental Engineering, Institute of Industrial Science, University of Tokyo
4-6-1 Komaba, Meguro-ku, Tokyo 153-8505

As the most abundant materials in our planet, water and silica play crucial roles in many biological, geological and industrial processes. Preferring local tetrahedral symmetry, they are both tetrahedral liquids. Water and silica have many similar but unique properties. For example, they both exhibit anomalous density maximum as a function of temperature in the liquid state [1]. Recently, we studied the density anomaly in water and silica by molecular dynamics simulations and found that the density anomaly commonly originates from the locally translational structural ordering in water and silica [2].

Besides density anomaly, water and silica also show unusual dynamics, known as " fragile-to-strong " transition [3, 4]. Their dynamic slowing down upon cooling shows a crossover from super-Arrhenius law at high temperature to Arrhenius law at low temperature. The origin of this dynamic anomaly is a hot topic and remains elusive until today.

Accessing to the microscopic information, molecular dynamics simulation provides a powerful tool to investigate the dynamic anomaly in water and silica. However, due to the extremely slow dynamics, the lack of simulation data at low temperatures largely obstructs the study of these important materials.

In this study, by utilizing the supercomputer at SCC-ISSP, the University of Tokyo, we are able to reach 2800 and 3000 K in our simulation of silica system, which is very low for this liquid.

For normal glass-forming liquids, dynamic heterogeneity, measured by dynamic susceptibility χ_4, monotonically increases with decreasing temperature. By analyzing the new data at low temperatures, however, we observed a maximum of dynamic susceptibility χ_4 at around 3500K for the first time, as shown in Fig.1. This is a crucial finding, since it suggests a two-state scenario, instead of popular glass transition scenario for the " fragile-to-strong " transition in silica.

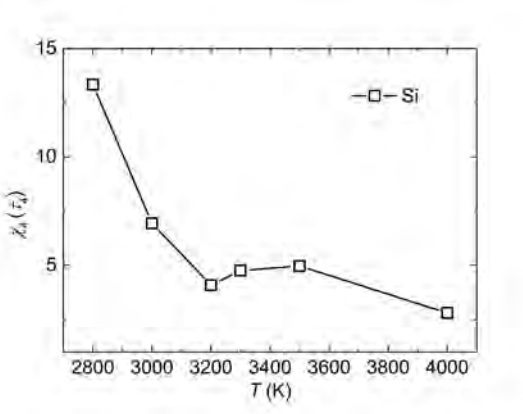

Figure 1: Dynamic susceptibility χ_4 of silicon in silica as a function of temperature. Based on this finding, we are now analyzing the local structure and dynamics of silica at these low temperatures.

Based on this finding, we are now analyzing the local structure and dynamics of silica at these low temperatures. We believe that the low temperature data of silica will provides new insight into the dynamic anomaly of the extremely important material, SiO2.

References

[1] CA. Angell, and H. Kanno: Science. 193 (1976) 1121.

[2] R. Shi, and H. Tanaka: Proc. Natl. Acad. Sci. U.S.A. 115 (2018) 1980.

[3] K. Ito, CT. Moynihan, and CA. Angell: Nature 398 (1999) 492.

[4] I. Saika-Voivod, PH. Poole, and F.Sciortino: Nature. 412 (2001) 514.

Study of finite-size effects on colloidal gelation originating from momentum conservation

Michio Tateno and Hajime Tanaka
Department of Fundamental Engineering, Institute of Industrial Science, University of Tokyo
4-6-1 Komaba, Meguro-ku, Tokyo 153-8505

The goal of this project is to reveal the physical mechanism of colloidal gel formation by focusing on the role of momentum conservation law imposed by a liquid component, i.e., hydrodynamic interactions (HI) between colloids. We previously showed that HI has crucial effects on the process of network structure formation in a colloidal suspension: hydrodynamic interactions tend to assist formation of elongated clusters rather than compact one due to "squeezing effects" originating from the imcompressibility of a liquid component, which is absent if HI is neglected [1, 2]. This further leads to the shift of the percolation threshold volume fraction toward a lower value compared to that of the corresponding Brownian dynamics simulation [2]. However, considering the nonlocal nature of HI, it is expected that these results may be affected by the system size. Moreover, colloidal gel intrinsically has a multiscale structure. Thus it is interesting to examine the influence of finite-size effects on the formation process of such structures in colloidal suspensions. To answer these questions, we numerically study the aggregation kinetics of colloidal particle with HI for different system sizes by using Fluid Particle Dynamics (FPD) method, which can properly incorporate many-body HI between colloids [3, 4].

In FPD method, we numerically solve the Navier-Stokes equation by approximating solid colloids as undeformable fluid particles. For simlations, however, there are two key time scales, the momentum diffusion time over the lattice unit and the colloid diffusion time over the size of a particle. Since there is a large gap between these two times scales, the study of slow dynamics of colloidal suspensions inevitably require an extremely high computational cost, which severely limits the size of simulations if we employ conventional codes (Open MP and/or MPI implementation). To overcome this problem, we implement GPU on our FPD codes utilizing a service provided by ISSP.

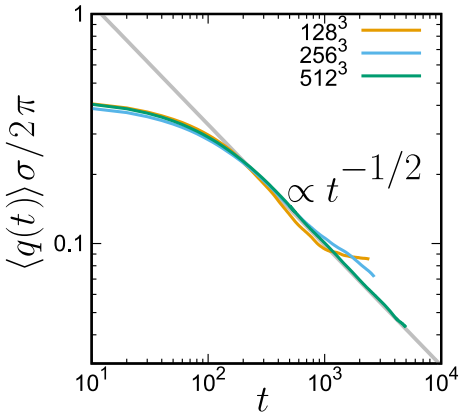

Figure 1: Time evolution of the characteristic wave number $\langle q(t)\rangle$ for various system sizes, $L^3 = 128^3, 256^3, 512^3$. Here we nomarilze $\langle q(t)\rangle$ with the diameter of colloids σ.

Figure 1 shows the temporal change of the characteristic wave number, $\langle q(t)\rangle$, defined as the first moment of the structure factor for different system sizes: $L^3 = 128^3, 256^3, 512^3$ in the lattice unit. (see Fig. 2) This characteristic wavenumber is inversely proportional to

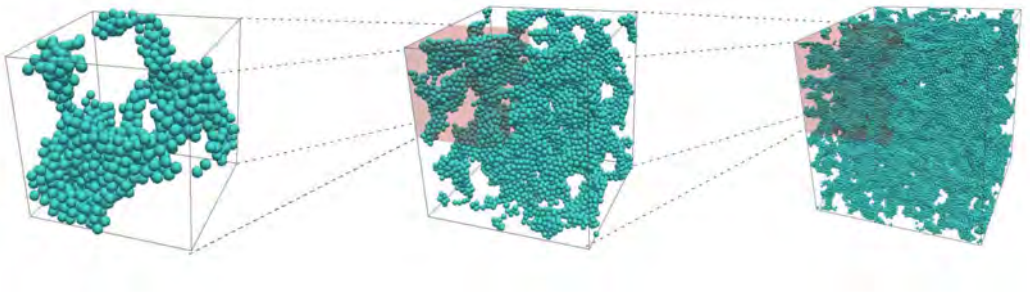

Figure 2: 3D structures of colloidal gels at time $t = 1000$ for different system size: $L = 128^3$(left), 256^3(middle), 512^3(right).

the typical size of the aggregates. Here we can see that all the samples show almost identical coarsening behaivour, decaying with power law whose the exponent is $1/2$ in the late stage. However, the results for $L^3 = 128^3, 256^3$ deviate from the power law decay at certain times. In contrast, the one for $L^3 = 512^3$ maintains the power law decay in the entire time range of the simulation. This tells us that the deviation from the power law decay should be a consequence of the finite size effects. We note that the similar exponent has been already reported in the network-forming process in colloidal systems [2, 5], but the range of the power law decay observed there was too narrow to justify its power law nature in a convincing manner. In the largest system, we can see, for the first time, that the power law regime can extend over one order of magnitude. Furthermore, we also analyze the data based on the dynamic scaling law and find that the distribution functions characterizing the phase-separation structures (more specifically, the structure factor and the chord distribution function) can be collapsed on single master curves after scaling with the growth exponent $1/2$. These results imply the self-similar nature of the coarsening of this phenomena and the presence of a unique physical mechanism behind this coarsening process.

In summary, we performed numerical simulations of colloid phase separation by the FPD method, which can deal with many-body hydrodynamic interaction between colloids, and systematically examined the system-size dependence of network-forming phase separation. We found that the power law growth of the exponent $1/2$ continues over one decade for a system of the largest size and the coarsening process has self-similarity. The physical mechanism responsible for such a power law growth is now under investigation. Our simulation method also allows us to access the detailed information during the process of coarsening, particularly, spatio-temporal organization of the flow field of a liquid component, which is induced by self-assembly of colloids and stress generated during aggregation. We are planning to address these interesting fundamental open questions.

References

[1] K. Kamata, T. Araki and H. Tanaka: Phys. Rev. Lett. **102**, (2010) 108303.

[2] A. Furukawa and H. Tanaka: Phys. Rev. Lett. **104**, (2010) 245702.

[3] H. Tanaka and T. Araki: Phys. Rev. Lett. **85**, (1999) 1338

[4] A. Furukawa, M. Tateno and H. Tanaka: accepted to Soft Matter.

[5] H. Tanaka, Y. Nishikawa and T. Koyama: J. Phys.: Condens. Matter **17** (2005) L143.

Calculation of ordered structures and their optical properties of soft materials

Jun-ichi FUKUDA

Department of Physics, Kyushu University, Motooka 744, Nishi-ku, Fukuoka 819-0395

In this project, we studied particularly the optical properties of exotic structures exhibited by a chiral liquid crystal confined between two parallel substrates. In previous numerical studies [1], I showed that a highly chiral liquid crystal under such circumstances exhibits various exotic structures containing topological defects, depending on the spacing between the confining substrates and temperature. These structures include a hexagonal lattice of half-Skyrmions whose typical spacing is a few hundred nanometers.

My experimental collaborators were motivated by my previous theoretical studies to carry out experiments, and observed a hexagonal array of dark spots in a thin film of a chiral liquid crystal under a conventional optical microscope with high numerical aperture. One of the main goals of this project was to confirm whether they really observed a lattice of half-Skyrmions. As mentioned above, the typical periodicity of the structures is a few hundred nanometers, and therefore theoretical interpretation of the microscope images is highly challenging because geometrical optics commonly used to explain the principles of optical microscopy is totally useless.

I solved the full Maxwell equations for the electromagnetic wave to investigate the response of the liquid crystal to monochromatic incident light. My calculation was based on plane-wave expansion along the in-plane directions, and finite-difference discretization along the direction normal to the confining substrates. The matrix for the resulting large set of linear equations was of tridiagonal form thanks to the above-mentioned finite-difference discretization, which reduced substantially the amount of numerical resources necessary for solving the equations. The profile of the dielectric tensor in the Maxwell equations was assumed to be linearly dependent of the orientational order parameter of second-rank tensor, which was determined by separate calculations minimizing the free energy functional of the liquid crystal in terms of the order parameter.

In Fig. 1, we show a typical profile of the liquid crystal exhibiting a hexagonal lattice of half-Skyrmions, and a calculated optical image. The calculated image contains a hexagonal array of dark spots as experimental ones do. We also did calculations for different structures of the liquid crystal, and compared the resulting

optical images with experimental ones. From all the calculation results, we concluded that the experimental microscope image with a hexagonal array of dark spots is indeed that of a hexagonal array of half-Skyrmions [2].

I also carried out calculations to elucidate the Kossel diagrams visualizing the directions of strong Bragg reflections from a sample with crystalline order. Some results on the exotic structures of a chiral liquid crystal known as cholesteric blue phases are presented in Ref. [3]. I am also investigating what Kossel diagrams for a thin system of a liquid crystal as mentioned above should be like, and I hope the results will be able to be presented next time.

References

[1] J. Fukuda and S. Žumer, Nature Commun. **2**, 246 (2011); Phys. Rev. Lett. **106**, 097801 (2011); Phys. Rev. Lett. **104**, 017801 (2010).

[2] A. Nych, J. Fukuda, U. Ognysta, S. Žumer and I Muševič, Nature Phys. **13**, 1215 (2017).

[3] J. Fukuda, Y. Okumura and H. Kikuchi, Proc. SPIE **10555**, 105550A (2018).

Fig. 1. Structure of a chiral liquid cell (top) and its calculated optical image (bottom). In the former, orientational order at the midplane (short rods) and topological defect lines (red surfaces) are shown. The optical image of the former corresponds to that in the rectangle in the latter.

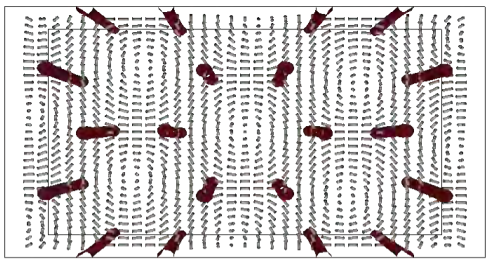

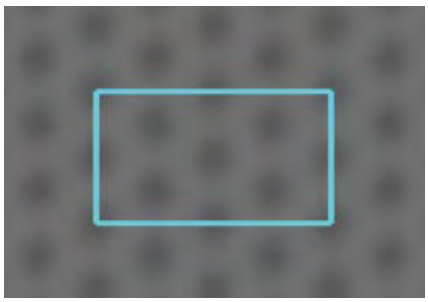

Ground State of an Anisotropic $S=1/2$ Two-Leg Ladder with Different Leg Interactions

Takashi Tonegawa

Professor Emeritus, Kobe Univ. and Visiting Professor, Osaka Prefecture Univ.

This report aims at exploring the ground-state phase diagram of an anisotropic $S=1/2$ two-leg ladder with different leg interactions by using mainly numerical methods. We express the Hamiltonian which describes this system as

$$\begin{aligned}\mathcal{H} = & J_{\rm leg,a}\sum_{j=1}^{L}[\vec{S}_{j,a},\,\vec{S}_{j+1,a}]_{\rm leg} \\ & + J_{\rm leg,b}\sum_{j=1}^{L}[\vec{S}_{j,b},\,\vec{S}_{j+1,b}]_{\rm leg} \qquad (1) \\ & + J_{\rm rung}\sum_{j=1}^{L}[\vec{S}_{j,a},\,\vec{S}_{j,b}]_{\rm rung}\end{aligned}$$

with

$$\begin{aligned}&[\vec{S}_{j,\ell},\,\vec{S}_{j+1,\ell}]_{\rm leg} \\ &\quad \equiv S^x_{j,\ell}S^x_{j+1,\ell}+S^y_{j,\ell}S^y_{j+1,\ell}+\Delta_{\rm leg}S^z_{j,\ell}S^z_{j+1,\ell}\,, \qquad (2)\\ &[\vec{S}_{j,a},\,\vec{S}_{j,b}]_{\rm rung} \\ &\quad \equiv \Gamma_{\rm rung}\{S^x_{j,a}S^x_{j,b}+S^y_{j,a}S^y_{j,b}\}+S^z_{j,a}S^z_{j,b}\,. \qquad (3)\end{aligned}$$

Here, $\vec{S}_{j,\ell}=\left(S^x_{j,\ell},\,S^y_{j,\ell},\,S^z_{j,\ell}\right)$ is the $S=1/2$ operator acting on the jth rung of the $\ell(=a$ or $b)$ leg; $J_{{\rm leg},a}$ and $J_{{\rm leg},b}$ denote, respectively, the magnitudes of the a and b leg interactions; $J_{\rm rung}$ denotes that of the rung interaction, $\Delta_{\rm leg}$ and $\Gamma_{\rm rung}$ are, respectively, the parameters representing the XXZ-type anisotropies of the former and latter interactions; L is the total number of rungs, which is assumed to be even. It should be noted that this system has a frustration when $J_{{\rm leg},a}J_{{\rm leg},b}<0$ irrespective of the sign of $J_{\rm rung}$.

There exist five interaction parameters in our Hamiltonian $\mathcal{H}$. Throughout the following discussions, we focus our attention upon the case where $J_{{\rm leg},a}=0.2$, $-2.0\le J_{{\rm leg},b}\le 3.0$, $J_{\rm rung}=-1.0$, $\Gamma_{\rm rung}=0.5$, and $0\le\Delta_{\rm leg}\le 1$. Here, we choose $|J_{\rm rung}|$ as the unit of energy. It is noted that the anisotropies of the leg and rung interactions are, respectively, of the XY and Ising types. The motivation of treating this case is as follows. When the ferromagnetic rung interactions with Ising-type anisotropy are much stronger than both of two kinds of the leg interactions ($|J_{{\rm leg},b}|\ll 1.0$), a pair of $S=1/2$ spins at each rung forms a bound state with $S^z_{j,a}+S^z_{j,b}=\pm 1$. This may lead to the spin-nematic Tomonaga-Luttinger liquid (TLL) state, which accompanies two-magnon bound states, as the ground state at least in the frustrated region. Furthermore, the XY-type anisotropy of the leg interactions is expected to stabilize the nematic TLL state.

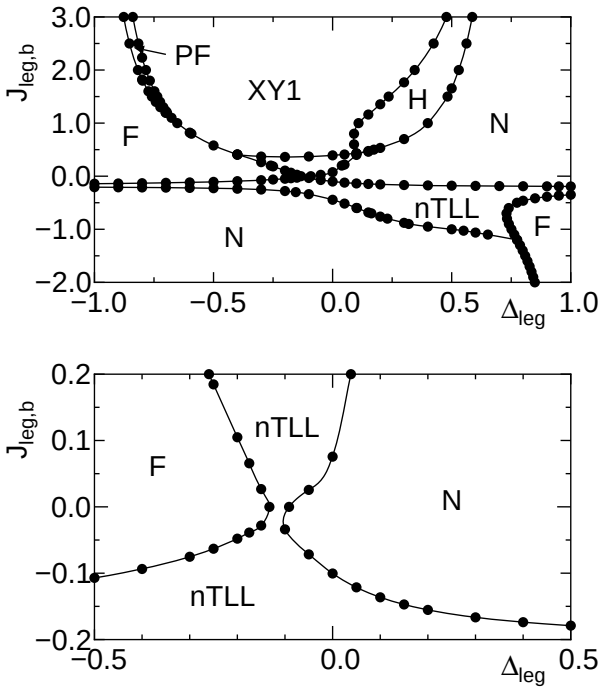

Figure 1: The whole view (top) and an enlarged view around the origin (bottom) of the ground-state phase diagram on the $\Delta_{\rm leg}$ versus $J_{{\rm leg},b}$ plane in the case where $J_{{\rm leg},a}=0.2$, $J_{\rm rung}=-1.0$, and $\Gamma_{\rm rung}=0.5$, obtained in the present work.

Figure 1 shows our final result for the ground-state phase diagram on the $\Delta_{\rm leg}$ versus $J_{{\rm leg},b}$ plane, which has been determined by using a variety of numerical methods based on the exact diagonalization (ED) calculation. This phase diagram consists of the six kinds of phases; these are the ferromagnetic (F), partial ferrimagnetic (PF), $XY1$, Haldane (H), Néel (N), and nematic TLL (nTLL) phases. It is noted that the nTLL phase appears as the ground state in the strong-rung frustrated region ($-1.0<J_{{\rm leg},b}<0.0$), as is expected, and survives even in the strong-rung unfrustrated region

($0.0 \leq J_{\mathrm{leg},b} \lesssim 0.4$).

At this junction, we denote, respectively, by $E_0^{\mathrm{P}}(L,M)$ and $E_1^{\mathrm{P}}(L,M)$, the lowest and second-lowest energy eigenvalues of the Hamiltonian $\mathcal{H}$ under the periodic boundary condition within the subspace characterized by L and M, where M is the total magnetization which is a good quantum number with the eigenvalues of $M=0$, ± 1, $\cdots$, $\pm L$. We also denote by $E_0^{\mathrm{T}}(L,M)$ the lowest energy eigenvalue of $\mathcal{H}$ under the twisted boundary condition within the subspace determined by L and M. We have numerically calculated these energies for finite-size systems with up to $2L=28$ spins by means of the ED method. The ground-state energy $E_{\mathrm{g}}(L)$ is given by the minimum value among $E_0^{\mathrm{P}}(L,0)$, $E_0^{\mathrm{P}}(L,\pm 1)$, $\cdots$, $E_0^{\mathrm{P}}(L,\pm L)$, and the ground-sate magnetization $M_{\mathrm{g}}(L)$ is the value of M giving $E_{\mathrm{g}}(L)$. It is noted that $M_{\mathrm{g}}(L)=0$ in the $XY1$, H, N, and nTLL states, $0<M_{\mathrm{g}}(L)<L$ in the PF state, and $M_{\mathrm{g}}(L)=L$ in the F state. Furthermore, we introduce the following three excitation energies:

$$\Delta E_0^{\mathrm{P}}(L,M) = E_0^{\mathrm{P}}(L,M) - E_0^{\mathrm{P}}(L,0)\,, \quad (4)$$

$$\Delta E_1^{\mathrm{P}}(L,0) = E_1^{\mathrm{P}}(L,0) - E_0^{\mathrm{P}}(L,0)\,, \quad (5)$$

$$\Delta E_0^{\mathrm{T}}(L,0) = E_0^{\mathrm{T}}(L,0) - E_0^{\mathrm{P}}(L,0)\,. \quad (6)$$

Let us now discuss how to numerically determine the phase boundary lines shown in Fig. 1. In the following way, we estimate the finite-size critical values of $J_{\mathrm{leg,b}}$ (or Δ_{leg}) for various values of Δ_{leg} (or $J_{\mathrm{leg,b}}$) for each phase transition. Then, the phase boundary line for the transition is obtained by connecting the results for the $L\to\infty$ extrapolation of the finite-size critical values.

Firstly, the phase transition between the N and nTLL phases is of the Berezinskii-Kosterlitz-Thouless (BKT) type [1] with accompanying the spontaneous translational-symmetry breaking [STSB], and therefore, as is well known, the phase boundary line can be accurately estimated by the level spectroscopy (LS) method developed by Okamoto and Nomura [2]. That is to say, we numerically solve the equation,

$$\Delta E_1^{\mathrm{P}}(L,0) = \Delta E_0^{\mathrm{P}}(L,2)/2 \quad (7)$$

to calculate the finite-size critical values.

Secondly, according to the above LS method [2], the finite-size critical values for the phase transition between the $XY1$ and nTLL phases are estimated from the equation,

$$\Delta E_0^{\mathrm{P}}(L,1) = \Delta E_0^{\mathrm{P}}(L,2)/2\,. \quad (8)$$

Thirdly, the phase transition between the $XY1$ and H phases is the BKT transition [1] without the STSB. It is also well known that, in this case, Nomura and Kitazawa's LS method [3] is very powerful to determine the phase boundary line. The finite-size critical values for this transition are calculated by using the equation,

$$\Delta E_0^{\mathrm{P}}(L,2) = \Delta E_0^{\mathrm{T}}(L,0)\,. \quad (9)$$

Fourthly, since the phase transition between the H and N phases is the 2D Ising-type transition, the phase boundary line between these two phases can be estimated by the the phenomenological renormalization group (PRG) method [4]. Then, the finite-size critical values for this transition are calculated by solving the PRG equation,

$$L\,\Delta E_1^{\mathrm{P}}(L,0) = (L+2)\,\Delta E_1^{\mathrm{P}}(L+2,0)\,. \quad (10)$$

Lastly, the results of our calculations show that the phase transition between the F and PF phases is of the second-order, and therefore the finite-size critical values for this transition are estimated from the equation,

$$\Delta E_0^{\mathrm{P}}(L,L) = \Delta E_0^{\mathrm{P}}(L,L-1)\,. \quad (11)$$

These results also show that the phase transition between the PF and $XY1$ phase is of the second-order or the first-order depending on whether $J_{\mathrm{leg},b} \gtrsim 1.55$ or $1.55 \gtrsim J_{\mathrm{leg},b} \gtrsim 1.2$. This means that the finite-size critical values for this transition in the former region of $J_{\mathrm{leg},b}$ are calculated from

$$\Delta E_0^{\mathrm{P}}(L,1) = 0\,, \quad (12)$$

while these in the latter region of $J_{\mathrm{leg},b}$ are from

$$\Delta E_0^{\mathrm{P}}(L,M_{\mathrm{g}}(L)) = 0\,, \quad (13)$$

where $1<M_{\mathrm{g}}(L)<L$. Furthermore, it is apparent that the finite-size critical values for the phase transitions between the F and one of the $XY1$, N, and nTLL phases, being of course the first-order ones, are estimated by using the equation,

$$\Delta E_0^{\mathrm{P}}(L,L) = 0\,. \quad (14)$$

This work has been done in collaboration with T. Hikihara, K. Okamoto, S. C. Furuya, and T. Sakai.

[1] Z. L. Berezinskii, Sov. Phys. JETP **34**, 610 (1971); J. M. Kosterlitz and D. J. Thouless, J. Phys. C **6**, 1181 (1973).
[2] K. Okamoto and K. Nomura, Phys. Lett. A **169**, 433 (1992); K. Nomura and K. Okamoto, J. Phys. Soc. Jpn. **62**, 1123 (1993); K. Nomura and K. Okamoto, J. Phys. A **27**, 5773 (1994).
[3] K. Nomura A. and Kitazawa, J. Phys. A **31**, 7341 (1998).
[4] M. P. Nightingale: Physica A **83** (1976) 561.

Effect of interface on the structure and properties of water confined in nanopore

Tomoko MIZUGUCHI[1], Katsumi HAGITA[2], and Susumu FUJIWARA[1]

[1]*Faculty of Materials Science and Engineering, Kyoto Institute of Technology, Matsugasaki, Sakyo-ku, Kyoto 606-8585*
[2]*Department of Applied Physics, National Defense Academy, 1-10-20, Hashirimizu, Yokosuka, Kanagawa 239-8686*

It is important to understand the properties of supercooled water in many fields such as life sciences, but the research of supercooled water is generally difficult since bulk water crystallizes at deeply supercooled conditions. S.-H. Chen and his co-workers investigated the dynamics of deeply supercooled water confined in nanopores where crystallization of water is prevented, and observed the crossover phenomenon that the temperature dependence of relaxation time changes at a certain temperature [1, 2]. However, it is premature to conclude that this phenomenon occurs in bulk water as well. Indeed, it was reported that confined water can be divided into bound water and free water by their diffusion coefficients [3]. The relationship between these two types of water dynamics and the dynamic crossover phenomenon is not necessarily clear. It is very important to accurately estimate the influence of the interface. To this end, we performed molecular dynamics (MD) simulations of water confined in a nanopore of amorphous silica using the reactive force filed (ReaxFF).

The pore system was created as follows. First, bulk amorphous silica was prepared at 3000 K and 1 atm in the NP_zT ensemble using Morse potential [4], where z direction is parallel to the axis of a cylindrical pore which was created later. Next, switching to ReaxFF MD simulation, the system was relaxed for 200 ps at 3000 K and 1 atm in the NP_zT ensemble, then quenched to 300 K at a cooling rate of 15 K/ps in the NVT ensemble. After 300 ps relaxation at 300 K and 1 atm in the NPT ensemble, a cylindrical pore with a diameter of 2.7 nm was created by removing atoms, and furthermore, some oxygen atoms at the pore surface were removed so that the ratio of the numbers of Si and O became 1:2. We then put water in the pore, and performed MD calculation for 20 ps only for water using TIP3P model with silica immobilized. Finally, ReaxFF MD simulation including silica was started at 300 K and 1 atm in the NPT ensemble. The ReaxFF parameters used in this study were developed in 2015 by Yeon and van Duin to simulate the water/silica interface [5]. All the simulations were conducted with LAMMPS [6], and the ReaxFF MD simulations were performed with the USER-REAXC package of LAMMPS.

Once the ReaxFF MD simulation was started in the system including silica and water, chemical reactions occured between silica surface and water, and silanol groups (-SiOH) were produced. Figure 1 shows the time evolution of the number of silanol groups. We determined the formation of a silanol group only by interatomic distances, and the number of silanol groups is set to 0 at the starting time of MD calculation. It is found that silanol groups are formed in a short time.

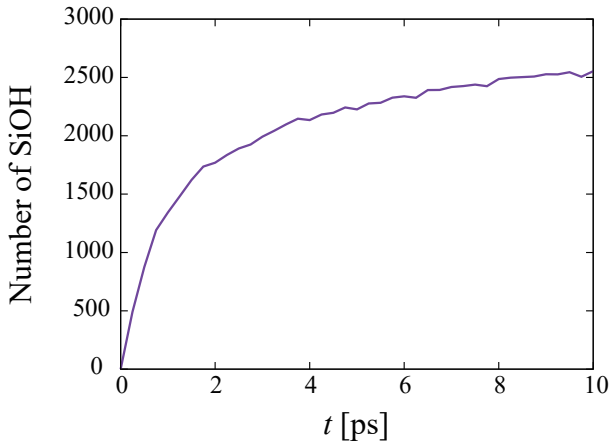

Figure 1: Time evolution of the number of silanol groups.

References

[1] A. Faraone, L. Liu, C.-Y. Mou, C.-W. Yen, and S.-H. Chen: J. Chem. Phys. **121** (2004) 10843.

[2] X.-Q. Chu, A. I. Kolesnikov, A. P. Moravsky, V. Garcia-Sakai, and S.-H. Chen: Phys. Rev. E **76** (2007) 021505.

[3] T. Yamada, R. Yonamine, T. Yamada, H. Kitagawa, M. Tyagi, M. Nagao, and O. Yamamuro: J. Phys. Chem. B **115** (2011) 13563.

[4] S. Leroch and M. Wendland: J. Phys. Chem. C **116** (2012) 26247.

[5] J. Yeon and A. C. T. van Duin: J. Phys. Chem. C **120** (2016) 305.

[6] S. Plimpton: J. Comput. Phys. **117** (1995) 1.

Transport phenomena and optical tomography

Manabu Machida
Institute for Medical Photonics Research
Hamamatsu University School of Medicine, Hamamatsu 431-3192

Let us begin with the time-independent radiative transport equation given by

$$\begin{cases} (\theta\cdot\nabla+\mu_a+\mu_s)\,I(x,\theta)=\mu_s \\ \times\int_{S^2}p(\theta,\theta')I(x,\theta')\,d\theta', \quad (x,\theta)\in R^3_+\times S^2, \\ I(x,\theta)=g(x,\theta), \quad (x,\theta)\in\Gamma_-, \end{cases}$$

where $I(x,\theta)$ $(x\in R^3,\ \theta\in S^2)$ is the specific intensity of light propagating in random media such as turbid liquids or biological tissue, $p(\theta,\theta')$ is the scattering phase function, and R^3_+ and $\Gamma_\pm$ are defined as $R^3_+ = \{x\in R^3;\, x_3>0\}$, $\Gamma_\pm=\{(x,\theta)\in\partial\Omega\times S^2;\, \mp\hat{z}\cdot\theta>0\}$, with $\hat{z}={}^t(0,0,1)$.

We assume that $\mu_s>0$ is a constant but μ_a spatially varies as

$$\mu_a(x)=\bar{\mu}_a+\delta\mu_a(x),$$

with a constant $\bar{\mu}_a$. We assume that $\mu_s,\bar{\mu}_a$ are known but $\delta\mu_a(x)$ is unknown. We also assume a spatially-varying boundary source given by

$$g(x,\theta)=e^{iq_0\cdot\rho}\delta(\theta-\theta_0),$$

where $\rho={}^t(x_1,x_2)$, $q_0\in R^2$, and $\theta_0\in S^2$. We suppose that the exitance or hemispheric flux J_+ is measured on the boundary at $x_3=0$. The exitance is defined as

$$J_+(\rho)=\int_{S^2_+}(\theta\cdot\hat{z})I(\rho,0,-\theta)\,d\theta.$$

Let $J^{(0)}_+(\rho)$ be the exitance in the absence of $\delta\mu_a$. We obtain within the first Born approximation

$$J^{(0)}_+(\rho)-J_+(\rho)=(\theta_0\cdot\hat{z})\int_{S^2}\int_{R^3_+}$$
$$\times\left[\int_{S^2_+}(\theta\cdot\hat{z})G(x',-\theta';\rho,0,\theta)\,d\theta\right]\delta\mu_a(x')$$
$$\times\left[\int_{R^2}G(x',\theta';\rho'',0,\theta_0)e^{iq_0\cdot\rho''}\,d\rho''\right]dx'd\theta'.$$

The absorption inhomogeneity $\delta\mu_a$ is thus reconstructed from the above inverse problem, which we can solve by singular value decomposition with a suitable regularization. We will use the three-dimensional F_N method [1] to compute the Green's function $G(x,\theta;\rho_0,0,\theta_0)$.

When the Green's function is calculated with the three-dimensional F_N method, the following functions $\mathcal{J}^{(-)jm'}_{lm}$ have to be computed.

$$\mathcal{J}^{(-)jm'}_{lm}=\frac{\mu_s\xi_j}{2}(-1)^{l+1}\sqrt{\frac{2l+1}{4\pi}\frac{(l-m)!}{(l+m)!}}$$
$$\times[\mathrm{sgn}(m')]^{m'}\frac{\sqrt{(2|m'|)!}}{(2|m'|-1)!!}\sum_{m''=-|m'|}^{|m'|}(-1)^{m''}$$
$$\times\sqrt{\frac{(|m'|-m'')!}{(|m'|+m'')!}}d^{|m'|}_{m'',-m'}[i\tau(\xi_j|q|)]$$
$$\times\int_{S^2_+}\frac{g^{m'}\left(-\xi_j,\hat{k}_z\mu+i\xi_j|q|\sqrt{1-\mu^2}\cos\varphi\right)}{\xi_j+\hat{k}_z\mu+i\xi_j|q|\sqrt{1-\mu^2}\cos\varphi}$$
$$\times\mu P^{m''}_{|m'|}(\mu)P^m_l(\mu)e^{i(m+m'')\varphi}\,d\theta,$$

where $\mu=\cos\vartheta$, $\hat{k}_z=\sqrt{1+(\xi_j|q|)^2}$, $g^{m'}\in C$ are some functions, $\xi_j\in R$ are eigenvalues of a matrix. Here, ϑ,φ are the polar and azimuthal angles of θ. This unavoidable heavy computation is helped by the use of the supercomputer.

References

[1] M. Machida: J. Phys. A: Math. Theor. **48** (2015) 325001.

The radiative transport equation with FDM and FEM

Manabu Machida
Institute for Medical Photonics Research
Hamamatsu University School of Medicine, Hamamatsu 431-3192

The specific intensity of light propagating in random media is governed by the radiative transport equation, which is a linear Boltzmann equation. A typical example of such light is near-infrared light in biological tissue. The equation is a first-order differential equation involving an integral term and has six variables, i.e., time t, positions x_1, x_2, x_3, and angular variables ϑ, φ. We consider light propagation in a domain $\Omega \subset R^3$. Let $I(x, \theta, t)$ ($x \in R^3$, $\theta \in S^2$, $t \in R$) be the specific intensity of light. Let c be the speed of light in the medium and $\mu_a(x), \mu_s(x)$ be the absorption and scattering coefficients, respectively. The radiative transport equation is given by

$$\begin{cases} \left(\frac{1}{c}\partial_t + \theta\cdot\nabla + \mu_a + \mu_s\right) I(x,\theta,t) \\ \qquad = \mu_s \int_{S^2} p(\theta,\theta') I(x,\theta',t)\, d\theta', \\ \qquad x \in \Omega, \quad \theta \in S^2, \quad t \in (0,T), \\ I(x,\theta,t) = g(x,\theta,t), \\ \qquad (x,\theta) \in \Gamma_-, \quad t \in (0,T), \\ I(x,\theta,0) = a(x,\theta), \quad x \in \Omega, \quad s \in S^2, \end{cases}$$

where $p(\theta, \theta')$ is the scattering phase function and $\Gamma_\pm$ is defined as

$$\Gamma_\pm = \left\{(x,\theta) \in \partial\Omega \times S^2;\, \pm\nu\cdot\theta > 0\right\},$$

with ν the outer unit vector normal to $\partial\Omega$.

If $I(x, \theta, t)$ is almost isotropic as a function of θ, we can write

$$I(x,\theta,t) = \frac{1}{4\pi}u(x,t) + \frac{3}{4\pi}J(x,t)\cdot\theta.$$

Then the fluence rate $u \in R$ and current $J \in R^3$ are given by $u(x,t) = \int_{S^2} I(x,\theta,t)\, d\theta$ and $J(x,t) = \int_{S^2} \theta I(x,\theta,t)\, d\theta$. From the radiative transport equation we see that J obeys the Fick law, $J(x,t) = -D\nabla u(x,t)$, where $D = [3(1-g)\mu_s]^{-1}$, $g = \int_{S^2}(\theta\cdot\theta')p(\theta,\theta')\, d\theta$, and u obeys the diffusion equation,

$$\left(\frac{1}{c}\partial_t - \nabla\cdot D\nabla + \mu_a\right) u(x,t) = 0.$$

Using this diffusion approximation, we have started with the numerical calculation of the above diffusion equation.

In finite element method (FEM) we divide the domain Ω into a mesh of nonoverlapping elements and define a basis $v_i(x)$ of limited support. Then the function $u(x,t)$ is approximated in this basis by the piecewise polynomial interpolation, $u^h(x,t) = \sum_i u_i(t)v_i(x)$, where u_i are basis coefficients. The superscript h denotes the finite element mesh basis expansion. The coefficients $D(x)$ and $\mu_a(x)$ are expanded in the same manner into $D^h(x)$ and $\mu_a^h(x)$. Thus we obtain

$$\left[K(D^h) + C(\mu_a^h) + \alpha A\right] U(t) + B\partial_t U(t) = 0,$$

where $U(t) = {}^t(u_1, u_2, \ldots)$,

$$\begin{aligned} K_{ij} &= \int_\Omega D^h(x)\nabla v_i(x)\cdot\nabla v_j(x)\, dx, \\ C_{ij} &= \int_\Omega \mu_a^h(x) v_i(x) v_j(x)\, dx, \\ B_{ij} &= \frac{1}{c}\int_\Omega v_i(x) v_j(x)\, dx, \\ A_{ij} &= \int_{\partial\Omega} v_i(x) v_j(x)\, d\sigma. \end{aligned}$$

Here, α is a parameter appearing in the boundary condition.

Molecular simulation of colloidal crystals

Takamichi TERAO
Department of Electrical, Electronic and Computer Engineering, Gifu university
Yanagido 1-1, Gifu 501-1193

Polymer-nanoparticle composites, also known as spherical polymer brushes, are a typical example of a soft colloidal system. Polymer brushes play an important role in regulating the stability of colloidal suspensions and also in tuning the effective interactions between fine particles due to the polymer-induced repulsive potential. Self-assembly of these particles is a fundamental topic in material science; arrays of these composites have industrial applications such as the production of photonic crystals with bandgaps that forbid the propagation of light from a certain frequency range. The property of effective potential between particles is important to determine the phase diagram of the system. For example, a Gaussian-core model shows re-entrant melting. These studies have implied that the self-assembly of soft colloidal systems exhibits characteristic features which are different from charge-stabilized colloidal systems.

Spherical polymer brushes contain a core particle inside where different core particles cannot overlap. The study of physical properties of these systems, such as structural formation and phase diagrams, has been gaining increasing attention. Recently, spherical dendritic brushes, where many dendrons are grafted onto the spherical surface of a core particle, have been investigated. Dendrimers are highly branched, tree-like macromolecules with numerous free ends and excess polymer densities at the periphery of the brushes. Dendritic polymer brushes comprise dendritic polymers anchored to a surface at one end. Recent theoretical studies have clarified the structural formation of dendritic polymer brushes on flat surfaces by means of self-consistent field theory and scaling analysis. Moreover, molecular simulations have been performed to study the structural formation of dendritic polymer brushes.

In this study, the nature of the effective interaction between a pair of dendritic spherical polymer brushes (Figure 1) was numerically investigated using Monte Carlo simulation. Since much stronger entropic repulsion between particles is expected compared with that of linear polymer brushes, the structural formation of these spherical dendritic brushes was studied. The transferability of the obtained coarse-grained potential at various temperatures was also confirmed.

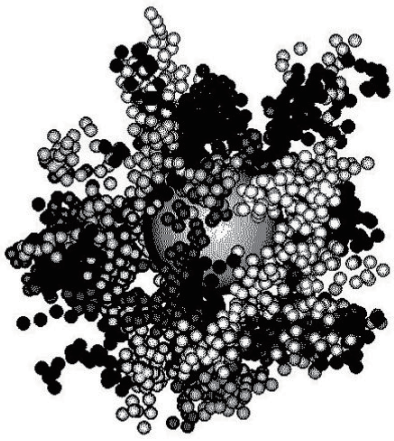

Figure 1: Spherical dendritic polymer brushes

Nonadiabatic Dynamics of Cooperative Domain Growth Triggered by THz-pulse Irradiation

Kunio ISHIDA

Department of Electrical and Electronic Engineering, School of Engineering, Utsunomiya University, Yoto, Utsunomiaya, Tochigi 321-8585

Photoinduced nucleation by THz pulses is studied by a model of localized electron couple with an optical phonon mode.

Based on the analogy to the photoinduced phase transitions observed in various materials, we consider that cooperative interactions between electrons and coherent phonons will lead to the multiplication of excited electrons and/or growth of a transient phase, which is understood by bifurcation of quantum-mechanical wavepackets on adiabatic potential energy surfaces. Taking a model of localized electrons coupled with a quantized optical phonon mode, we discuss the dynamics of the cooperative phenomena by THz-pulse irradiation and, in particular, the role of the number and/or the initial distribution of phonons in the initial creation process of transient phases.

We employ a model of localized electrons coupled with an optical phonon mode which describes the general properties of the photoinduced structural change. In the present study we consider an array of molecules (unit cells) on a square lattice with two electronic levels and a single phonon mode interacting with each other, which is described by the following Hamiltonian:

$$H = \sum_{\vec{r}}\left[\frac{p_{\vec{r}}^2}{2}+\frac{\omega^2 u_{\vec{r}}^2}{2}+(\sqrt{2\hbar\omega^3}s u_{\vec{r}}+\varepsilon\hbar\omega+s^2\hbar\omega)\tilde{n}_{\vec{r}}+\lambda\sigma_{\vec{r}}^x\right] - \sum_{<\vec{r},\vec{r}'>}\left[\alpha\omega^2(u_{\vec{r}}-\beta\tilde{n}_{\vec{r}})(u_{\vec{r}'}-\beta\tilde{n}_{\vec{r}'})+\{V-W(u_{\vec{r}}+u_{\vec{r}'})\}\tilde{n}_{\vec{r}}\tilde{n}_{\vec{r}'}\right]$$

We calculated the dynamics of coupled electron-phonon system excited by THz optical pulses. Since the lattice vibration frequency is of the order of THz, we consider that the applied THz pulses act as an external electric field that directly induces deformation of the lattice. Thus, the initial condition of the simulations is set to be deformed lattice with electrons occupying the ground state.

As a lot of computational resources are required to calculated the dynamics of the system, we used the System B with MPI parallelization[1] and 4 nodes were used in each simulation run.

We found that the electronic transition between the ground state and an excited state is induced by the propagation of phonons, and the region of excited molecules extends over the whole system, although initial deformation of the lattice is limited to the molecules in the vicinity of the surface of samples. As a result, the population of excited electrons increases, which

shows that the multiplication of excited electrons is possible by the injection of phonons. Although these features are similar to the photoinduced cooperative phenomena, we also found that the nonadiabatic interaction λ is enhances the nucleation as shown in Fig.1. The present results show that the irradiation of intense THz-pulses is effective to induce the multiplication of excited electrons in various systems, and that it will be another method to discuss the dynamical behavior and/or the hidden phase[1] which is able to access via photoexcited states.

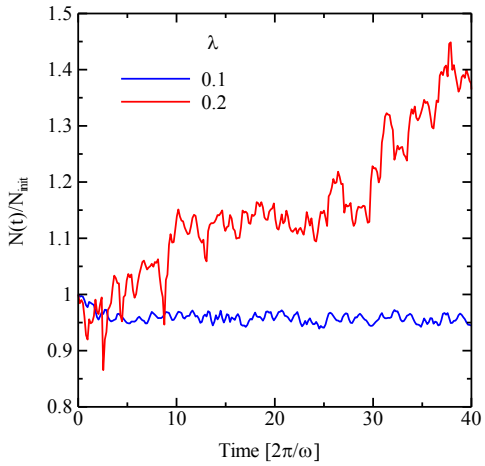

Fig.1 Excited state population as a function of time for λ = 0.1 and 0.2.

References

[1] K. Ishida and K. Nasu, Comp. Phys. Commun. **180**, 1489 (2009).

[2]"Photoinduced phase transitions" ed. K. Nasu (World Scientific, Singapore).

Nonadiabatic Wavepacket Dynamics of Electron-phonon-photon Systems

Kunio ISHIDA

Department of Electrical and Electronic Engineering, School of Engineering, Utsunomiya University, Yoto, Utsunomiya, Tochigi 321-8585

Since the adaptive control method in coherent regime[1] was proposed to control the reaction rate with certain chemical species, ultrafast coherent control of electron-phonon systems has been studied by many authors. When the quantum-mechanical nature of the electromagnetic field is taken into account, the nonadiabaticity of the electronic transition is relevant to the absorption/emission of photons in femto/picosecond regime. Though this effect is neglected particularly for intense incident light, we still require to understand the interplay of phonons and photons in the case of strongly coupled electron-phonon systems.

We study the wavepacket dynamics of electron-phonon-photon systems in order to clarify the role of nonadiabaticity of electronic transitions. We stress that Raman process which involves creation/annihilation of both phonons and photons is important.

Employing a simple model of an electronic system coupled with both phonons and photons, we numerically solved the time-dependent Schrödinger equation for systems with a single phonon mode and three photon modes. We chose the Fock states as a basis for the vibration mode and the photon modes, and the equation of motion is expressed by the diabatic picture. Since a lot of computational resources are required even for three photon modes, numerical simulations were performed on the System B with hybrid parallelization using up to 18 nodes. We found that induced Raman process enhances the electronic transition and that the trajectories of wavepackets deviate from those under semiclassical approximation as shown in the figure.

As discussed in previous studies[2,3], the conical intersection(CI) in the “adiabatic potential energy surfaces” for phonons and photons is important to reveal the dynamics of the system in this case. The wavepackets always pass the crossing region of the (one-dimensional) PESs in the semiclassical approximation, while they move around the CI in the case of quantized light. Hence, the bifurcation of the wavepackets caused by the nonadiabatic matrix elements of the Hamiltonian takes place in a different manner between quantum-mechanical calculations and semiclassical calculations, which implies that the dressed-state picture is important to discuss

the transient dynamics of photoirradiated systems in coherent regime.

References

[1] R. S. Judson and H. Rabitz, Phys. Rev. Lett. **68**, 1500 (1992).

[2] M. Kowalewski, K. Bennett, and S. Mukamel, J. Chem. Phys. **144**, 05439 (2016).

[3] F. Bouakline, Chem. Phys. **442**, 31(2014).

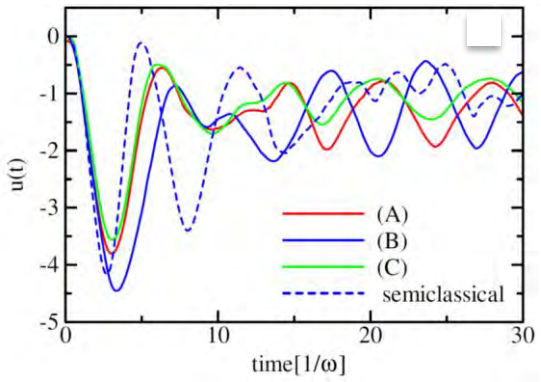

Fig.1 Dynamics of lattice deformation u(t) taking into account: (A) single photon mode, (B) two photon modes with induced Raman process, and (C) two photon modes with spontaneous Raman process. ωdenotes the frequency of the phonon.

Conformational dynamics of proteins studied by molecular dynamics simulations

Yuma SUEMATSU and Munehito ARAI

Department of Life Sciences, Graduate School of Arts and Sciences,

The University of Tokyo, Komaba, Meguro, Tokyo 153-8902

Proteins exert their functions through dynamic motions in general, and thus, elucidation of conformational dynamics of a protein is necessary to understand the mechanism of its action and to improve its biological activity. Cyanobacteria are known to synthesize alkanes/alkenes corresponding to diesel oils using the proteins inside the organism. Because these hydrocarbons are produced from carbon dioxide by photosynthesis, such sustainable “bio-energies” are expected to be substitutes for petroleum-based hydrocarbons [1,2]. In 2010, Schirmer *et al.* revealed that cyanobacteria use an aldehyde-deformylating oxygenase (ADO) to convert aldehydes into alkanes/alkenes [3]. However, the catalytic mechanism of ADO has been poorly understood.

To elucidate the conformational dynamics of ADO, here we performed molecular dynamics (MD) simulations of the ADO protein from a cyanobacterium *Nostoc punctiforme* PCC 73102, which has been reported to have the highest activity among ADOs from various cyanobacterial strains [3]. Because ADO is known to bind two metal ions, we performed MD simulations both in the presence and absence of zinc ions. In addition, we did simulations in the presence and absence of a heptadecane (C17) molecule, resulting in four types of MD simulations (-Zn/-C17; -Zn/+C17; +Zn/-C17; +Zn/+C17). Preliminary simulations have been performed last year, and thus longer simulations up to 400 ns were performed here for each types of simulations.

All MD simulations were performed using the AMBER12 software. The ADO protein was immersed in TIP3P water molecules with periodic boundary conditions. The force fields of ff98SB were used for the protein, while those for C17 were calculated using the ANTECHAMBER program. After energy minimization, the temperature of the system was raised up to 298 K with restraints on protein structure. Finally, the MD simulations were performed for ~400 ns at 298 K without structural restraints.

Our simulations showed that the metal-free forms of ADO exhibited large structural fluctuations around the metal-binding sites, consistent with crystal structures of metal-free ADOs. Interestingly, we could observe

conformational changes of the C17 molecule inside the ADO protein. Moreover, the open/close dynamics was observed at the product-exit site of ADOs, and the dynamics was dependent on the presence/absence of the metals and product in the ADO molecule.

These results suggest that the conformational dynamics of ADO is controlled by the binding/release of the metals and product during the catalytic cycle. Further studies by longer simulations will elucidate the time scale of the open/close dynamics of the substrate-entry/product-exit site of ADO. The open/close dynamics may be directly related to the catalytic efficiency of ADO, and manipulation of the conformational dynamics may enable us to improve the alkane-producing activity of ADO.

References

[1] Y. Hayashi, Yasugi, F. and M. Arai: PLoS ONE, **10** (2015) e0122217.

[2] H. Kudo, R. Nawa, Y. Hayashi, and M. Arai: Biotechnology for Biofuels, **9** (2016) 234.

[3] A. Schirmer, M.A. Rude X. Li, E. Popova, and S.B. del Cardayre: Science, **329** (2010) 559-562.

Spin-lattice-coupling effects in pyrochlore antiferromagnets

Kazushi AOYAMA
Department of Earth and Space Science, Graduate School of Science, Osaka University
Machikaneyama-cho, Toyonaka-shi, Osaka 560-0043

In frustrated magnets, it often happens that spins are coupled to the lattice degrees of freedom and the underlying lattice is distorted spontaneously to resolve the magnetic frustration, leading to a long-range magnetic order. The spinel chromium oxides ACr_2O_4 provide a typical example of such a spin-lattice-coupled (SLC) ordering, where the magnetic ion Cr^{3+} forms the pyrochlore lattice, a three-dimensional network of corner-sharing tetrahedra. Of recent particular interest is antiferromagnets on a breathing pyrochlore lattice realized in the chromium oxides AA'Cr_4O_8. In the breathing case, the lattice nonuniformity of the breathing structure, the alternating array of small and large tetrahedra, should be reflected in the system parameters such as the ratio of the nearest neighbor interaction for large tetrahedra to that for small ones J'/J. In this work, we investigate effects of the breathingness measured by J'/J on the SLC ordering.

Our model Hamiltonian is given by $\mathcal{H}_{\rm eff} = \mathcal{H}_0 + \mathcal{H}_{\rm SL}$,

$$\begin{aligned}
\mathcal{H}_0 &= J \sum_{\langle i,j\rangle_s} \mathbf{S}_i \cdot \mathbf{S}_j + J' \sum_{\langle i,j\rangle_l} \mathbf{S}_i \cdot \mathbf{S}_j, \\
\mathcal{H}_{\rm SL} &= -Jb \sum_{\langle i,j\rangle_s} (\mathbf{S}_i \cdot \mathbf{S}_j)^2 - J'b \sum_{\langle i,j\rangle_l} (\mathbf{S}_i \cdot \mathbf{S}_j)^2 \\
&- \Big\{ Jb \sum_{\langle i,j,k\rangle_s} + J'b \sum_{\langle i,j,k\rangle_l} \Big\} (\mathbf{S}_i \cdot \mathbf{S}_j)(\mathbf{S}_i \cdot \mathbf{S}_k) \\
&- b\sqrt{JJ'} \sum_i \sum_{j\in N_s(i)} \sum_{k\in N_l(i)} \mathbf{e}_{ij} \cdot \mathbf{e}_{ik} \\
&\qquad \times (\mathbf{S}_i \cdot \mathbf{S}_j)(\mathbf{S}_i \cdot \mathbf{S}_k), \qquad (1)
\end{aligned}$$

where $\mathbf{S}_i$ is a classical Heisenberg spin, the dimensionless parameter b measures the strength of the SLC, and $\mathbf{e}_{ij}$ is a unit vector connecting sites i and j

To investigate ordering properties of the model (1), we perform Monte Carlo simulations by using the facilities of the Supercomputer Center, ISSP, the University of Tokyo. In the simulation, we basically perform 10^6 Metropolis sweeps under periodic boundary conditions, where the first half is discarded for thermalization. Our single spin flip at each site consists of the conventional local update and a successive over-relaxation process in which we try to rotate a spin by the angle π around the local mean field.

By measuring various physical quantities such as the spin collinearity and the spin structure factor, we determined the low temperature phases. It is found that the system exhibits the first order transition into collinear spin states characterized by $(1,1,0)$ or $(\frac{1}{2},\frac{1}{2},\frac{1}{2})$-type magnetic Bragg peaks. The $(1,1,0)$ state is realized in the weaker SLC regime, while the $(\frac{1}{2},\frac{1}{2},\frac{1}{2})$ states, which have three ordering patterns (type I, II, and III) depending on the ratio J'/J and the strength of the SLC, are favored in the relatively stronger SLC regime. In contrast to the $(1,1,0)$ and the type I $(\frac{1}{2},\frac{1}{2},\frac{1}{2})$ states appearing in the uniform case, the type II and III phases are peculiar to the breathing pyrochlores. It is also found that the difference in the ordering patterns of three $(\frac{1}{2},\frac{1}{2},\frac{1}{2})$ phases is reflected in the residual entropy, which could be observed as signatures of the type II, III orders.

Computer-simulated *n*-beam X-ray pinhole topographs based on the Ewald-Laue dynamical diffraction theory and FFT

Kouhei OKITSU

Institute of Engineering Innovation, School of Engineering,

The University of Tokyo, 2-11-16 Yayoi Bunkyo-ku Tokyo 113-8656

The difficulty of phase determination in X-ray crystal structure analysis has been overcome by the direct method invented by Hauptman and Karle for small molecular-weight crystals. However, it is almost not effective for protein crystals whose molecular sizes are significantly large. Then, non-native protein crystals in which heavy atoms or selenium atoms are introduced, are usually used for phase determination.

The idea of '*n*-beam method' to solve the phase problem was reported by Lipscomb in 1949 for the first time. However, this method has not been successfully used to extract phase information of protein crystals up to today. The ultimate purpose of the present study is to give the final solution of the phase problem for native protein crystals by using the *n*-beam method.

Incidentally, the present author has two hypothesizes about too large *R*-factor (up to 20-30%) for protein crystals. The former is that *R*-factor can be decreased by using '*n*-beam approximation' in place of usually used two-beam approximation when estimating the *R*-factor. The above hypotheses is based on an assumption that intensity perturbation is caused by interference effect among simultaneously reflected X-rays. A large number of reflection spots are taken simultaneously on two-dimensional detector for protein crystals since their reciprocal lattice node density is extremely high compared with small molecular-weight crystal.

The latter hypothesis is that the phase information can be extracted only by taking into account the crystal orientation that is not usually used but has information about reflection indices giving simultaneous Bragg reflections.

The purpose of the present report is describing a method to calculate X-ray intensity from a crystal whose orientation is known and shape is complex.

A numerical method to solve the Ewald-Laue (E-L) dynamical diffraction theory for an *n*-beam case was reported by Colella in 1974 for the first time. However, it was effective only for a parallel plate crystal. The present author extended the Takagi-Taupin (T-T) equation to *n*-beam condition and gave a numerical method to solve it [1-3]. Further, it has been clarified that the *n*-beam T-T equation can be numerically solved for an arbitrary-shaped crystal from a comparison between experimentally obtained and computer-simulated six-beam pinhole topographs for a channel-cut silicon crystal [4,5].

He has also reported three-, four-, five-, six-, eight- and twelve-beam pinhole topographs experimentally obtained and computer-simulated

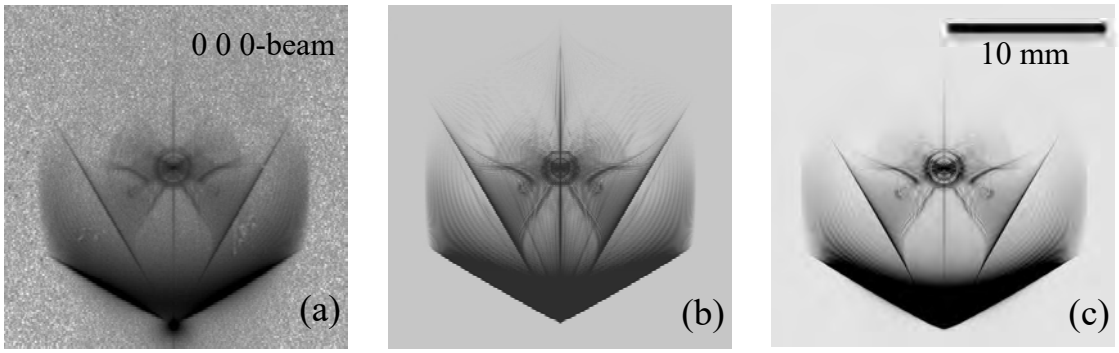

Fig.1 Six beam pinhole topographs (a) Experimentally obtained at SPring-8 and computer-simulated based on (b) the T-T equation and (c) E-L theory and FFT. The photon energy was 18.245 keV. The thickness of the silicon crystal was 9.6 mm. (a) and (b) have been published in reference [3].

based on the T-T equation and has verified the equivalence between the *n*-beam E-L and T-T theories, for the first time [6]. The applicable number of waves comes from a restriction that the *n* reciprocal lattice nodes should be on a circle in the reciprocal space. (circular case).

However, he has not found a method to solve the T-T equation for non-circular n-beam case, unfortunately, in spite that *n*-beam condition in a protein crystal is always non-circular. On the other hand, the *n*-beam E-L theory can be solved even for a non-circular case.

Recently in 2016-2017, a numerical method to solve the E-L theory and then Fourier-transform the solution to obtain a six-beam pinhole topograph has been reported by Kohn. The present author has got an inspiration to solve the eigen value problem of the E-L theory and apply a fast Fourier transform (FFT) to the solution to obtain a non-circular case *n*-beam pinhole topgraph.

Figure 1 shows forward-diffracted images of six-beam pinhole topographs (a) experimentally obtained, computer-simulated based on (b) the T-T equation and (c) the E-L theory and FFT. This method can be applied to calculation of pinhole topographs even for a protein crystal whose shape is complex in general since it has been found that pinhole topographs for a complex-shaped crystal can be simulated by piecing together several parts of topographs for parallel plate crystals simulated by using the E-L theory and FFT. Then, the present author has prepared to calculate reflected X-ray intensity for a non-native protein crystal to verify the first hypothesis [7].

References

[1] K. Okitsu: Acta Cryst. **A59** (2003) 235-244.

[2] K. Okitsu et al.: Acta Cryst. **A59** (2003) 311-316.

[3] K. Okitsu et al.: Acta Cryst. **A62** (2006) 237-247.

[4] K. Okitsu et al.: Acta Cryst. **A67** (2011) 550-556.

[5] K. Okitsu: Acta Cryst. **A67** (2011) 559-560.

[6] K. Okitsu, Y. Imai and Y. Yoda: InTech *Resent Advances in Crystallography* (2012) 67-86 [Invited].

[7] K. Okitsu: Submitted to Acta Cryst. **A77** (2018).

Transport properties of one-dimensional interacting electron systems by a quantum Monte Carlo method

Takeo KATO
Institute for Solid State Physics, University of Tokyo
Kashiwa-no-ha, Kashiwa, Chiba 277-8581

Conductance quantization in electron transport through a quantum contact is one of highlights in mesoscopic physics because it clearly demonstrates importance of quantum mechanics. However, appearance of another non-quantized conductance plateau, which is called "0.7 anomaly", has been a mystery for long time from the first discovery of the conductance quantization. This phenomenon is thought to be a many-body effect due to Coulomb interaction between electrons near the point contact. For example, numerical calculation for zero-temperature transport based on functional renormalization group indicates suppression of conductance due to singularity induced by exchange interaction [1]. The entire feature of the 0.7 anomaly has, however, not been understood yet.

To tackle this problem, we have tried to construct a procedure to obtain information of conductance from numerical data for a finite one-dimensional lattice model with Coulomb interaction and one-body potential energy by scatterers (point contacts) with a finite width. We employed the stochastic series expansion (SSE) method [2], which is one of quantum Monte Carlo methods, and calculated current-current correlation functions as a function of the imaginary time. Because only finite systems can be treated in the SSE method, the procedure to obtain linear conductance is nontrivial. We first showed that zero-frequency current-current correlation function obtained by a naive analytic continuation loses the information of electronic transport. We found that by introducing an additional broadening factor, we can recover information of phase shift of electrons across a scatter, and succeeded in reproducing a known result, i.e., the Landauer formula if the Coulomb interaction is switched off. We also demonstrated that conductance of a point-like scatterer in the Luttinger liquid obtained from this procedure is consistent with renormalization group analysis [3]. Our method is naturally connected to the formula for the Drude weight in the thermodynamic limit [4].

The present study provides a foundation for calculation of conductance in interacting electron systems. We are now trying to extend our idea toward general one-dimensional interacting electron systems, by reformulating it in terms of the field theory for electronic transport [5].

References

[1] J. Heyder et al., Nature **501** (2013) 73.

[2] A. W. Sandvik, Phys. Rev. B **59** (1999) R14157; A. W. Sandvik, J. Phys. A: Math. Gen. **25** (1992) 3667.

[3] C. L. Kane and M. P. A. Fisher, Phys. Rev. Lett. **68** (1992) 1220.

[4] D. J. Scalapino, et al., Phys. Rev. Lett. **68** (1992) 2830.

[5] N. Shimada and T. Kato, in preparation.

Numerical Large Deviation Analysis of Eigenstate Thermalization Hypothesis

Eiki Iyoda
Department of Applied Physics,Institute for Solid State Physics, the University of Tokyo
Hongo, Bunkyo-ku, Tokyo 113-8656

Recently, thermalization in isolated quantum systems attracts attention, and a plausible mechanism of thermalization is based on the strong version of the eigenstate thermalization hypothesis (ETH) [1]. The ETH states that all the energy eigenstates in the microcanonical (MC) energy shell have thermal properties. Here, the word *thermal* means the expectation value of an observable $\hat{O}$ equals the MC average:

$$O_i := \langle E_i|\hat{O}|E_i\rangle \simeq \langle \hat{O}\rangle_{\rm MC} \tag{1}$$

We have numerically investigated the ETH by focusing the large deviation property, in other words, we focused on *athermal* eigenstates. We refer to an energy eigenstate $|\rangle E_i$ as athermal eigenstate if $|O_i - \langle \hat{O}\rangle_{\rm MC}| > \varepsilon$ is satisfied, where ε is a threshold. We define the number of the athermal eigenstates $D_{\rm out}$ as

$$D_{\rm out} \equiv \sum_{|E_i\rangle \in \mathcal{M}(E,\Delta E)} \theta\left(|O_i - \langle \hat{O}\rangle_{\rm MC}| - \varepsilon\right), \tag{2}$$

where $\mathcal{M}(E, \Delta E)$ is the microcanonical energy shell with $[E - \Delta E, E]$. We also refer to D as the dimension of the energy shell.

The strong ETH implies that $D_{\rm out}$ is zero if the system size L is sufficiently large. There is a mathematical theorem which gives an upper bound of the ratio $D_{\rm out}/D$:

$$D_{\rm out}/D \leq e^{-\gamma L}, \tag{3}$$

where $\gamma > 0$. If the ratio $D_{\rm out}/D$ decays faster than exponentially, $D_{\rm out}$ will become zero with large but finite L.

We have calculated $D_{\rm out}$ by using numerically exact diagonalization and Sakurai-Sugiura method [2]. We used one-dimensional quantum spin chain (XXX model) with next nearest interaction. The XXX model can be represented with hard core bosons, and we used the filling of hard core bosons at 1/3 in this model. The system sizes are taken as $L = 12, 15, 18, 21, 24$. The dimension of the Hilbert space is 735471 for $L = 24$. By using the translation invariance, we divide the whole space into L sectors. We should diagonalize matrices with ~ 30465 dimension. For $L = 24$, we use the Sakurai-Sugiura method to investigate the parameter dependence.

As a result [3], we have obtained $D_{\rm out}/D$ for some observables by changing the integrability breaking parameter. When the system is non-integrable, we have showed $D_{\rm out}/D$ are fitted well with a function $f(L) = a - b\exp(cL)$ with positive constants a, b and c. This implies the strong ETH. This double exponential behavior is seen even in the near integrable system.

References

[1] M. Rigol, V. Dunjko, and M. Olshanii, Nature **452**, 854 (2008).

[2] T. Sakurai and H. Sugiura, J. Comput. Appl. Math. **159**, 119 (2003).

[3] T. Yoshizawa, E. Iyoda, and T. Sagawa, arXiv:1712.07289.

Tensor Renormalization Group with Randomized Algorithm for Singular Value Decomposition

Satoshi MORITA

Institute for Solid State Physics,

The University of Tokyo, Kashiwa-no-ha, Kashiwa, Chiba 277-8581

Tensor network method is a powerful tool for quantum and classical many-body systems. The tensor renormalization group (TRG) method is an efficient method for contracting tensor networks [1]. Its main operations, "decomposition" and "contraction" have the computational complexity proportional to the sixth power of the bond dimension.

We proposed an efficient algorithm of the tensor renormalization group based on a randomized algorithm for singular value decomposition [2]. Avoiding explicit creation of a four-leg tensor reduces the computational complexity to the fifth power of the bond dimension. The oversampling parameter tunes accuracy of the randomized algorithm. We showed that the oversampling parameter larger than the bond dimension is sufficient to reproduce the same result of the full singular value decomposition [3].

References

[1] M. Levin and C. P. Nave, Phys. Rev. Lett. **99** 120601 (2007)

[2] N. Halko, P. G. Martinsonn, J. A. Tropp, SIAM Review **53**, 217 (2011).

[3] SM, R. Igarashi, H.-H. Zhao, and N. Kawashima: Phys. Rev. E **97**, 033310 (2018)

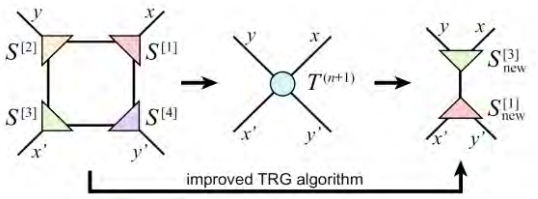

Fig. 1: The chain of deformation in the TRG algorithm [3].

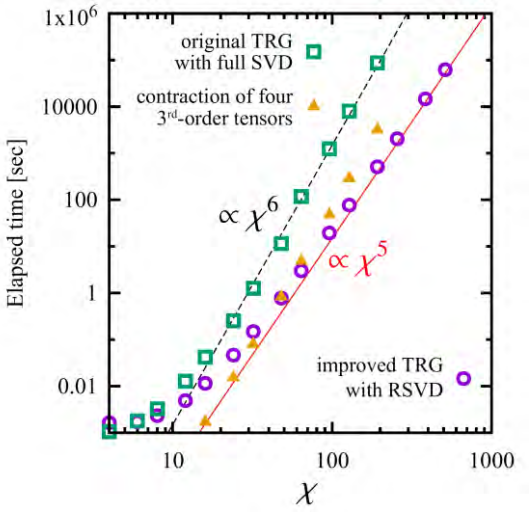

Fig. 2: Elapsed time per TRG step as a function of the bond dimension [3].

Coarse-Grained Molecular Dynamics Simulations of Slide-Ring Gel Networks

Koichi Mayumi[1], Yusuke Yasuda[1], Masatoshi Toda[2], Hideaki Yokoyama[1], Hiroshi Morita[2], and Kohzo Ito[1]

[1] *Dept. of Advanced Materials Science, Graduate School of Frontier Sciences, the Univ. of Tokyo.*

[2]*National Institute of Advanced Industrial Science and Technology*

We have studied the relationship between mechanical properties and the orientation of molecules in slide-ring gels [1] using parallel computer simulations. This year, we focused on orientation of molecules in networks.

Generally conventional fixed-crosslink gels have chemical bond between axle chains, while slide-ring gels fabricated by Ito et. al., do not have direct crosslinks, but have figure-of-eight crosslinks. Slide-ring gels show high extensibility and toughness because figure-of-eight crosslinks act like pulleys and prevent stress concentration on short axle chains, which is called "pulley effect" (Fig. 1). This time we tried to visualize pulley effect, using coarse-grained molecular dynamics simulation.

We have constructed a coarse-grained model of slide-ring gels with beads-spring model established by Kremer and Grest [3]. 20,000 up to 35,000 beads system was used for simulation, and equilibration simulation was performed using OCTA/COGNAC engine for $1.0 \times 10^7\ \tau$ time steps, where simulation step was $\Delta t = 1.0 \times 10^{-2}\tau$. We carried out elongation simulation in the range of extension ratio λ = 1-10 at a strain speed $1.0 \times 10^{-5}\ \lambda / \tau$ for slide-ring gels with 4 different crosslinking densities.

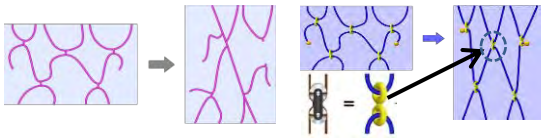

Fig. 1: Stress concentration in conventional gel (left) and pulley effect in slide-ring gel (right)

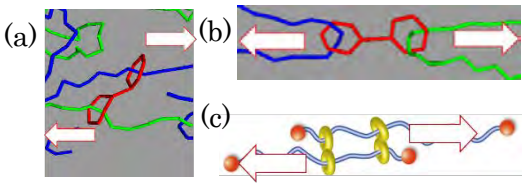

Fig. 2: (a) Orientation of figure-of-eight crosslinks parallel to stretching (b) Orientation of figure-of-eight crosslinks perpendicular to stretching, which leads to the pulley effect (c) Stress relaxation mechanism caused by the orientation of cross-links shown in (a).

We observed the orientation of axial chain and figure-of-eight crosslinks in slide-ring gels under uniaxial deformation. Like pulleys shown in Fig. 1, some figure-of-eight cross-links are oriented parallel to stretch (Fig. 2 (b)). On the other hand, some other cross-linking points are aligned in the direction perpendicular to stretching (Fig. 2 (a)), which suggests a novel stress-relaxation mechanism (Fig. 2(c)).

References

[1] K. Ito et. al., Adv. Mater. **13**(2001) 485.

[2] K. Ito, Polym. J. 39, 489 (2007).

[3] K. Kremer & G. S. Grest, J. Chem. Phys., 92, 5057 (1990).

Manipulation of Topological States by Real-Space Structure

Toshikaze Kariyado
International Center for Materials Nanoarchitectonics, National Institute for Materials Science
Namiki, Tsukuba, Ibaraki 305-0044

This year, we have mainly focused on the analysis of the electronic structure of i) antiperovskite family A_3EO (A=Ca,Sr,Ba, and E=Sn,Pb) [1], and ii) graphene nanomesh (graphene with antidot lattice) [2]. The main part of the analysis was relying on the density functional theory, and was performed using the parallelized version of Quantum Espresso package [3]. As we will see in the following, the systems to be considered in our work contain superstructures or many orbitals, and therefore, the parallelized computational programs play an essential role in our study. The parallelized version of the Quantum Espresso package works fine on the ISSP supercomputing facility.

For the antiperovskite family, we attempted to obtain electronic band structure for $Ca_{3(1-x)}Sr_{3x}SnO$, in relation to the pseudo gauge field, which might be generated by appropriate band structure engineering [1]. For this purpose, we take two approaches. In the first approach, effective models for two end materials ($x = 0$ and $x = 1$) are constructed, and then, effective models for intermediate values of x are obtained by interpolating parameters in the effective models for the two end materials. In the second approach, we consider superstructures like those in Fig. 1. In the two shown structures, the ratios between the number of Sr and Ca atoms are 4/9 and 5/9, respectively. The electronic band structures obtained in this way are reported in ref. 1.

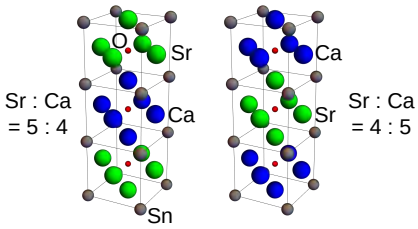

Figure 1: Crystal structures corresponding to $x = 4/9$ and $5/9$.

For graphene nanomesh, the computing facility is used to analyze lattice distortion effects, which are inevitable at the perimeter of antidot (nano-sized hole). For this purpose, we derive Wannier orbitals for relevant bands, and estimate effective transfer integrals. Because of the symmetry breaking at the perimeter of nanoholes (inside vs outside), the centers of Wannier orbitals can be off from the atomic positions. Consequently, transfer integrals are not determined by the distance between atoms alone, rather we have to take the Wannier centers into consideration. However, overall the lattice distortion effects are small and the most of the properties of graphene nanomesh can be addressed by a simple tight-binding model with uniform transfer integrals [2].

References

[1] T. Kariyado: arXiv:1707.08601.

[2] T. Kariyado, Y.-C. Jiang, H. Yang, and X. Hu: arXiv:1801.03115.

[3] P. Giannozzi *et al.*: J. Phys.: Condens. Matter **21** (2009) 395502.

Large-scale Molecular-dynamics Simulation with ANN Potentials: nm-scale Domain Structure in Densified Silica Glass

Daisuke WAKABAYASHI[1] and Fuyuki SHIMOJO[2]

[1]*Institute of Materials Structure Science, High Energy Accelerator Research Organization (KEK), Tsukuba 305-0801*

[2]*Department of Physics, Kumamoto University, Kumamoto 860-8555*

Silica glass is well known as an archetypal oxide glass and its compression behavior has attracted considerable attention in various fields of physical sciences. Recent small-angle X-ray scattering measurements have revealed the appearance of subnanometer-scale domains for low-pressure and high-pressure phases in silica glass during the pressure-induced structural transformations [1].

To reveal the detailed structure of subnanometer-scale domains, we conducted some calculations for large-scale molecular-dynamics (MD) simulations with a system of ~10,000 atoms. We have confirmed that ab-initio methods can simulate the compression behavior of silica glass accurately [2]. On the basis of the results of ab-initio calculations, we fitted the potential with a machine-learning technique (ANN potential) and applied it for the calculations with an extended system.

To obtain the data for fitting ANN potentials, we conducted ab-initio calculations. The configurations of six-coordinated and densified four-coordinated glasses (corresponding to high- and low-pressure phases) were prepared by gradually cooling silica melt from 4,000 K at 40 and 15 GPa, respectively, and then the decompression and recompression processes were calculated. There is remarkable agreement between the densities on decompression and recompression and therefore six-coordinated and densified four-coordinated glasses behave in an elastic manner as a single phase. In addition, six-coordinated glass was retrieved, in contrast to the case for experiments, implying that a six-coordinated structure remains at ambient conditions after decompression on a picosecond timescale.

We tested the MD simulations with a system of about 30,000 atoms using the ANN potential determined from the data at 40 GPa. However, the calculations at high temperatures cannot be made due to the numerical divergence, which implies that more machine-learning training is needed to refine the ANN potential.

References

[1] T. Sato, N. Funamori, D. Wakabayashi, K. Nishida, and T. Kikegawa: submitted.

[2] E. Ryuo, D. Wakabayashi, A. Koura, and F. Shimojo: Phys. Rev. B **96** (2017) 05420.

Giant and cross response with ferroelectric-antiferroelectric phase transitions

Kyohei Takae and Hajime Tanaka
Institute of Industrial Science, University of Tokyo
4-6-1 Komaba, Meguro-ku, Tokyo 153-8505, Japan

The dielectric properties and related cross coupling effects such as electromechanical and electrocaloric effects are strongly influenced by structural phase transitions. Here we focus on ferroelectric–antiferroelectric phase transitions, where basic physical picture controlling phase transitions with spontaneous arrangement of crystalline structure still remains elusive. To obtain physical insight into such phase controllability, we construct a molecular model exhibiting ferroelectric–antiferroelectric phase transitions with structural rearrangement. The pair interaction consists of dipolar interaction and Lennard-Jones interaction but slightly modified to realise anisotropic molecular interaction between spheroids. The key point of this model is interplay between the anisotropy of dipolar interaction (changing its sign depending on the direction of the relative position between adjacent particles) and steric (Lennard-Jones) interaction. By varying temperature and the aspect ratio of the spheroids, we realise ferroelectric–antiferroelectric phase transition with spontaneous rearrangement of crystalline structure, where the ferroelectric (antiferroelectric) phase is stable for small (large) aspect ratio. In this year we study electrical, mechanical and thermal control of this phase transitions [1] by molecular dynamics simulations.

Firstly, we examine mechanical switching from antiferroelectric to ferroelectric state under Parrinello-Rahman barostat. The Parrinello-Rahman barostat is necessary since phase transitions involves structural rearrangement. We apply anisotropic uniaxial stress on antiferroelectric states to study mechanical switching. Depending on temperature and the direction of stretching/compression, phase transitions from antiferroelectric state to another antiferroelectric state, ferroelectric state, and paraelectric state are observed, where both the dielectric and mechanical properties are greatly changed. Thus we realise selective mechanical switching of dielectric and electromechanical properties.

Secondly, we examine electrocaloric effects. The electrocaloric effect stands for temperature change induced by applying/removing external electric field. In particular, antiferroelectric phase has lower entropy in our system and hence temperature decreases (increases) by applying (removing) external electric field to induce phase transitions. This effect is called inverse electrocaloric effect, since the sign of temperature change is inverted compared with usual electrocaloric effect. By calculating the dynamical structure factors concerning rotational motions, we reveal that the suppression of rotational vibrations is the origin of small entropy in antiferroelectric state, resulting in the inverse electrocaloric effect.

References

[1] K. Takae and H. Tanaka, submitted.

Nonequilibirum phase transition and shock wave phenomena in the dense hard sphere systems

Masaharu ISOBE
Nagoya Institute of Technology
Gokiso-cho, Showa-ku, Nagoya, 466-8555

As one of the simplest model, the hard disk/sphere systems have been investigated in the field of both equilibrium and non-equilibrium statistical physics. In this project, we investigated non-equilibrium phenomena in the hard disk/sphere model system with modern algorithms, especially for Event-Chain Monte Carlo(ECMC) [1] and Event-Driven Molecular Dynamics(EDMD) [2], where we propose the "Hybrid Scheme", namely, ECMC for equilibration and EDMD for calculation of dynamical properties [3, 4].

Clustering impact regime with shocks in freely evolving granular gas:

Clustering of the granular gas is one of the fascinating phenomena. An evolving process of cooling granular gas systems without gravitational force is usually starting from the initial homogeneous state to the inhomogeneous clustering state, in which the energy decay deviates from the classical Haff's law. Previously [5, 6, 7, 8], we investigated the macroscopic behaviors on the evolving quasi-elastic Inelastic Hard Sphere (IHS) model by performing a microscopic event-driven molecular dynamics with mainly 512^2 [5], 4096^2 [7] in two-dimensional system (2D) and 128^3 [8] in three dimensional system (3D). These large-scale numerical simulations have revealed similarity with fluid Navier-Stokes turbulence, such as enstrophy cascade (Kraichnan-Leith-Bachelor theory), Kolmogorov scaling and Bose-Einstein condensation, which are well-known n the fluid turbulence. The rough estimate of Reynolds number with Taylor's microscale reveals that the IHS system at the onset of clustering regime grow up to $R_\lambda \sim 327$ (2D) and ~ 1470 (3D) [7, 8] respectively.

In this study [9], we focus on the inhomogeneous clustering regimes of evolving granular gas via event-based molecular dynamics simulation [2, 3] with up to 16.7 million disks to clarify the validity of asymptotic behaviors of energy predicted by a couple of theories. Although we confirmed that the theories are consistent in relatively dilute and small system, we found the novel regime regarding on collisions between "clusters" spontaneously appearing after the clustering regime in dense case, which can only be identified more than a few million particles systems. The two-step energy relaxation can be considered as follows: At first, several string-like clusters are organized as an aggregation of inelastic hard spheres, which are sparsely distributed. Those string-like clusters moved actively and are gradually aggregating. Next, a certain amount of cluster begins to collide each other. This giant impact between clusters preceded collectively and made round shape density wave propagation on the cluster. This shock propagation results in the rapid growth of dissipation. The volumetric dilatation pattern of semicircular shape originated from shock density propagation in the clusters after cluster impact can be detected. Our analyses clarify the cause of giant impact between cluster, which is an entirely novel physical mechanism in the field of cooling granular

gas.

References

[1] E. P. Bernard, W. Krauth, and D. B. Wilson: Phys. Rev. E **80** (2009) 056704.

[2] M. Isobe: Int. J. Mod. Phys. C **10** (1999) 1281.

[3] M. Isobe: Mol. Sim. **42** (2016) 1317.

[4] M. Isobe: "Advances in the Comutational Sciences — Proceedings of the Symposium in Honor of Dr Berni Alder's 90th Birthday", edited by Eric Shwegler, Brenda M. Rubenstein, and Stephen B. Libby, World Scientific, **Chapter 6** (2017) 83.

[5] M. Isobe: Phys. Rev. E **68** (2003) 040301.

[6] M. Isobe: Proceedings in Powders and Grains 2005, Garcia-Rojo, Herrmann and McNamara(eds), (2005) 1123.

[7] M. Isobe: Int. J. Mod. Phys. C **23** (2012) 1250032.

[8] M. Isobe: J. Phys: Conf. Ser. **402** (2012) 012041.

[9] M. Isobe: EPJ Web Conf., **140** (2017) 04006.

Theoretical study for hydration effects on emitter of bioluminescence

Miyabi HIYAMA
Graduate School of Science and Technology, Gunma University, Tenjin-cho, Kiryu, Gunma 376-8515

In this year, we calculated the instantaneous absorption spectra of phenolate-keto, phenolate-enol, and enolate aqueous oxyluciferin anions, shown in Figure 1, at room temperature from QM/MM calculations using an explicit solvent. The absorption energies are computed as the ensemble average of 1000 different structures of hydrated clusters of oxyluciferin anions for each isomeric form. All calculations were performed using the GAUSSIAN09 [1] program on system B of Super Computer Center in ISSP.

It was demonstrated that the calculations reproduce experimental results concerning spectral shifts and broadening, for which traditional methods based on quantum chemistry and the Franck-Condon approximation fail because of the molecular vibrations of oxyluciferin anions and dynamical fluctuations of their hydration structures [2].

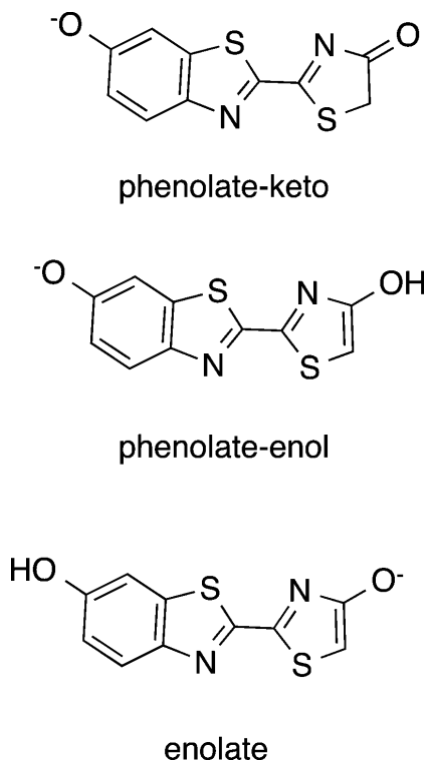

Figure 1: Molecular structures for oxyluciferin anions [2]

References

[1] Gaussian 09, Revision D.01, M. J. Frisch et al.
[2] M. Hiyama et al. Phys. Chem. Chem. Phys. 19 (2017) 10028.

Colloidal suspensions in binary liquid mixtures

Takeaki Araki and Armand Barbot
Department of Physics, Kyoto University
Kitashirakawa-oiwake-cho, Sakyo-ku, Kyoto 606-8505

We numerically study behaviors of colloidal suspensions in one-phase mixed solvents under shear flows (Fig. 1). Far from the phase separation point of the binary solvent, the colloid particles are dispersed well and the suspension shows a Newtonian viscosity (Fig. 2b). When the mixture is brought near the coexistence curve, the colloidal particles are aggregated by attractive interactions due to the concentration heterogeneity caused by the surface wetting. This aggregating interaction is enhanced when the component favored by the colloidal surface is poor. We found its viscosity is increased with approaching to the phase separation point. Near the coexistence curve the suspension shows a shear thinning behavior (Fig. 2b), since the aggregated structure is rearranged into small clusters under the shear flow (Fig. 2a). Our simulations also suggest that the shear flow does not change the concentration profiles around the particles so importantly at the onset of the rearrangement of the aggregates. Thus, we can consider that the effective interaction is almost free from the shear flow and remains isotropic.[1]

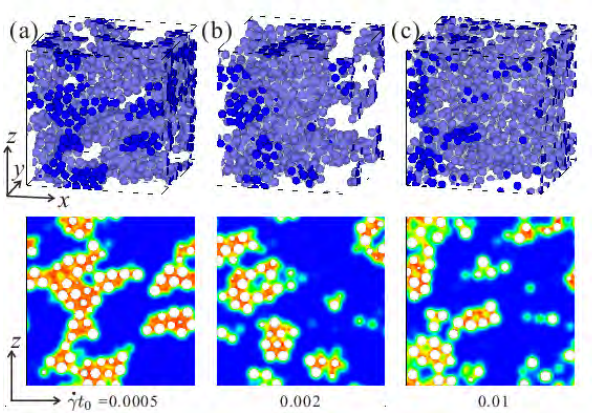

Figure 1: Snapshots of the particle distribution under shear flow (upper panels). The concentration fields are shown in the lower panels. The mixing fraction of the binary solvent is $\bar{\phi} = 0.35$ and the particle fraction is $\psi = 0.128$. The mixtures are at the coexistence curve.

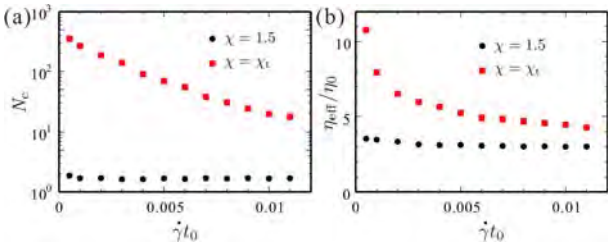

Figure 2: (a) The shear rate dependence of the cluster size. The mixture is in the one phase mixed state far from the coexistence curve (black circle, $\chi = 1.5$) and at the coexistence curve (red squares, $\chi = \chi_t$). (b) The shear rate dependence of the effective viscosity.

References

[1] A. Barbot and T. Araki: Soft Matter **13** (2017), 5911.

Microscopic theory of magnon physics in a three-dimensional chiral magnets

Naoya ARAKAWA

Department of Physics, Toho University, Funabashi, Chiba 274-8510

Magnons can describe low-energy physics of magnets. In contrast to the understanding for nonchiral magnets (e.g., ferromagnets and antiferromagnets), magnons for chiral magnets, magnets with finite spin scalar chirality, remains poor understood. In particular, the differences between magnons of nonchiral and chiral magnets and the differences between magnons of different chiral magnets are unclear.

To improve this situation, we studied the magnon dispersion curve and specific heat of chiral magnets on the pyrochlore lattice [1] by using the linearized-spin-wave approximation. We used an effective spin model consists of the Heisenberg interactions and the Dzyaloshinsky-Moriya interactions, and considered the all-in/all-out (AIAO) type and the three-in-one-out (3I1O) type chiral magnets.

We obtained two main results. The first one is that in all the chiral magnets considered, the magnon dispersion has no gapless excitation. Since nonchiral magnets usually have a Goldstone type gapless excitation, the first main result shows that the absence of the gapless excitations is a characteristic property of the chiral magnets. The second is that the magnon dispersion of the 3I1O type chiral magnets has not only the quasiacoustic branches, but also the optical branch, while those of the AIAO type chiral magnets are all quasiacoustic branches. We have defined a quasiacoustic and an optical branch of the magnon dispersion as follows: a quasiacoustic branch increases with the displacement from $\boldsymbol{q}=\boldsymbol{Q}$, the ordering vector; an optical branch decreases with the displacement. The above difference between the AIAO type and the 3I1O type chiral magnets is a characteristic, experimentally distinguishable difference between these chiral magnets.

We acknowledge support from the Super Computer Center in this study.

References

[1] N. Arakawa: Magnon Dispersion and Specific Heat of Chiral Magnets on the Pyrochlore Lattice, Journal of Physical Society of Japan, 86 (2017) 094705.

A series expansion study on the magnon spectrum of a kagome antiferromagnet in $Cs_2Cu_3SnF_{12}$

Yoshiyuki Fukumoto
Department of Physics, Faculty of Science and Technology, Tokyo University of Science
2641 Yamazaki, Noda, Chiba 278-8510

A spin-1/2 kagome-lattice antiferomagnet $Cs_2Cu_3SnF_{12}$ has a magnetic order with the $q = 0$ structure. Ono *et al.* observed the magnon dispersion curve via inelastic neutron scattering and pointed out that Dzyaloshinskii-Moriya (DM) interactions stabilizes the $q = 0$ structure [1]. It was also reported that the spin-wave analysis with the lowest order of quantum corrections result in exchange parameter as large as about 40% of that determined by a susceptibility measurement. In order to resolve this discrepancy, we intended to make a series expansion study from a Ising limit [2]. However, our obtained series coefficients are up to the second order at this stage, and the development of source codes for higher-order calculations is now in progress. The delay is due to the complexity in generating clusters that contribute to the series.

We used the supercomputer to make exact-diagonalization studies on a similar system, spin-1/2 spherical kagome cluster realized in $\{W_{72}V_{30}\}$ [3], which consists of 30 vertices and 20 corner-sharing triangles. We consider model Hamiltonians with terms which break the conservation of total S^z, as suggested by experiments on magnetization process. Then, the dimension of the Hilbert space is $2^{30} \simeq 1.07\times10^9$, and the memory usage of three complex vectors in this space amounts to 48 GB. We performed our numerical calculations on the SGI Altix ICE 8400EX at the Supercomputer Center, Institute for Solid State Physics, using OpenMP parallelization with up to 24 cores.

For cluster magnets, in general, stepwise structures are expected in zero-temperature magnetization curves. However, for a 30-site cluster $\{W_{72}V_{30}\}$, it was reported that there is no such structure up to 50 T in a magnetization measurement at 0.5 K[4]. In order to understand this behavior, we study the effects of Dzyaloshinsky-Moriya (DM) interactions and tilts of the g tensors, both of which lead to the breaking of the total-S^z conservation [5]. It is found that the D vector component parallel to the radiation direction of the polyhedron cancels out the staircase in a low magnetic field region efficiently. The tilts of the g tensors are inherent to systems defined on the polyhedrons and lead to induced magnetic fields varying site by site. This induced magnetic field affects the magnetization only at high magnetic fields. We also discuss two existing experimental results on the basis of our calculated results.

Next, we turn to the study of temperature dependence of the magnetic susceptibility for the spherical kagome cluster with DM interactions to compare with an existing experimental result [6]. Needless to say, the DM interaction breaks the conservation of total spin and get the evaluation of magnetic susceptibility to be more difficult. As for kagome-lattice antiferromagnets with DM interactions, Rigol and Singh calculated susceptibility up to a 15-site cluster to understand the experimental susceptibility of Herbertsmithite [7]. They calculated all eigenvalues under magnetic fields H,

and evaluate magnetic susceptibility from the second-order coefficient in H of the free energy. Instead, we use the method of microcanonical thermal pure quantum (mTPQ) states to carry out calculations for the 30-site spherical kagome cluster.

The mTPQ state is configured to reproduce the equilibrium value in the smooth microcanonical ensemble with a density operator $(l - h)^k$, where h is the Hamiltonian density and l is an arbitrarily real number not less than the maximum eigenvalue of h [8]. We first show that the mTPQ states with sufficiently large l reproduce the equilibrium value in the canonical ensemble. In our susceptibility calculations, we apply magnetic fields, whose strength is chosen to be 10% of the exchange parameter, and calculate the induced magnetizations by using the mTPQ states. The susceptibility is obtained by dividing the magnetizations by the field strength. Although mTPQ expectation values contain statistical errors and the division process by a small field strength enhances the error, we find the present calculation procedure results in meaningful results. It is also found that the DM interaction moves the theoretical susceptibility closer to the experimental one [4].

References

[1] T. Ono, K. Matan, Y. Nambu, T. J. Sato, K. Katayama, S. Hirata, and H. Tanaka, J. Phys. Soc. Jpn. 83, 043701, 2014.

[2] W. Zheng, J. O. Fjaerestad, R. R. P. Singh, R. H. McKenzie, and R. Coldea, Phys. Rev. B 74, 224420, 2006.

[3] A. M. Todae, A. Merca, H. Bögge, T. Glaser, L. Engelhardt, R. Prozorov, M. Luban, and A. Müller, Chem. Commun., 3351, 2009.

[4] J. Schnack, A. M. Todea, A. Müller, H. Nojiri, S. Yeninas, Y. Furukawa, R. Prozorov, and M. Luban, arXiv:cond-mat/1304.2603v1.

[5] Y. Fukumoto, Y. Yokoyama, and H. Nakano: submitted to J. Phys. Soc. Jpn. (arXiv:1803.06485).

[6] Y. Maeda, Tokyo University of Science, 2018, master thesis.

[7] M. Rigol and R. R. P. Singh, Phys. Rev B 76, 184403, 2007.

[8] S. Sugiura and A. Shimizu, Phys. Rev. Lett. 108, 240401, 2012.

Theory of the multiple spin density waves and the magnetic skyrmions in the triangular-lattice Hubbard model

Takashi UCHIDA
Hokkaido University of Science
4-1, 7-15, Maeda, Teine-ku, Sapporo 006-8585

Magnetic skyrmions are topological stable vortex-like magnetic structures with the spin directions distributing in all directions. It has been found that the skyrmions emerge as 3Q multiple helical spin density waves in B20 transition metal compounds and their alloys. Because of the lack of inversion symmetry, the formation of magnetic skyrmions in these materials are well explained by a competition between the ferromagnetic exchange interactions and the Dzyaloshinskii-Moriya (DM) interaction under magnetic field. Recently, frustrated classical systems without the DM interaction have been found to reveal magnetic skyrmions at finite temperatures [1]. The purpose of the present research is to explore theoretically the multiple spin density waves in the frustrated itinerant systems, where the 3Q structures including skyrmions might be expected near the half-filled region. For this purpose, we have investigated the magnetic structure of the single-band Hubbard model on the triangular lattice on the basis of the molecular spin dynamics (MSD) method [2].

The MSD method is based on the functional integral method for the spin fluctuation theories and the isothermal molecular dynamics method. The method allows us to find automatically the magnetic structure of a large system with thousands of atoms in a unit cell at finite temperatures. Starting from the Hamiltonian expressed in terms of the locally rotated coordinates and by adopting the static approximation to the functional integral technique, the MSD method reduces to the generalized Hartree-Fock approximation at the ground state. In the numerical calculations the most time-consuming process is the magnetic force calculation at each time step, where the local electronic structures are calculated in the real space by means of the recursion method. In order to perform the recursion calculation efficiently, we have adopted the automatic parallel calculation scheme.

The magnetic structure is calculated on the supercell with 40×40 triangular lattice, which is embedded in a large cluster consisting of 3×3 supercells, each of which are connected by the periodic boundary condition. For the Coulomb interaction strength $U/t = 8$ and the temperature $T/t = 0.001$, the MSD yields modulated 120° structures for $n = 0.8$ and 0.9, 3Q structures for $n = 0.95$, 1.00 and 1.05, 2Q structure for $n = 1.10$, collinear antiferromagnetism for $n = 1.20$, and ferromagnetism for $n = 1.40$. The 3Q states are found to be skyrmion-like structures with the magnetic moment directions distributing in all directions, where the three Q vectors are directed along the axes of the triangular lattice.

References

[1] T. Okubo, S. Chung, and H. Kawamura, Phys. Rev. Lett. **108** (2012) 017206

[2] Y. Kakehashi, S. Akbar, and N. Kimura, Phys. Rev. B**57** (1998) 8354.

Microscopic description of optical bistability

Tatsuhiko SHIRAI
Institute for Solid State Physics, University of Tokyo
Kashiwa-no-ha, Kashiwa, Chiba 277-8581

We developed an efficient numerical algorithm to treat the quantum master equation (QME) for hybridized systems of many photons and a large number of two-level atoms. The scheme of numerical calculation consists of the parallelization in photon space by making use of the fact that the time-evolution operator of the QME, L, is a sparse matrix. For the Hilbert space representing the atom, we use the permutation symmetry of L, by which we can reduce the number of dimensions drastically from 2^{2N} to $O(N^3)$. The photon number n should be infinite in principle, but we found that the system is well described if we set the upper limit of the photon number, $n_{\max}$, to be larger than a few times of N. With this method, we performed numerical simulations for the system with up to $N = 25$ and $n_{\max} = 57$.

We also study the efficiency of the parallelization in terms of the photon space. The core labeled by the pair of integers (n_1, n_2) stores elements of $\langle n_1|\rho|n_2\rangle$ where ρ is a density matrix, and $\{|n\rangle\}$ are photon number states and the integer n runs from 0 to the cutoff $n_{\max}$. Thus, the total number of cores is $n_{\text{core}} = (n_{\max} + 1)^2$. The main part of the numerical calculation is the Bi-CG method, consisting of the multiplication of L and $L^\dagger$ on ρ. The calculation of (n_1, n_2)-elements of L and $L^\dagger$ requires only six elements of ρ as depicted in Fig. 1. Due to the local nature of the calculation independent of $n_{\max}$, good efficiency should be achieved.

By using the above numerical methods, we give size dependences of both static and dynamic properties of the optical bistability, and moreover discuss the weak scaling to evaluate the efficiency of the parallelization [1].

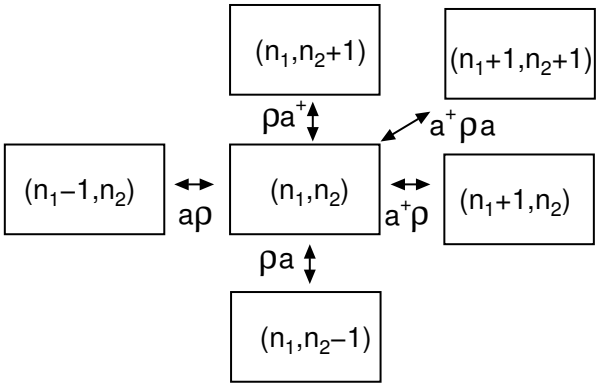

Figure 1: Data exchange among neighboring cores necessary for the multiplication of L on ρ in the parallelization method.

References

[1] T. Shirai, S. Todo, H. De Raedt, and S. Miyashita: submitted to Phys. Rev. A.

Numerical Study of One Dimensional Frustrated Quantum Spin Systems

Kazuo HIDA
Division of Material Science, Graduate School of Science and Engineering
Saitama, Saitama 338-8570

1 Introduction

In this project, we investigate the ground state phase diagram of spin-1 distorted diamond chains with two types of distortion called types A and B. They are described by the following Hamiltonians

type A :

$$\mathcal{H}_{\rm A} = \sum_{l=1}^{N}\Big[(1+\delta_{\rm A})\boldsymbol{S}_l\boldsymbol{\tau}_l^{(1)} + (1-\delta_{\rm A})\boldsymbol{\tau}_l^{(1)}\boldsymbol{S}_{l+1} + (1-\delta_{\rm A})\boldsymbol{S}_l\boldsymbol{\tau}_l^{(2)} + (1+\delta_{\rm A})\boldsymbol{\tau}_l^{(2)}\boldsymbol{S}_{l+1} + \lambda\boldsymbol{\tau}_l^{(1)}\boldsymbol{\tau}_l^{(2)}\Big], \quad (1)$$

type B :

$$\mathcal{H}_{\rm B} = \sum_{l=1}^{N}\Big[(1+\delta_{\rm B})\boldsymbol{S}_l\boldsymbol{\tau}_l^{(1)} + (1+\delta_{\rm B})\boldsymbol{\tau}_l^{(1)}\boldsymbol{S}_{l+1} + (1-\delta_{\rm B})\boldsymbol{S}_l\boldsymbol{\tau}_l^{(2)} + (1-\delta_{\rm B})\boldsymbol{\tau}_l^{(2)}\boldsymbol{S}_{l+1} + \lambda\boldsymbol{\tau}_l^{(1)}\boldsymbol{\tau}_l^{(2)}\Big], \quad (2)$$

where $\boldsymbol{S}_l$, $\boldsymbol{\tau}_l^{(1)}$, $\boldsymbol{\tau}_l^{(2)}$ are spin-1 operators.

2 Undistorted case

For $\delta_{\rm A} = \delta_{\rm B} = 0$, $\boldsymbol{T}_l^2 = T_l(T_l+1)(\boldsymbol{T}_l \equiv \boldsymbol{\tau}_l^{(1)}+\boldsymbol{\tau}_l^{(2)})$ are conserved for each l as $T_l = 0, 1,$ and 2. A pair of spins $\boldsymbol{\tau}_l^{(1)}$ and $\boldsymbol{\tau}_l^{(2)}$ with $T_l = 0$ is called a dimer. The interaction between the spins on both sides of a dimer is decoupled. The ground state of the whole system can be written as a direct product of dimers and the ground states of clusters (called cluster-n) consisting of n nonvanishing $\boldsymbol{T}_l$'s and $n+1$ $\boldsymbol{S}_l$'s between two dimers. The ground state phase consisting of an infinite array of dimers and cluster-n's is called DCn phase. In the absence of distortion, the ground-state phase diagram of the whole system consists of DCn phases with $n = 0, 1, 2,$ and 3, a uniform spin-1 Haldane (UH) phase, a ferrimagnetic phase with spontaneous translational symmetry breakdown (STSB) with $m(\equiv M/M_{\rm s}) = 1/6$ ($\rm F_{1/6}$ phase), and a ferrimagnetic phase without STSB with $m = 1/3$ ($\rm F_{1/3}$ phase) as shown in Fig. 1, where M is the spontaneous magnetization and $M_{\rm s}(= 3N)$ is the saturated magnetization. [1, 2]

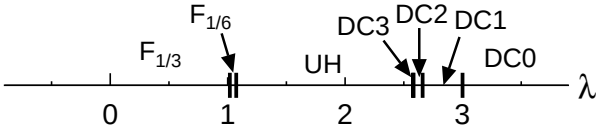

Figure 1: Ground-state phase diagram of undistorted diamond chains with $S = 1$.

3 Distorted Cases

3.1 Type A distortion

The ground-state phase diagram obtained by the DMRG and exact numerical diagonalization for $3N = 18$ is shown in Fig. 2. The $\rm F_{1/3}$ phase survives distortion, although it shifts to smaller λ regime. The $\rm F_{1/6}$ phase narrows rapidly with the increase of $\delta_{\rm A}$, and becomes numerically undetectable for large $\delta_{\rm A}$. The DCn phases turn into the Haldane phases

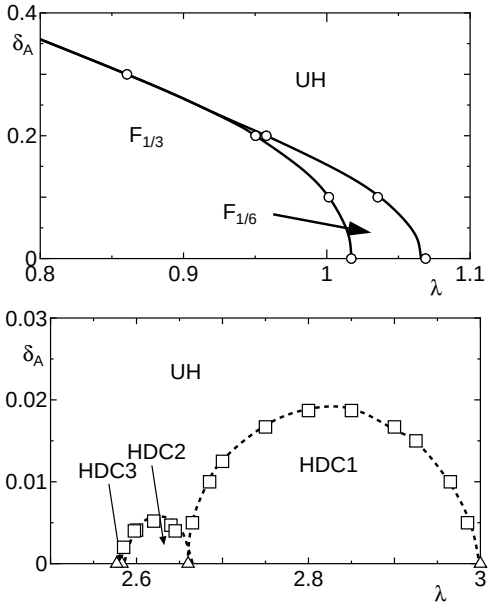

Figure 2: Ground-state phase diagram for type A distortion. Upper panel shows the region with small λ and lower panel, large λ.

with spontaneous $(n+1)$-fold STSB (HDCn phases) as in the mixed diamond chain with $(S,\tau)=(1,1/2)$[3]. For large enough $\delta_{\rm A}$, they undergo phase transitions to a UH phase. This phase is continuously connected to the UH phase at $\delta_{\rm A}=0$ for $1.0726\leq\lambda\leq 2.577$.

3.2 Type B distortion

The ground-state phase diagram obtained by the exact numerical diagonalization for $3N=18$ is shown in Fig. 3. The DCn phases turn into ferrimagnetic phases with $(n+1)$-fold STSB (FDCn phases) as in the mixed diamond chain with $(S,\tau)=(1,1/2)$[3]. In these phases, the spontaneous magnetization is given by $m=1/(3(n+1))$. Hence, they can be regarded as F$_m$ phases. The F$_{1/3}$ phase for $\delta_{\rm B}=0$ survives the distortion and shifts to smaller λ regime. The F$_{1/6}$ phase narrows rapidly with the increase of $\delta_{\rm B}$, and becomes numerically undetectable for $\delta_{\rm B}\sim 1$. The width of the UH phase remains finite unless $\delta_{\rm B}=1$. It has been confirmed by the DMRG calculation with $3N=72$ that narrow partial ferrimagnetic (PF) phases with continuously

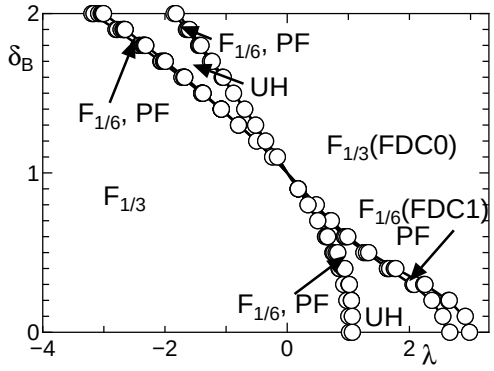

Figure 3: Ground-state phase diagram for type B distortion.

varying m are present between these ferrimagnetic phases and UH phase.

This work is supported by JSPS KAKENHI Grant Number JP25400389.

(collaborator Ken'ichi Takano)

References

[1] K. Takano, K. Kubo, and H. Sakamoto: J. Phys.: Condens. Matter **8** 6405 (1996).

[2] K. Hida and K. Takano: J. Phys. Soc. Jpn. **86**, 033707 (2017).

[3] K. Hida, K. Takano and H. Suzuki : J. Phys. Soc. Jpn. **79** 114703 (2010).

Heat Transfer Characteristics of Condensate Film Flow along Vertical Plates with Microscopic Grooves

Takahiro ADACHI
Department of Mechanical Engineering, Akita University
Tegata-Gakuen 1-1, Akita, Akita 010-8502

The characteristics of thin, falling liquid films due to condensation along a vertical plate have been of interest to engineers, for example, in plate-type absorber, plate-type condenser and so on. In order to enhance the heat transfer, fluted parts along the streamwise direction have been established on the plate. This is because the liquid film spreads as thinly as possible over the plate surface since strong surface tension aids in the removal of film from the top to bottom of the fluted parts, thereby producing a very thin liquid film. This is called a drainage effect[1].

However, it is difficult to clarify the detailed mechanism of the heat transfer enhancement, because the film flow has thin, three-dimensional and unsteady behaviour. Actually, it has been shown that the film flow on the flat plate behaved like a wave and thickness of the film flow became thinner locally in the wavy flow regime, which leads to the enhance of the heat transfer enhancement. In case of the fluted plate, the situation must be more complicated. So, it is greatly depends on numerical calculations to clarify the flow and temperature characteristics.

In this study, we numerically investigate the thin liquid film flow on the vertical rectangular fluted plates in laminar flow resume. Our objective is to clarify effects of grooved geometries and surface tension on both the flow patterns and the heat transfer by setting the fluted parts on the vertical flat plate. Then, we treat our study under the well-known Graetz-Nusselt's problem. This means that the film flow is three-dimensional and fully developed in the stream-wise direction, while the temperature is developing in the thermally inlet region. We will try to show the relation among the heat transfer, fluted geometries and the surface tension effect.

We consider a liquid film flow along a plate with a rectangular groove setting along the stream-wise direction on its surface. Figure 1 shows a geometry of the problem and the coordinate system. The x-axis is taken to be parallel to the vertical direction and the y-axis to be perpendicular to it. Nondimensional parameters to characterize the plate configuration, height h of the groove, width of the groove w_b, inlet length w_i and outlet length w_o are, using δ_0^* at the inlet as a characteristic length, defined as

$$h = \frac{h^*}{\delta_0^*}, \quad w_b = \frac{w_b^*}{\delta_0^*}, \quad w_i = \frac{w_i}{\delta_0^*}, \quad w_o = \frac{w_o}{\delta_0^*} \quad (1)$$

where we represent physical quantities with their dimensions by attaching a superscript $*$ to them, and the total plate length is $L = w_i + w_b + w_o$.

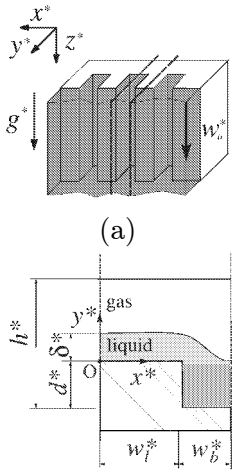

Fig.1 Geometry and coordinates.

The governing equations for the velocity and pressure are written in non-dimensional forms as

$$\frac{\partial u}{\partial x} + \frac{\partial v}{\partial y} = 0, \tag{2}$$

$$\rho\left(\frac{\partial u}{\partial t} + u\frac{\partial u}{\partial x} + v\frac{\partial u}{\partial y}\right) = \frac{1}{Re}\{\frac{\partial}{\partial x}\left(2\mu\frac{\partial u}{\partial x}\right) + \frac{\partial}{\partial y}\left(\mu\frac{\partial v}{\partial x} + \mu\frac{\partial u}{\partial y}\right)\} - \frac{\partial p}{\partial x}, \tag{3}$$

$$\rho\left(\frac{\partial v}{\partial t} + u\frac{\partial v}{\partial x} + v\frac{\partial v}{\partial y}\right) = \frac{1}{Re}\{\frac{\partial}{\partial x}\left(\mu\frac{\partial v}{\partial x} + \mu\frac{\partial u}{\partial y}\right) + \frac{\partial}{\partial y}\left(2\mu\frac{\partial v}{\partial y}\right)\} - \frac{\partial p}{\partial y}, \tag{4}$$

$$\rho\left(u\frac{\partial w}{\partial x} + v\frac{\partial w}{\partial y}\right) = \frac{1}{Re}\{\frac{\partial}{\partial x}\left(\mu\frac{\partial w}{\partial x}\right) + \frac{\partial}{\partial y}\left(\mu\frac{\partial w}{\partial y}\right)\} + \rho Fr - \frac{\partial p}{\partial z}, \tag{5}$$

where velocity gradient in z direction is ignored such as $\partial u/\partial z = \partial v/\partial z = \partial w/\partial z = 0$ in the equations (2), (3), (4) and (5) because of assumption as velocity u is unchanged in z direction.

We show the temporal evolution of the film flow at $t = 0$, 30, 100 and 250 in Fig.**??** for $d = 3$ and $Bo = 10$. At the initial state shown in Fig.2 (a), the liquid film is distributed so as to be the same quantity as Nusselt's distribution on the flat plate, which means that the cross sectional area for the liquid phase is $1 \times w_l \times w_b = 5$. The film flow is developing temporally along the fluted plate surface from the initial distribution as shown in Fig. 2 (a). Thickness of the film flow is decreased at groove edge due to an effect of surface tension seen in Fig. 2 (b)-(d). It is evident that the averaged thickness of liquid film decreases for the fluted plate compared with thickness for the flat plate because the heat transfer area increases in the fluted plate more than one in the flat plate by setting the fluted part. Therefore, it is expected that the heat transfer increases for the fluted plate greater than that for the flat plate.

Film flow falling along vertical rectangular fluted plates is investigated in this study. We have calculated the temporal evolution of the film flow by using the Combined Level Set and Volume of Fluid(CLSVOF) and Ghost Fluid(GF) methods, and obtained the steady state film and velocity distributions. It is found that the film flow goes inside the fluted part due to the effect of the surface tension for the fluted plate and the thickness near the fluted edge is thinner.

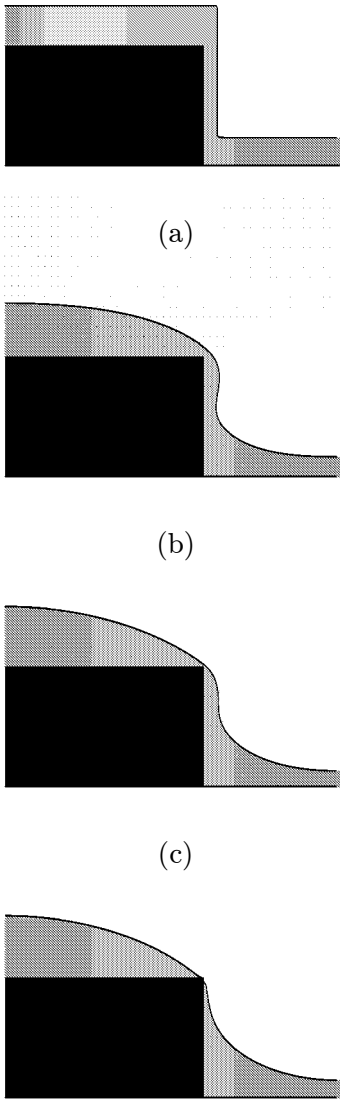

Fig. 2 Time evolution of the film flow.

References

[1] R. Gregorig, Z. Angew. Math. Phys., Vol. 5, (1954) 36.

Designing novel quantum materials based on space group symmetries, from filling-enforced quantum band insulators to novel quantum spin liquids

Masahiko G. YAMADA, Masaki OSHIKAWA
Institute for Solid State Physics, University of Tokyo
Kashiwa-no-ha, Kashiwa, Chiba 277-8581

First, we have searched for realistic cadidates for filling-enforced quantum band insulators (feQBI) [1]. The feQBI is a novel quantum phase protected by the space group symmetry of the material. They are distinct from a trivial atomic insulator in the sense that it cannot be adiabatically connected to any atomic insulators unless the energy gap closes or the space group symmetry is broken. In this sense, we can regard the feQBI as an intrinsic band insulator where the band gap is opening purely because of the quantum interference of the Bloch wave functions. In addition, it is known that this band gap can open only by including the spin-oribit coupling (SOC).

It was suggested that the hyperkagome system with SOC can host such phases [1], so we explored some metal-organic frameworks (MOFs) as the first candidate for feQBI. There already exists a material with a space group No. 220 in MOFs [2], which is one of few space groups hosting feQBI, so it is natural to seek first in MOFs. However, after many attempts for the first-principles band calculations for those materials, the gap for the feQBI filling never opens in such MOF-type materials. While this was a negative result on our initial objective, later it was found to be physically reasonable. In fact, a microscopic investigation based on the perturbation theory has revealed that the SOC in the d-orbital transition metal systems cannot open the gap for feQBI.

Therefore, we have changed our objective from the search for feQBI to the search for a new candidate for quantum spin liquids with a kagome or hyperkagome lattice structure. This is a natural extension of the feQBI because these lattices are known to host flat-band ferromagnetism or quantum spin liquid with another filling condition. After materials search using first-principles calculations, we discovered [3] some new kagome spin liquid candidates, which can be compared to herbertsmithite. In addition, by increasing the strength of SOC a new type of Dzyaloshinskii-Moriya interactions apper in those materials coming from the SOC hopping similar to the model for feQBI [1].

References

[1] H. C. Po, H. Watanabe, M. P. Zaletel, and A. Vishwanath, Sci. Adv. **2**, e1501782 (2016).

[2] L. E. Darago, *et al.*, J. Am. Chem. Soc. **137**, 15703 (2015).

[3] M. G. Yamada and M. Oshikawa, in preparation